POLITECNICO DI MILANO

Facoltà di Ingegneria Industriale

Corso di Laurea Magistrale in
Ingegneria Spaziale

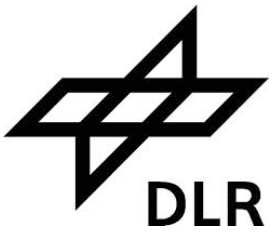

Viscosity and Regression Rate Measurements of Paraffin-Based Hybrid Solid Fuels

Advisor: Prof. Luigi T. DE LUCA

Co-Advisor: Ing. Mario KOBALD

Tesi di Laurea di:

Serenella DI BETTA Matr. 751178

Anno Accademico 2012 - 2013

Acknowledgements

First I would like to thank my parents for having been close to me during all long years spent at Politecnico.
Thanks to Professor De Luca for the opportunity to do this thesis work and thanks to Mario Kobald and Dr. Ciezky for making it possible.
Thanks to Elena for supervising me during this period and for her great helpfulness.
Thanks to Michele for revealing me the rheology secrets.
A special thanks to Veronica, unfailing source of knowledge and course notes that clear a lot of doubts during these years.
Thanks to Aikido dojo mates, with whom i shared a lot of experiences, for giving the way of relieving and manage stress, and thanks to my friends for standing always beside me.
A very huge thanks to wohnheim fellas for making my stay abroad unforgettable. Last but not least, thanks to german food, beer, supermarkets, frogs, cold weather and snow for constantly putting me to the test during seven months spent in Germany.

In primo luogo vorrei ringraziare i miei genitori per essermi stati accanto e avermi sostenuto durante tutti i lunghi anni trascorsi al Politecnico.
Grazie al Professor De Luca per avermi dato l'opportunità di svolgere questo lavoro di tesi e a Mario Kobald e al Dr. Ciezky per averlo reso possibile.
Grazie ad Elena per avermi seguito durante il periodo di svolgimento della tesi e per la sua infinita disponibilità, e grazie a Michele per avermi svelato i segreti della reologia.
Uno speciale ringraziamento a Veronica, inesauribile fonte di sapere e di appunti che hanno dissolto molti dubbi durante questi anni di corso di laurea.
Grazie ai compagni del dojo di Aikido con cui ho condiviso un sacco di esperienze, per avermi dato modo di sfogare e gestire lo stress e grazie ai miei amici per essermi accanto sempre.
Un Enorme grazie a tutti i ragazzi del wohnheim per aver reso indimenticabile la permanenza all'estero. E ultimi ma non meno importanti, grazie alle rane, al freddo, alla neve, alla birra, al cibo e ai supermercati tedesci per avermi messo costantemente alla prova durante i sette mesi passati in Germania.

Abstract

Hybrid rocket systems have been studied and experimented with since the 30s in Russia, Austria and Germany. In hybrid rocket engines the propellant is stored into two different aggregation states: solid and liquid (or gaseous). Typical configuration is the so-called "direct hybrid" in which the fuel is solid and the oxidizer is liquid or gaseous. Another configuration is possible, even if less used, with solid oxidizer and liquid fuel. This configuration is called "reverse hybrid".
Due to its particular storage configuration, hybrid propulsion combines the advantages of liquid and solid propellants. Its main characteristics are: safety, due to the separately storage of fuel and oxdizer the possibility of explosion or detonation during fabbrication, storage and operation is really low; possibility of multiple shut on and shut off; low costs compared to liquids due to the relative simplicity of the system; higher specific impulse than solid rocket motors.
Despite all these advantages hybrid propulsion has some important limitations: due to rough combustion process, the combustion efficiency is lower with respect to solid and liquid propellants; time variation of key-parameters complicates the effective control of the thrust; the thrust is limited by low regresion rate values. The latter is the mainly studied shortcoming and different solutions have been proposed to overcome this problem. Most effective solution is to use a new class of fuels in hybrid rockets. This fuels are called "liquefying fuels" due to the fact that they produce a liquid layer on their surface during the combustion process. The instability of the liquid layer leads to the entrainment of liquid droplets from the melt layer as additional mass transfer. This phenomenon increases the regression rate of 2-5 times with respect to classical hybrid fuels as HTPB.
In this work a special group of liquefing hybrid propellants is studied. The attention is focused on wax-based fuels. Since the regression rate is strongly dependent on the viscosity of the melt layer, the rheological behavior of the different waxes has been characterized measuring their viscosity at different temperatures and shear rates. Waxes have been studied both pure and with some additives. Additives change the rheological behavior of the wax, in particular adding carbon black leads to a non-Newtonian behavior of the melted wax. Correlation between the percentage of carbon black and non-Newtonian behavior is also investigated in this work.
The regression rate of waxes has been measured by means of a 2D slab burner at test complex M11 at DLR Lampoldshausen. Waxes have been tested at constant oxidizer mass flow (53 g/s) and at ambient pressure. Burning tests have been performed on pure waxes and on mixtures of 88% wax, 10% stearic acid and 2% carbon black. Results show the link between the regression rate and the viscosity of the wax. Higher is the viscosity, lower is the instability of the melt layer and so the regression rate. It is found that paraffin waxes have the highest regression rate. Results of burning tests are then qualitatively compared with data found at SPLab at Politecnico di Milano.

Contents

Nomenclature

Acronyms

ABC	Asymptotic behavior correlation
AFRL	Air force research laboratories
AMROC	American rocket society
BET	Specific surface area analysis
C.B.	Carbon Black
DLR	Deutsches Zentrum fuer Luft und Raumfahrt - German Aerospace Center
GIRD	Gruppa Isutcheniya Reaktinovo Dvisheniya (Group of Investigation on Reactive Motion)
HAST	High altitude supersonic target
HDPE	High density polyethylene
HTPB	Hydroxyl-terminated polybutadiene
NASA	National aeronautics and space administration
PD	Polydispersity
S.A.	Stearic Acid

Greek symbols

α	Absorption coefficient, m^{-1}
ϵ	Emissivity coefficient
$\dot{\gamma}$	Shear rate, $1/s$
η	Dynamic viscosity, $Pa \cdot s$
ρ	Density, kg/m^3
σ	Stefan-Boltzmann constant, W/m^2K^4
τ	Shear stress, Pa

Physical quantities

a_0	First power law interpolation coefficient (regression rate)
B	Blowing parameter
C_f	Friction coefficient
C_{f0}	Friction coefficient without blowing
C_h	Stanton number
c_p	Specific heat, J/kgK
e_0	Entrainment parameter
G	Mass flux, kg/m^2s
h	Enthalpy, J/kg
k	Thermal conductivity, W/mK
L	Length of fuel grain, mm
$\dot{m}$	mass flow rate
n	Carbon number
n_r	Second power law interpolation coefficient (regression rate)
p	pressure, Pa
P_d	Dynamic pressure, Pa
P_r	Prandtl number
$\dot{q}$	Heat flux, W/m^2
$\dot{r}$	Regression rate, mm/s
R_e	Reynolds number
T	Temperature, K
u	Velocity, m/s
x	Axial distance along the axis of the port
Y	General property value

Subscripts

c	Chamber
$conv$	Convective
e	Free stream
ent	Entrainment
f	Fuel
g	Gaseous phase
l	Liquid phase
m	Melting
ox	Oxidizer
rad	Radiative
s	Solid phase
v	Vaporization
w	Wall

List of Figures

List of Tables

Estratto

Nonostante siano nati nello stesso periodo di solidi e liquidi, i sistemi a propulsione ibrida sono stati i meno studiati ed utilizzati. I primi studi inerenti a questa configurazione risalgono alla prima metà degli anni '30 e hanno avuto luogo in Russia, Austria e Germania. Gli esperimenti hanno poi preso piede anche negli stati uniti, dove si è recentemente arrivati al volo di *SpaceShipOne*, uno spazioplano suborbitale propulso con HTPB e monossido di azoto (N_2O).
Nei sistemi a propulsione ibrida il combustibile e l'ossidante sono immagazzinati in due diversi stati di aggregazione: uno solido e l'altro liquido o gassoso. La configurazione più comune prevede combustibile solido e ossidante liquido (o gassoso), non mancano però studi sui cosidetti ibridi inversi in cui è l'ossidante ad essere solido mentre il combustibile è liquido.
Grazie alla loro particolare configurazione, i sistemi ibridi combinano alcuni vantaggi sia dei sistemi a propulsione solida che di quelli a propulsione liquida. In essi infatti lo stoccaggio separato di combustibile e ossidante rende molto improbabile la possibilità di accensioni accidentali ed esplosioni. Hanno inoltre il grande vantaggio di permettere spegnimenti e riaccensioni multiple, permettono di modulare la spinta, hanno costi inferiori e sono più semplici rispetto ai sistemi a liquido, e l'impulso specifico presenta valori più elevati se comparati ai propellenti solidi. Nonostante tutti questi vantaggi, i sistemi a propulsione ibrida hanno alcune grosse limitazioni che hanno fatto sì che il loro studio ed utilizzo sia stato messo da parte durante gli anni. La loro combustione risulta infatti essere alquanto ruvida, questo porta ad una bassa efficienza di combustione (circa 95%), inoltre la variazione nel tempo di importanti parametri, quali i valori di O/F e la geometria del porto, rende complesso l'effettivo controllo della spinta. Un altro importante difetto sono i bassi valori di velocità di regressione che limitano la spinta. Il problema legato alla velocità di regressione è il maggiormante studiato e diverse soluzioni sono state proposte al fine di risolverlo: l'aggiunta di additivi energetici, l'incremento della turbolenza del flusso e l'utilizzo di combustibili detti bassofondenti. Quest'ultimo è risultato essere il più efficace: i combustibili bassofondenti infatti, durante la combustione, formano uno strato liquido sulla superficie del combustibile solido che causa il fenomeno di entrainment. A seguito di instabilità dello strato liquido dovute al flusso di ossidante, delle gocce di combustibile vengono staccate dalle creste delle onde di instabilità e vengono trascinate nel flusso di ossidante. Questo fenomeno aumenta la velocità di regressione, facendola arrivare a valori 2-5 volte superiori rispetto a quelli dei combustibili ibridi classici come l' HTPB.
Nel presente lavoro è studiato e discusso un gruppo di combustibili appartenti alla classe dei combustibili bassofondenti: le cere paraffiniche.
Dal momento che la velocità di regressione risulta strettamente correlata alla viscosità dello strato liquido, è stato caratterizzato il comportamento reologico di diversi tipi di paraffine, di una cera microcristallina e di una cera con additivi precedentemente

inseriti dal produttore. La viscosità è stata misurata sia per le cere pure che per miscele con additivi di diversa tipologia (alluminio, acido stearico e carbon black). Gli additivi cambiano in maniera significativa l'andamento della viscosità delle cere, aumentandola nella maggior parte dei casi. La presenza di carbon black inoltre porta la miscela ad avere un comportamento non-Newtoniano, il che comporta che la viscosità non risulti più costante al variare del gradiente di velocità.
Sono stati inoltre eseguiti dei test in camera di combustione, al fine di misurare la velocità di regressione del combustibile. I test sono stati eseguiti presso il complesso M11 del centro di ricerche DLR a Lampoldshausen. Sono state sottoposte a test di combustione sia cere pure che in miscela con 10% acido stearico e 2% carbon black. I risultati sono quindi stati confrontati con i dati ottenuti dalla caratterizzazione balistica delle stesse cere eseguita nel laboratorio SPLab del Politecnico di Milano.

Combustibili bassofondenti

I primi test riguardanti i combustibili bassofondenti sono stati condotti da AFRL e ORBITEC utilizzando combustibili criogenici. Lo stesso comportamento balistico si può tuttavia osservare in sostanze che sono solide in condizioni standard e che producono uno strato liquido sulla supeficie durante la combustione. Tra questi materiali troviamo le cere paraffiniche. Oltre al tipico fenomeno di gassificazione, questi materiali presentano anche un fenomeno di trasferimento di massa dovuto alle goccioline che si staccano dalle creste delle onde, dovute all'instabilità dello strato liquido. Questo fenomeno prende il nome di *entrainment*. L'effetto più importante dell'entrainment è quello di aumentare la velocità di regressione senza aumentare il parametro di soffiamento. L'entrainment è legato alle proprietà del motore e del combustibile secondo la relazione:

$$\dot{m}_{ent} \propto \frac{P_d^{\alpha} h^{\beta}}{\eta^{\gamma} \sigma^{\pi}} \tag{1}$$

Dove P_d è la pressione dinamica, h, η e σ sono rispettivamente lo spessore, la viscosità e la tensione superficiale dello strato liquido. α, β, γ e π sono costanti determinate sperimentalmente, il cui valore differisce a seconda della fonte:

Reference	α	β	γ	π
Gater and L' Ecuyer	1.5	2	1	1
Nigmatulin et al.	1	1	-	-
Karabeyoglu	1-1.5	-	$> \pi$	$< \gamma$

Tabella 1: Valore degli esponenti per l'entrainment.

E' stato provato sperimentalmente [38] che la velocità di regressione dipende dalla viscosità con una proporzionalità del tipo $\eta^{1/6}$ per i combustibili a base paraffinica. Dato che l'entrainment in generale si sviluppa in condizioni supercritiche di pressione e temperatura, non è facile valutare le proprietà del combustibile alle condizioni operative. Per fare questo sono stati sviluppati diversi modelli [21] [24] che valutano l'andamento delle proprietà in relazione al numero di atomi di carbonio presenti nelle molecole.

Combustibili testati

Le cere paraffiniche sono delle miscele di idrocarburi solidi, in prevalenza alcani che hanno formula chimica C_nH_{2n+2}. Le paraffine sono caratterizzate da lunghe catene carboniose con un numero di atomi di carbonio superione a 20 ($n > 20$). Hanno temperature di fusione piuttosto basse e la loro densità si aggira intorno ai 900 kg/m^3. Tre cere paraffiniche sono state testate nell'ambito di questa tesi, due prodotte da Sasol (6003 e 6805) e una prodotta da Carlo Erba. Si è testata anche una cera microcristallina e una cera con all'interno degli additivi inseriti in fase di produzione, rispettivamente Sasolwax 0907 e 1276.
Le cere microcristalline sono caratterizzate da peso molecolare e temperatura di fusione piu elevati rispetto alle paraffine. Inoltre le loro molecole risultano più ramificate, questo si traduce in una maggior resistenza allo scorrimento delle molecole stesse.

Tali cere sono state sottoposte a test sia pure che miscelate con diversi additivi:

- Acido stearico: è un è un acido carbossilico con formula chimica $CH_3(CH_2)_{16}CO_2H$. Viene aggiunto alle cere per aumentare le loro proprietà meccaniche.
- Carbon Black: è un pigmento ottuneto dalla combustione incompleta di idrocarburi pesanti. Generalmente utilizzato come pigmento e rinforzo nella produzione di pneumatici, viene aggiunto alle cere per diminuire l'energia di radiazione trasmessa dalla fiamma alla superficie del grano solido.
- Alluminio: è uno dei metalli leggeri più comunemente utilizzato in propulsione per aumentare le prestazioni dei combustibili. Si sono utilizzate particelle di micro-alluminio con grandezza di circa 44 micron.

Caratterizzazione reologica

La viscosità è una grandezza fisica che caratterizza la resistenza di un fluido allo scorrimento. Dipende dalle proprietà chimiche del fluido, dalla temperatura e dal gradiente di velocità all'interno del fluido stesso. Il comportamento di un fluido ideale sottoposto ad uno sforzo tangenziale è descritto dalla legge di Newton:

$$\tau = \eta \cdot \dot{\gamma} \tag{2}$$

Dove τ è lo sforzo tangenziale, η la viscosità dinamica e $\dot{\gamma}$ rappresenta il gradiente di velocità. Nella sopracitata legge di Newton la viscosità risulta essere una costante, non varia dunque al variare del gradiente di velocità. I fluidi che seguono questo tipo di comportamento si dicono Newtoniani.
Esiste tuttavia un diverso numero di fluidi, per i quali la viscosità risulta essere dipendente dal valore di $\dot{\gamma}$, detti non-Newtoniani. I fluidi non-Newtoniani possono essere suddivisi in due grosse categorie: fluidi pseudoplastici e fluidi dilatanti. Nei fluidi pseudoplastici la viscosità diminuisce all'aumentare del gradiente di velocità, mentre quelli dilatanti tendono a cristallizzare se sottoposti a sforzo, questo porta ad un aumento della viscosità con il gradiente di velocità.

La viscosità è stata misurata per mezzo del reometro rotazionale RheoStress 6000 utilizzando due diverse configurazioni per le piastre. La prima configurazione usata è la cosiddetta cone-plate. Essa consiste in una piastra piana sulla quale viene posizionato il fluido da testare ed in una sovrastante piastra a geometria conica che permette di ottenere una distribuzione del gradiente di velocità omogenea. Questa configurazione

è stata utilizzata per le cere pure e per le miscele con acido stearico. Per le miscele con presenza di particelle (alluminio e carbon black) si è preferito utilizzare una configurazione plate-plate, ovvero con entrambe le piastre piane. Questo è dovuto al fatto che le particelle presenti nella miscela avrebbero potuto rovinare la piastra conica renendola non più utilizzabile.

I test sono stati condotti prima variando il gradiente di velocità tra $0.001s^{-1}$ e $3300s^{-1}$, a temperatura costante ($120°C$) in modo da individuare il range all'interno del quale il fluido si comporta come Newtoniano. All'interno di questo range è stato quindi scelto un valore del gradiente di velocità al quale eseguire i test per determinare l'andamento della viscosità al variare della temperatura. Questi test sono stati eseguiti tra $190°C$ e $70°C$, l'unica variazione nel range di temperatura si ha per la cera Sasolwax 0907 che, avendo un punto di fusione più elevato, è stata testata tra 190° C e $90°C$.

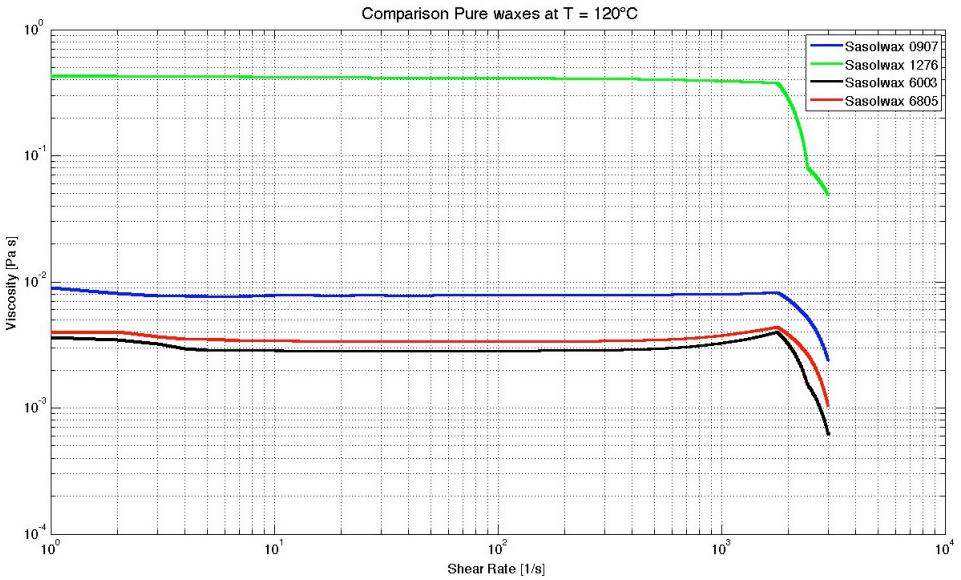

Figura 1: Andamento della viscosità delle cere pure a $T = 120°C$.

Per quanto concerne le cere pure si nota immediatamente che Sasolwax 1276 presenta una viscosità di due ordini di grandezza maggiore rispetto alle altre. Tra le altre è la cera microcristallina 0907 ad avere più alta viscosità, questo è dovuto alla sua struttura molecolare che risulta essere più ramificata rispetto alle altre due cere paraffiniche. Le ramificazioni si oppongono allo scorrimeto del fluido e ciò porta ad un aumento della viscoistà.

Sono stati eseguiti test anche su miscele con additivi. Alcuni valori di viscosità ottenuti sono riportati in tabella 2. In generale l'aggiunta di additivi aumenta i valori di viscosità. Fa eccezione la cera 1276 che con l'aggiunta di acido stearico presenta una viscosità minore rispetto alla cera pura. Un comportamento interessante è quello mostrato dalle miscele in cui è stato aggiunto carbon black. A partire da una percentuale di carbon black di 1.8% la miscela smette di essere Newtoniana e comincia a comportarsi come un fluido pseudoplastico. Questo fenomeno è stato investigato con diversi test su miscele con Sasolwax 0907 e diverse percentuali di carbon black (da 1.5% a 3%).

Miscela	Viscosità [Pa s] a T = 120°C	Differenza percentuale dalla cera pura [%]
0907 pura	0.0078	-
1276 pura	0.4116	-
6003 pura	0.0028	-
6805 pura	0.0034	-
0907 +10%S.A	0.0074	−5.10
1276 +10%S.A	0.3112	−24.39
6003 +10%S.A	0.0032	14.28
6805 +10%S.A	0.0036	5.88
0907 +10%Al	0.0093	19.23
1276 +10%Al	0.4769	15.86
6003 +10%Al	0.0033	17.86
6805 +10%Al	0.0042	23.53
0907 +10%S.A +2%C.B	0.0184	135.90
1276 +10%S.A +2%C.B	0.4397	6.83
6003 +10%S.A +2%C.B	0.0064	128.57
6805 +10%S.A +2%C.B	0.0071	108.82

Tabella 2: Valori di viscosità a $T = 120°C$ e $\dot{\gamma} = 100\ s^{-1}$.

Caratterizzazione balistica

I test di combustione sono stati effettuati presso il DLR Lampoldshausen nel complesso M11. Il banco prova è compoto da una camera di combustione, tre sistemi di alimentazione, un sistema di controllo da remoto e un sitema di registrazione video. La camera di combustione a una sezione di 150x45 mm. L'accensione avvine tramite un sistema di iniezione, posizionato al di sotto di essa, che inizia a bruciare una miscela di ossigeno e idrogeno gassosi. Sui lati della camera di combustione sono presenti due finestre in quarzo che permetto l'ispezione e la registrazione video dei test.
I test sono stati tutti eseguiti a pressione ambiente (1 bar) e a portata in massa di ossidante costante (53 g/s). Come ossidante è stato usato ossigeno gassoso.
Le cere sono state testate sia pure che in una miscela di 88% cera, 10% acido stearico e 2% carbon black.

Al fine di variare il rapporto di miscela due tipologie di slab con diverse dimensioni sono state testate. Gli slab più piccoli hanno dimensioni 100x70x14 mm e con essi si ottiene un valore di O/F che supera il 70. Gli slab più grandi hanno dimensioni 180x90x18 mm e portano ad avere un rapporto di miscela tra 5 e 15.

In generale la velocità di regressione può essere valutata teoricamente utilizzando la formula empirica:

$$\dot{r}_f = a_0 G_{ox}^{n_r} \tag{3}$$

Tuttavia i valori delle costanti a_0 ed n_r trovati in letteratura riguardano geometrie cilindriche. Non è quindi possibile un confrono diretto tra i dati sperimentali qui discussi e i valori teorici in quanto le due geometrie risultano differenti. Nella configurazione con slab infatti i flussi radiativi e convetti sono differenti.

In questo lavoro la velocità di regresione è stata stimata utilizzando il flusso di massa dallo slab alla zona di combustione $\dot{m}_f$ che risulta essere proporzionale alla densità del combustibile ρ_f, alla sua superficie A_s, e appunto alla velocità di regressione $\dot{r}_f$:

$$\dot{m}_f = \rho_f A_s \dot{r}_f \tag{4}$$

Invertendo l'equazione di cui sopra si possono trovare i valori di velocità di regressione mediati su tempo e spazio. Nelle misurazioni sono in oltre presenti alcune incertezze dovute al fatto che parte del combustibile, sciogliendosi, va a posizionarsi sul fondo della camera di combustione e non brucia. Questa parte di combustibile non bruciata è stata, dove possibile, raccolta e tenuta in conto nel calcolo della velocità di regressione.

I risultati dei test condotti confermano che le cere paraffiniche, che hanno viscosità minore, mostrano valori più elevati di velocità di regressione. Inoltre si evince che in generale le miscele con carbon black e acido stearico bruciano in maniera minore rispetto alle cere pure. Questo è dovuto proprio alla presenza di additivi che, nonostante aumentino le proprietà meccaniche del combustibile, provocano un innalzamento della viscosità e quindi diminuiscono l'instabilità dello strato liquido sulla superficie solida del combustibile limitando il fenomeno di entrainment. In figura 2 sono rappresentati i valori medi di velocità di combustione sia per le cere pure che per le miscele. L'unica eccezione risulta essere la miscela a base di Sasolwax 1276 che mostra valori di velocità di regressione maggiori rispetto alla cera pura. Questo è probabilmente dovuto al fatto che l'aggiunta di acido stearico a questo particolare tipo di cera comporta una diminuzione della viscosità e quindi rende più facile l'instabilizzarsi dello strato liquido.

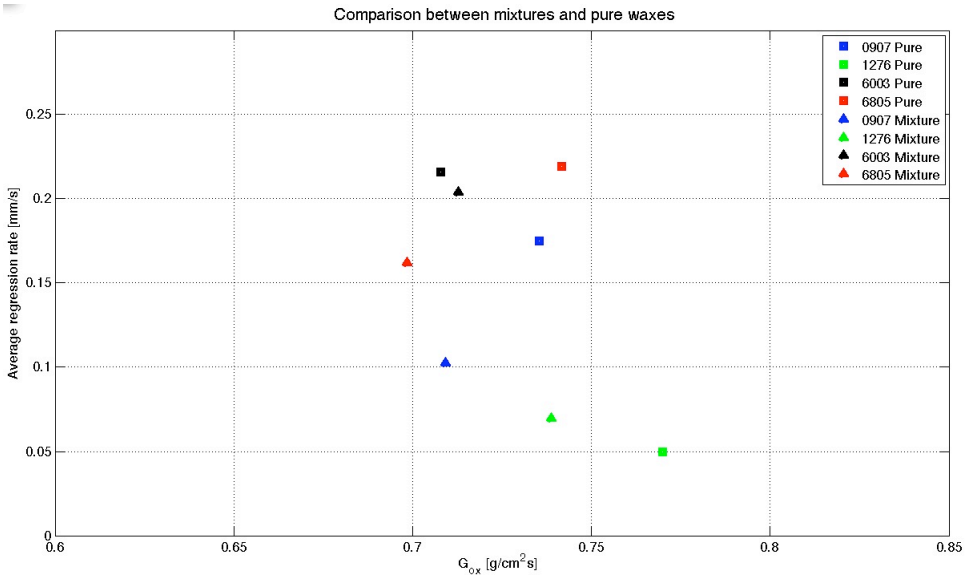

Figura 2: Confronto tra i valori medi di velocità di regressione delle cere pure e delle miscele.

Cambiando il rapporto di miscela inoltre cambia la temperatura in camera di combustione. Simulazioni eseguite con il sofware CEA infatti dimostrano che il rapporto stechiometrico si ottiene attorno a valori di $O/F = 3$, superato il quale la temperatura

in camera di combustione decresce rapidamente. Di conseguenza il calore trasmesso dalla fiamma al grano solido diminuisce e ciò porta ad una diminuzione della velocità di regressione. Questo fenomeno è apprezzabile anche confrontando i valori di velocità di regressione per i due diversi tipi di slab. Gli slab più piccoli, che hanno O/F maggiore, presentano velocità di regressione minori.

I dati ottenuti sono stati confrontati con i risultati di test condotti presso il laboratorio SPLab del Politecnico di Milano. Il confronto purtroppo è stato fatto solo in modo qualitativo in quanto le condizioni operative e le geometrie utilizzate risultano differenti. Si può tuttavia affermare che il comportamento delle diverse cere risulta simile: anche nei dati ottenuti al SPLab le cere paraffiniche risultano essere quelle con la più alta velocità di regressione.

Conclusioni

In questo lavoro sono state analizzate le caratteristiche reologiche di diversi tipi di cera, pura e additivata. Si è notato che la struttura molecolare del materiale influenza pesantemente la viscosità: più le molecole sono ramificate maggiore è la viscosità. La presenza di additivi inoltre cambia significativamente il comportamento del fluido, che arriva in alcuni casi a discostarsi dal classico comportamento newtoniano esibendo un chiaro andamento pseudoplastico.
Sono stati inoltre svolti dei test in camera di combustione che hanno portato ad evidenziare la dipendenza della velocità di regressione dalla viscosità. Questo è dovuto al fatto che una viscosità più bassa porta ad una maggiore instabilità dello strato liquido che dà origine al fenomeno di entrainment.
In futuro sarà necessario svolgere ulteriori test balistici, aumentando il tempo di combustione e variando la pressione e la portata in masa di ossidante, al fine di estendere la conoscenza sui valori di velocità di regressione ottenibili da questo particolare tipo di combustibile. Inoltre andrebbero svolti dei test al fine di determinare le caratteristiche meccaniche delle cere testate, in modo da poter ampliare e completare il databese delle proprietà del materiale.

Chapter 1

Introduction

1.1 Work Motivation

Despite being born in the same time of solid and liquid propellants, hybrid propulsion systems have been the least studied and used for different reasons: economic, political and practical. Recently, thanks to the SpaceShipOne project, the hybrid propulsion returned to world's attention.
In hybrid propellant rockets one component is stored in liquid phase while the second is stored in solid phase.

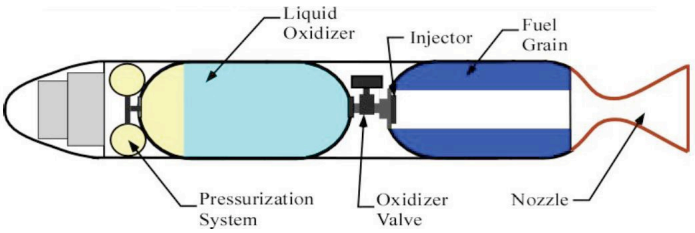

Figure 1.1: General configuration for hybrid rocket systems.

Hybrid propulsion has been of considerable interest in the commercial rocket business and in-space applications. It combines the advantages of solid and liquid propellants. The main advantages are: enhanced safety from explosion or detonation during fabbrication, storage and operation; start-stop-restart compatibilities; relative simplicity wich may translate into low overall system costs compared to liquids; higher specific impulse than solid rocket motors and higher density-specific impulse than liquid bipropellant engines; the ability to smoothly change thrust over a wide range on demand [1].
However hybrid systems have some disadvantages compared to traditional propulsion systems: low combustion efficiency with respect to solids and liquids, in fact due to rough combustion the efficiency of hybrid propellant systems is about 95%; time variation of main parameters governing the engine operations, such as oxidizer to fuel ratio and geometry of grain port; low regression rate values that limit the thrust. It is very difficult to obtain fuel regression rates comparable with the regression rate values of

solid propellants, this brings to a very complex grain geometry with multiple ports to produce the required surface area. Research about hybrid rocket motors and propellants aims to overcome this problem, one of the solution is to use fuels that produce a liquid layer on the burning surface. Under high shear stresses due to oxidizer mass flow, droplets are drawn from the liquid layer to the combustion flow. This phenomenon, called "entrainment" has the primary effect to increase the regression rate of the solid fuel. Paraffin waxes behave in this way and their regression rate will reach values 2-5 times higher than classical hybrid fuels like HTPB.

1.2 Thesis Objectives

Purpose of this work is to characterize rheological behavior and regression rates of different waxes used as hybrid rocket fuels. Since the regression rate is strongly dependent on the viscosity of the melt layer, viscosity of paraffin waxes and microcrystalline waxes, both pure and with some additives, has been measured by means of a rotational rheometer. Results are compared against previous one obtained with a different rheometer set-up in order to provide tabulated values of these new fuels.
Another objective of this work is to experimentally measure the regression rate of the mentioned fuels. Several hot tests have been run at test complex M11 at DLR Lampoldshausen using a 2D combustion chamber with optical access. All tests have been performed at ambient pressure. Results are then compared with values found at SPLab at Politecnico di Milano.
Finally, effect of additives, such as stearic acid and carbon black, is also investigated in order to create an experimental database.

1.3 Presentation Plan

The content of each chapter is briefly summarized below.

Chapter 2

An overview on the hybrid rocket technology is given. Advantages and disadvantages with respect to solid and liquid propulsion are listed. Combustion model and entrainment theory are presented.

Chapter 3

Definition of the key-property viscosity and difference between Newtonian and non-Newtonian fluid are recalled. A sum-up of most used viscous model is given. The measurement technique of viscosity by means of a rheometer is described.

Chapter 4

Role of alkanes in hybrid propulsion and how their properties change with the carbon number are presented. Wax and additives used in this work are described.

Chapter 5

In this chapter the experimental apparatus used to perform viscosity measurements is described. Results and discussion of viscosity measurements and of investigation on

carbon black effect on rheological behavior are shown. Comparison with previous data is also done.

Chapter 6

Description of the test bench used to perform the combustion tests is given. Fuel tested and experimental condition are resumed. Slab manufacturing process is described. Combustion tests results are presented and comparison with SPLab data is done.

Chapter 7

The outcomes of this work are drawn and future work are recommended.

Chapter 2

Review of Hybrid Rocket Systems

2.1 Hybrid propulsion hystory and state of the art

First experiments on hybrid rocket took place in Russia in 1933, Korolev and Tickhonravov developed a rocket, the *GIRD-09*, that had a thrust of 500N and it reached an altitude of 400m. They used liquid oxygen and a mixture of petroleum with collophonium as a propellant [2] [3]. In the end of 30s in Austria Oberth performed tests with liquid oxygen and a tar wood potassium nitrate. Afterwards more tests were performed in Germany between 1937 and 1943. It was used gaseous oxygen as oxidizer and a stack of multi-perforated coal disks as fuel. These tests were unsatisfactory due to the very low regression rate.
The United States started to investigate hybrid rocket in the 40s. Californian Pacific Rocket society performed tests with liquid oxygen and different kinds of fuels [4]. This leads in 1951 to launch a rocket propelled with liquid oxygen and gum that reached ad altitude of $9000m$. The experiment showed that presence of fissures or cracks in fuel grain does not have catastrophic effects.
Studies on hybrid systems kept on in the U.S. after the world war II with the first theoretical model of hybrid combustion by Bartel and Rannie [5]. Between 1951 and 1956 General Electric company studied a configuration with hydrogen peroxyd and polyethylene and they showed the possibility of modulating the thrust by simply controling of oxidizer flow. In 1960 Chemical Systems Division of United Technology Center (CSD/UTC), sponsored by the Navy, conducted a group of foundamentals investigations on internal ballistic and combustion behavior of hybrid motors. These researches led to the formulation of a combustion model by Marxman. Developed assuming a model of diffusive flame placed in a turbulent boundary layer, Marxman theory allowed to evaluate the regression rate.
In the 60s ONERA in France developed and hypergolic combination of nitric acid and metatoluene diamine/nylon. They performed eight launches, reaching an altitude of $10km$. In the same period in Sweden, Volvo Flygmotor also studied hybrid systems using hypergolic combinations. Their rocket reached an altitude of $80km$ in 1969.
In order to satisfy the request of U.S. Air Force of a drone for supersonic flight in the upper atmosphere for more than 5 minutes, United Technologies (CSD/UTC) proposed a *Sandpiper* that used a combination of storable propellant. The missile was larger than the ONERA one and its thrust duration was in excess of 300 seconds, it

was also throttleable. Another U.S. Air Force program requiring an higher payload, led to design the High Altitude Supersonic Target (*HAST*) whose combustion chamber had a larger diameter and the grain port was changed from cylindrical to cruciform. The upgrade of the HAST was the *Firebolt* built in 1980.
In the mid 80s the Challenger disaster and the failure of the Titan III enhanced the concern of the storage and handling of the shuttle solid rocket boosters. Therefore Nasa sponsored studies on using hybrid systems for Shuttle boosters. The new system performances should be at least double than the shuttle boosters' one. There were some problems due to the fact that no ballistic data were available for the propellants, so there was no agreement between the prediction of the four industrial group engaged by NASA.
Motivated by the growing business in commercial satellite, AMROC performed many successful tests with hybrid rocket motor with thrust values between $4.5kN$ and $1.1MN$. There were many difficulties when the motor was scaled up, low regression rate leads to a very complex grain configuraion, with 15 ports. This design caused problems with grain integrity.
In 1995 several industries and government agency started a new program, the Hybrid Propulsion Demostration Program (HPDP), with the aim to develop hybrid propellant boosters.
In 2004 *SpaceShipOne*, a suborbital air-launched spaceplane, completed the first manned private spaceflight winning the Ansari X Prize. Its hybrid rocket motor used HTPB and nitrous oxide (N_2O) as a propellant and it had a four-port grain configuration. The mission planned that the spaceplane was transport to an altitude of 15km by a mothership (*White Knight*) and then it reached $100km$ altitude by an autonomus boost phase. The return into atmosphere was performed by a gliding flight.
SpaceShipTwo, a suborbital, air-launched spaceplane, is currently under development by the Spaceship Company, a join venture between Scaled Composites and Virgin Group. As SpaceShipOne it has an hybrid rocket motor. On 29 April 2013, after nearly three years of unpowered testing, the spacecraft successfully performed its first powered test fligh. Virgin Galactic, a company within the Virgin Group, plans to operate a fleet of five SpaceShipTwo spaceplanes in a private passenger-carrying service, starting in 2014.

Hybrid systems are theoretically usefull for substituting solid rocket boosters. In fact using hybrid technology it is possible to increase the payload and the system is safer. However, with the same total impulse, the hybrid booster should be larger, due to the lower average density. One of the main problems that makes hybrid rocket motors not competitive is the low regression rate that results in a low thrust value. Several research groups are investigating the hybrid field to find a solution to overcome this problem. Stanford University proposes a very interesting solution using the class of liquefying fuels that increases the regression rate through a phenomenon called entrainment.

2.2 Hybrid versus liquid and solid rockets

In hybrid rocket engines the propellant is stored in two different aggregation states, solid and liquid or gaseous. Two main kinds of configurations exist, one with solid fuel and liquid or gaseous oxidizer that is called "direct hybrid", and the other that has liquid fuel and solid oxidizer and it is called "reverse hybrid". Hybrid configuration combines the advantages of solid and liquid propulsion systems: it is safer due to the

separate storage of fuel and oxidizer that can not allow accidental ignition, it enables multiple ingnition and shut down and it permits thrust modulation. It is also simpler and cheaper if compared to a liquid system. From the poin of view of the propulsive performances, hybrid systems are placed between liquid and solid engines. The specific impulse of the hybrids is higher than the one of the solid or monopropellant liquid systems. However it is lower then the specific impulse of the bipropellant liquid system, that can reach a value of specific impulse of about $460s$ with cryogenic propellants. The volumetric specific impulse of hybrid propellants is lower then the solids' one, especially when multi-port grain geometries are requested to increase the regression rate value. Their overall characteristics make hybrid systems suitable for suborbital launchers, upper rocket stages, small satellites and de-orbiting missions.

2.3 Combustion model

As said before, Marxman et al.[6] [7] developed a combustion model for hybrid systems in 60s. The model assumes a turbulent diffusion flame developed in the fluid dynamic boundary layer. The flame takes place where the stoichiometric ratio is reached. The flame gives energy to the solid fuel grain surface both by convective and radiative processes. The fluid gasifies and then it reacts with the oxidizer, substaining the combustion. The convective flux carries the combustion product downstream, they are mixed with oxidizer in the reagion above the flame and with fuel in the region below. The first region extends from the flame to the end of the fluid-dynamic boundary layer, while the second one extends from the regression surface to the flame. The temperature grows from the wall value up to a maximum in correspondence to the flame, then it decreases until it reaches the free stream value. The velocity follows the typical fluid-dynamic trend of the boundary layer, starting for the null value at the wall, up to the free stream value u_e as can be seen in Figure 2.1

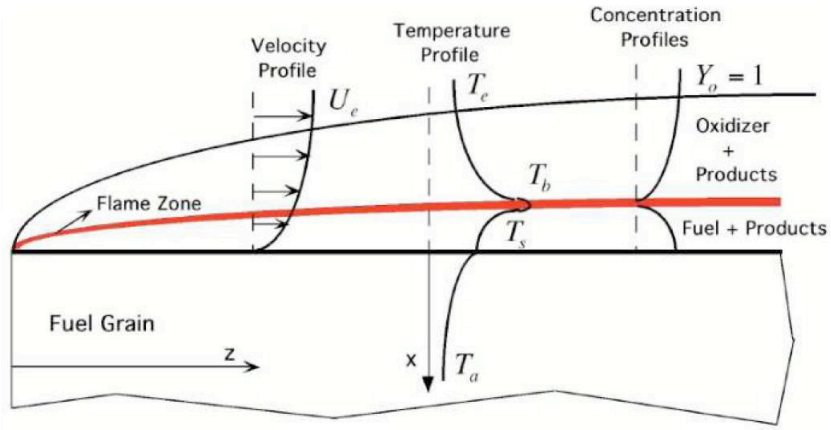

Figure 2.1: Diffusive flame structure.

Neglecting the contribution of radiation and convection in the deepest part of the solid grain, the energy conservation at the regression surface is:

$$\dot{q}_s = \rho_f \dot{r}_f h_f \tag{2.1}$$

Where the ρ_f is the fuel density, $\dot{r}_f$ is the fuel regression velocity and h_f is the entalpy of vaporization of the fuel. $\dot{q}_s$ is the boundary layer heat flux evaluated at the gas side: $\dot{q}_s = k_g \frac{T}{y}|_{y=0}$. Considering the Reynolds analogy, the transfer mechanism of turbulent enthalpy and momentum are similar, the heat flux can be written using the Stanton number C_h:

$$\dot{q}_s = C_h u_e \rho_e \Delta h \tag{2.2}$$

Where u_e and ρ_e are free stream values of velocity and the density of the oxidizer respectively. The enthalpy absorbed in the combustion process Δh is equal to the difference between the enthalpy of the flame zone and the one at the surface of the solid fuel grain. Using the definition of Stanton number that is the ratio between covective heat flux and fluid heat capacity, it can be written in term of Prandtl number Pr and friction coefficiet C_f:

$$C_h = \frac{C_f}{2} Pr^{-\frac{2}{3}} \tag{2.3}$$

Combining the equations 2.1 and 2.2 the regression rate of the solid fuel grain can be calculated:

$$\dot{r}_f = Pr^{-\frac{2}{3}} \frac{C_f}{2} \frac{\Delta h}{h_f} \frac{\rho_e}{\rho_f} u_e \tag{2.4}$$

2.3.1 Blowing

The boundary layer considered is a particular one, in which there is mass injection from the gasification of the solid fuel, this effect is called blowing. This phenomenon causes a reduction of friction coefficient and of heat transfer, called blocking effect. The parameters must be corrected taking into account this phenomenon. The ratio between the friction coefficient under blowing condition and the one without blowing, $\frac{C_f}{C_{f0}}$, was derived by Marxman:

$$\frac{C_f}{C_{f0}} = \left[\frac{\ln(1+B)}{B}\right]^{0.8} \left[\frac{1+1.3B+0.364B^2}{(1+B/2)^2(1+B)}\right]^{0.2} \tag{2.5}$$

Where B is the non-dimensional blowing parameter:

$$B = \frac{1}{C_f/2} \frac{\rho_s v_s}{\rho_e u_e} = \frac{1}{C_f/2} \frac{\dot{m}_f}{G} \tag{2.6}$$

Where $\dot{m}_f$ is the fuel mass flow rate and G is the total mass flux that is the sum of oxidizer mass flux G_{ox} and fuel mass flux G_f. The blowing parameter B shows the importance of the transversal mass flow injected in the boundary layer by the fuel gasification with respect to the free stream value.
In general, for classical hybrid fuels, the blowing parameter is in the range $5 < B < 100$ and the equation 2.5 can be approximated as:

$$\frac{C_f}{C_{f0}} = 1.27 B^{-0.77} \tag{2.7}$$

Considering a turbulent boundary layer ($Pr \cong 1$) and neglecting the radiation effect, the blowing parameter is $B = \frac{\Delta h}{h_f}$ and the friction coefficient without blowing

depends on Reynolds number $\frac{C_{f0}}{2} = 0.029Re^{-0.2}$. So the regression rate in a pure convective/conductive regime becomes:

$$\dot{r}_f = 0.036\frac{G^{0.8}}{\rho_f}\left(\frac{\eta}{x}\right)^{0.2} B^{0.23} \tag{2.8}$$

Where η is the oxidizer dynamic viscosity and the numerical coefficient 0.036 comes from Imperial units. The above formula shows a strong dependence of regression rate on the mass flux G that is typical for hybrid systems. There is also no explicit dependence on pressure and the thermochemical properties of the fuel influence the regression rate through the blowing parameter that is powered 0.23.

Usually, in practical application, to compute the regression rate a simpler formula is used:

$$\dot{r}_f = ax^m G^n = ax^m[G_{ox} + G_f] \tag{2.9}$$

where the constants a, n and m are experimentally found. Due to the dependence of G on the posizion along the grain, the regression rate is not constant in the perforation length. On the other hand, the term related to the boundary layer thickness growth x^m counteracts this effect due to its exponent that is equal to -0.2. The two effects balance each other, so the regression rate results almost uniform. This behavior, experimentally confirmed, allows to use a regression rate formula that is averaged on the length of the perforation:

$$< \dot{r}_f >= aL^m < G >^n \tag{2.10}$$

Where $< G >$ is the mean total mass flux, evaluated as the ratio between the total mass and the mean perforation area, and L is the grain perforation length.
The regression rate formulation written above are in an implicit form, they depend on regression rate itself through the value of G_f. This involve an iterative process that could become very demanding. To overcome this problem, for hybrid motors with prescribed length, a different formula is used:

$$\dot{r}_f = a_0 G_{ox}^{n_r} \tag{2.11}$$

This formulation uses only measurable input parameters and the values of the constant a_0 and n_r must be avaluated through a series of burning tests. The typical value of n_r is between 0.4 and 0.8.

2.3.2 Radiation effect

With the presence of metal additives or when the formulation of fuel is rich in hydrocarbons, the radiative heat transfer becomes important. So the energy balance must be rewritten taking into account the radiation [3]:

$$\dot{q}_s + \dot{q}_{rad} = \rho_f \dot{r}_f h_f \tag{2.12}$$

Where $\dot{q}_{rad}$ is the flame radiative flux absorbed by fuel surface:

$$\dot{q}_{rad} = \sigma\epsilon_s(\epsilon_g T_f^4 - T_s^4) \tag{2.13}$$

Where σ is the Stefan-Boltzmann constant, ϵ_s and T_s are respectively the the emissivity coefficient and the temperature of the solid grain surface, T_f is the flame

temperature and ϵ_g is the emissivity coefficient of the gas phase.
The radiative heating increases the regression velocity but this increase in heating leads also to an increase of the blocking effect that decreases the contribution of the convective heat transfer. To take into account this effect a correction of the blowing parameter is introduced:

$$\frac{B_{rad}}{B} = 1 + \frac{\dot{q}_{rad}}{\dot{q}_{conv}} \left(\frac{B_{rad}}{B} \right)^{0.77} \tag{2.14}$$

And also the regression rate must be corrected as:

$$\frac{\dot{r}_f}{\dot{r}_{f,conv}} = e^{(-0.75 \frac{\dot{q}_{rad}}{\dot{q}_{conv}})} + \frac{\dot{q}_{rad}}{\dot{q}_{conv}} \tag{2.15}$$

or

$$\frac{\dot{r}_f}{\dot{r}_{f,conv}} = e^{(0.37 \frac{\dot{q}_{rad}}{\dot{q}_{conv}})} \tag{2.16}$$

If the radiative heat transfer is comparable with the convective one an increse in the regression rate is achieved, but if the radiative contribution is small with respect to the convective heat transfer, the increase of the radiative heat flux is almost equal to the decrease of the convective one due to the blocking effect. So in the latter case, the theory neglecting the radiative part is still valid.

2.3.3 Pressure effect

In many practical applications, regeression rate is considered independent from pressure. However it has been demostrated that, at low presure, the regression rate shows a dependence on pressure. This dependence increases increasing the mass fluxes [8]. As it can be seen in Figure 2.2, three different regions can be identified: at low mass fluxes the regression rate is independent from pressure and it is dependent on flux with an exponential coefficient of 0.8, predicted by Marxman's model; at high mass fluxes the dependence of the regression rate on the mass flux is reduced but it is strongly influenced by pressure; at intermediate mass flux values the regression rate is influenced from both pressure and mass flux. In the latter region the regression rate follows the relation:

$$\dot{r}_f = \frac{aG^{0.8} b p_c^n}{aG^{0.8} + b p_c^n} \tag{2.17}$$

Where a and n are experimentally found.

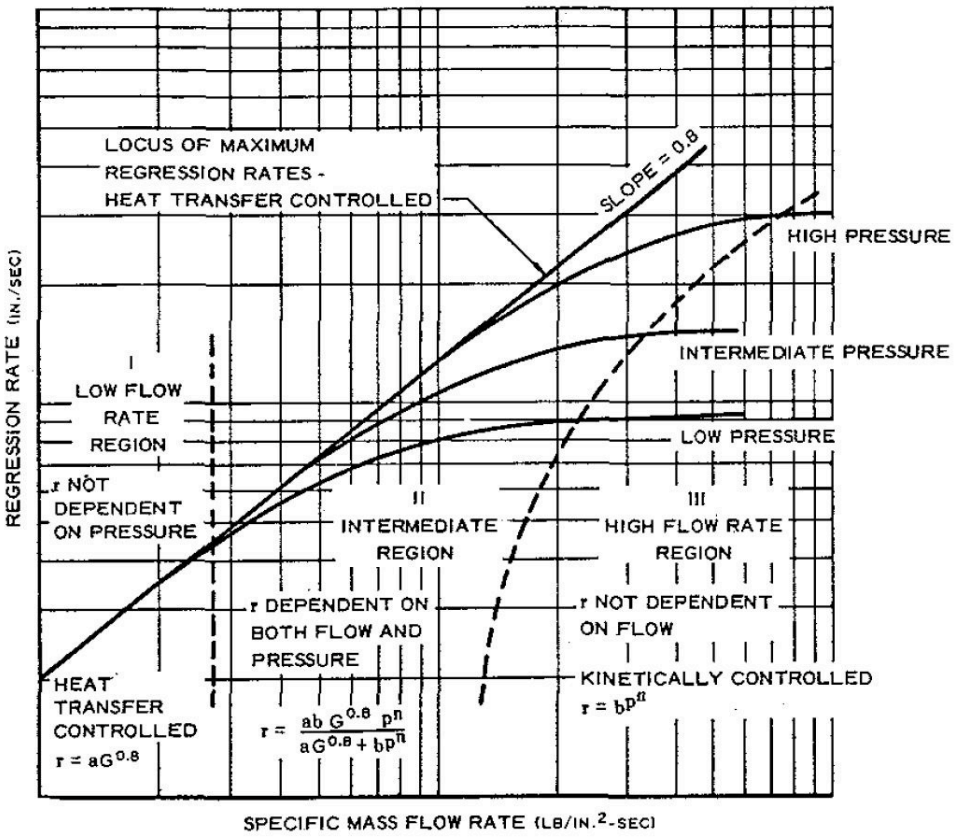

Figure 2.2: Pressure and mass flux dependence of typical hybrid systems.

This behavior is due to the fact that at low pressure the reaction rate is low and the process of combustion tends to the one of a turbulent premixed flame. In this case the characteristic time of reaction becomes greater than the characteristic time of the turbulent transport. Thus the first becomes the limiting factor of the regression rate, while at high pressure faster chemical kinetics lead to an higher reaction rate. The characteristic time of reaction is now lower than the characteristic time of the turbulent transport. So the regression rate becomes higher with increasing temperature.
The regression rate can be evaluated using a new relation that takes into account the pressure effect:

$$\dot{r}_f = a_0 G_{ox}^n p_c^l \tag{2.18}$$

Where $n = 0.4$ and $l = 0.5$ [9] are experimental coefficients. In the regime dominated by chemical kinetics, the regression rate depends on the mass flux weakly than the one given by equation 2.11. At very low mass fluxes the effect of pressure disappears and the effect of radiation may become important. The effect of the pressure on the regression rate is summarized in Figure 2.3

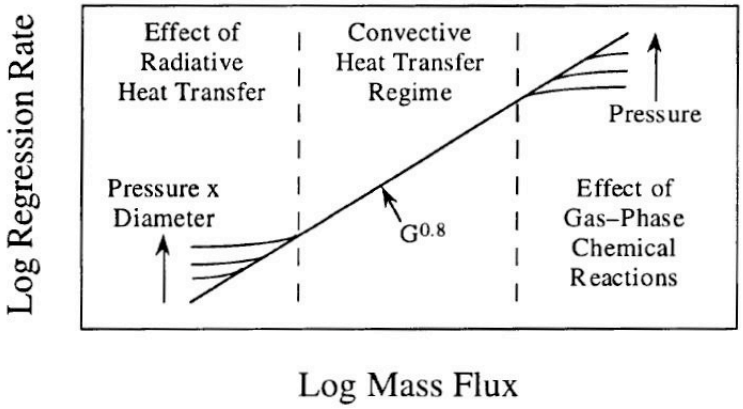

Figure 2.3: Scheme of pressure effect in hybrid combustion process [10].

2.4 Liquefying hybrid fuels

The physical phenomenon of heat and mass transfer from the relatively remote diffusive flame zone to the fuel surface limits the rate of vaporization of the solid fuel grain. This leads to low fuel mass flux, low regression rate that involves low thrust densities with respect to solid systems.
Low regression rate is a key problem on which there has been considerable research. Various methods to solve this problem have been suggested, including the increasing of combustion surface, this lead to a complex multi-port grain geometry that generates a non-uniform burning from port to port, problems in grain structural integrity and big quantities of unburned fuel [11]. Other techniques consist in adding high energy additives, that leads to increase performances only of few percentage [12], or reducing gasification heat flux, but the effectiveness of the method is reduced by the increased blowing surface. One of the best way to increase the regression rate seems to be to use a class of fuels that produces a melting layer on the burning surface. They are called *liquefying fuels*.
First experiments were done using liquid or gasses at standard condition that are frozen to form solid like H_2, liquid amines and hydrocarbons. Some tests on cryogenic fuels were performed by Air Force Research Laboratories (AFRL) and ORBITEC [13]. The same internal ballistic behaviour however is seen in materials that are solid at standard conditions, if they produce a melting layer when burnt. This category includes materials with low viscosity and low surface tension like paraffin-based fuels. In addition to classical gasification these fuels show an additional mass transfer due to the entrainement of liquid droplets from the melt layer. This phenomenon is due to instabilities of the liquid layer subjected to the high shear stress due to the oxidizer flow in the port. In thin film with large Reynolds number non-linear "Roll Waves" are formed, the droplets are drawn from the tips of these waves by the stresses exerted by local gas flow rate as sown in Figure 2.4 [11]. The primary effect of the entrainment mass transfer is to increase the regression rate of the fuel without increasing the thermochemically defined blowing parameter.

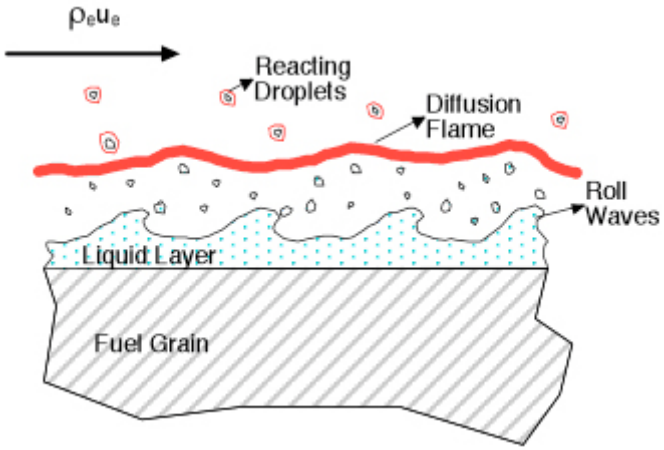

Figure 2.4: Entrainment of droplets in a liquefying fuel

2.4.1 Entrainment

Karabeyoglu et al. [13] [14] developed a mathematical formulation of the entrainment phenomenon. This formulation is an extension of the classical combustion model presented in section 2.3.

Melt layer thickness

The mathematical model considers the liquid layer thickness formed on the solid fuel surface under the actions of both convection and radiation. It depends on the energy transfer balance both in the solid and in the liquid phase (Figure 2.5). The velocity of the liquid-gas interface and the one of the liquid-solid interface are assumed to be equal and constant, so the thickness of the liquid layer is constant. In this way the regression rate of the fuel can be considered to be steady.

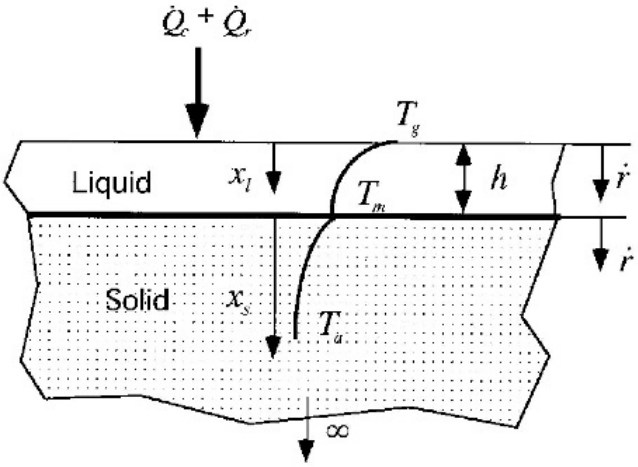

Figure 2.5: Schematic of thermal model used in melt layer thickness estimation.

Also the thermochemical properties of the fuel, both in the solid and liquid phase, are considered constant and the convective effect in the liquid layer is neglected due to the small thickness of the melt layer. The radiative flux field is assumed to be constant and the solid and liquid material are assumed to behave like a grey body, so the absorption coefficient is independent on the frequency of the radiation. Under this hypotesis the radiative energy flux in the liquid and solid phases are respectively:

$$\dot{q}_{rad}(x_l) = \dot{Q}_{rad} e^{-\alpha_l x_l} \tag{2.19}$$

$$\dot{q}_{rad}(x_s) = \dot{q}_r ad(h) e^{-\alpha_s x_s} = \dot{Q}_{rad} e^{-\alpha_l h} e^{-\alpha_s x_s} \tag{2.20}$$

Where $\dot{Q}_{rad}$ is the total collimated radiative flux impinging on the surface, α_l and α_s are the absorption coefficient of liquid and solid phases.
The radiative heating of material at any position can be expressed as the divergence of the radiative flux $\nabla \cdot \mathbf{q}_{rad}$. Considering a one-dimensional radiative flux field the radiative heating in liquid and solid phase becomes:

$$-\frac{dq_{rad}}{dx_l} = \alpha_l \dot{Q}_{rad} e^{-\alpha_l x_l} \tag{2.21}$$

$$-\frac{dq_{rad}}{dx_l} = \alpha_s \dot{Q}_{rad} e^{-\alpha_l h} e^{-\alpha_s x_s} \tag{2.22}$$

It can be shown that the total heating of the fuel by radiation is equal to the radiative heat input:

$$\int_0^h \alpha_l \dot{Q}_{rad} e^{-\alpha_l x_l} dx_l + \int_0^\infty \alpha_s \dot{Q}_{rad} e^{-\alpha_l h} e^{-\alpha_s x_s} dx_s = \dot{Q}_{rad} \tag{2.23}$$

Now the energy equations for the liquid and the solid phases can be written:

$$\frac{d^2T}{dx_l^2} = \frac{1}{\delta_l}\frac{dT}{dx_l} = -\frac{\alpha_l \dot{Q}_{rad}}{\kappa_l \rho_l c_{pl}} e^{-\alpha_l x_l} \tag{2.24}$$

$$\frac{d^2T}{dx_s^2} = \frac{1}{\delta_s}\frac{dT}{dx_s} = -\frac{\alpha_s \dot{Q}_{rad}}{\kappa_s \rho_s c_{ps}} e^{-\alpha_s x_s} \tag{2.25}$$

Where c_{pl} and c_{ps} are the the specific heats of the liquid and solid phases and the characteristic thermal thickness for the two phases are defined respectively as $\delta_l = \frac{\kappa_l \rho_l}{r_f \rho_s}$ and $\delta_s = \frac{\kappa_s}{r_f}$. κ_l, κ_s, ρ_l and ρ_s are the thermal diffusivities and densities of the liquid and solid.
Solutions of the above differential equations can be found considering their boundary conditions: for equation 2.24 $T(0) = T_v$ and $T(h) = T_m$, while for equation 2.25 $T(0) = T_m$ and $T(h) = T_\infty$ as can be seen also in Figure 2.5.
Now the energy balance at the liquid-solid interface can be evaluated, taking into account that the energy transfer from the liquid to the interface must be equal to the heat conducted into the solid from the interface and the energy required for the phase transformation:

$$-\lambda_l \left.\frac{dT}{dx_l}\right|_{x_l=h} + \lambda_s \left.\frac{dT}{dx_s}\right|_{x_s=0} - L_m \rho_s \dot{r}_f = 0 \tag{2.26}$$

In which L_m is the latent heat of melting and λ_l and λ_s are the thermal conductivities of liquid and solid.
The energy balance at the liquid-gas interface can also be written in the analogous way:

$$\dot{Q}_{conv} + \lambda_l \frac{dT}{dx_l}\bigg|_{x_l=0} - L_v \rho_s \dot{r}_v = 0 \tag{2.27}$$

In which it is that the convective heat transfer from the gas to the interface must be equal to the conductive heat transfer into the liquid and the heat required for the phase transformation. L_v is the latent heat of vaporization and $\dot{r}_v$ is the evaporative contribution to total regression rate. In equation 2.27 the possibility of entrainment mass transfer from the liquid surface, other than the mass transfer by vaporization, is allowed. Combining this equation with equation 2.26 it can be found that the total energy transferred from the wall ($\dot{Q}_w$) must be equal to the total energy absorbed in the fuel grain, that is composed by the total energy required to heat the liquid and the solid phases and the energy needed for the phase transformation:

$$\dot{Q}_w = \dot{Q}_{conv} + \dot{Q}_{rad} = h_e \rho_s \dot{r}_f + L_v \rho_s \dot{r}_v \tag{2.28}$$

Where h_e is the total heat of entrainment. Using the above formula the heat of gasification can be defined as:

$$h_v = \frac{\dot{Q}_w}{\rho_s r_f} = c_{pl}\Delta T_1 + c_{ps}\Delta T_2 + L_m + L_v \frac{\dot{r}_v}{\dot{r}_f} \tag{2.29}$$

With $\Delta T_1 = T_v - T_m$ and $\Delta T_2 = T_m - T_a$ (T_a is the ambient temperature of the solid fuel grain). The equation found for h_v is different from the classical one found in literature because the heat required to vaporize the material transported by means of entrainment is zero.
From equation 2.26, inserting known temperature derivatives, and combining it with equation 2.29, a non-linear equation for the thickness parameter $\phi = e^{\frac{-h}{\delta_l}}$ can be written as follows:

$$\phi = \frac{h_m(R_l - 1) + h_v(\dot{Q}_{rad}/\dot{Q}_w)\phi^{R_l}}{h_e(R_l - 1) + h_v(\dot{Q}_{rad}/\dot{Q}_w)} \tag{2.30}$$

In which $R_l = \alpha_l \delta_l$ is the ratio of the thermal thickness to the radiative penetration thickness in the liquid layer.
A general solution for the algebraic non-linear equation 2.30 can not be achieved. So it is preffered to focus on two limitig cases of practical interest:

- $R_l >> 1$: in this case the absorption of the radiation in the liquid layer is large, so all the radiative heat is absorbed at the liquid-gas interface. The thickness of the melted layer becomes:

$$h = \delta_l \ln\left(1 + \frac{C_l \Delta T_1}{h_m}\right) \tag{2.31}$$

  This is the case of fuel loaded with strongly absorbing material like carbon black.

- $R_l << 1$: this case represents the one in wich the absorption of the radiation in the liquid layer is small, so all the radiative heat is absorbed by the solid. The melted layer thickness becomes:

$$h = \delta_l \ln\left(1 + \frac{C_l \Delta T_1}{h_m - h_v(\dot{Q}_r/\dot{Q}_w)}\right) \tag{2.32}$$

  In this case the dependence of the thickness on the regression rate is explicit, in fact $h_v = f(\dot{r}_v/\dot{r})$.

It is important to notice that in both cases the melt layer thickness is proportional to the characteristic thermal length of the liquid δ_l and inversely proportional to the regression rate.
Also an increase in ambient temperature results in an increase of the melt layer thickness. The maximum thickness is reached when the ambiet temperature is equal to the melting temperature.

Liquid layer stability

Karabeyoglu et al. [13] demostrates that the instability of the liquid layer is essential for the formation of entraiment droplets. Under strong blowing conditions the liquid film is unstable in large range of parameters. Empirical relations for the entrainment are developed using some experimental data. It is found that the entrainment mass transfer per unit area $\dot{m}_{ent}$ is proportional to the liquid mass flow rate per unit width of the liquid $\dot{m}_l$:

$$\dot{m}_{ent} = 13.3 e_0(X_e)\dot{m}_l \tag{2.33}$$

$e_0(X_e)$ is an non-dimensional proportionality function formulated in terms of dynamic pressure of the gas flow P_d, surface tension σ and the ratio between the gas temperature T_g and the temperature of vaporization T_v:

$$X_e = \frac{P_d^{0.5}}{\sigma(T_g/T_v)^0.25} \tag{2.34}$$

$$e_0(X_e) = 1 + e^{-1.06\cdot 10^{-4}(X_e - 2109)} \tag{2.35}$$

Taking into account the theory and the experimental results, they suggested a relation for the entrainment rate of liquid droplets in terms of the relevant properties of hybrid motors:

$$\dot{m}_{ent} \propto \frac{P_d^{\alpha} h^{\beta}}{\eta_l^{\gamma} \sigma^{\pi}} \tag{2.36}$$

Where α, β, γ and π are experimental parameters. Literature values for the exponents are shown in table 2.1
The equation for $\dot{m}_{ent}$ shows that viscosity and surface tension of the melt layer play an important role on the formation of entrainment mass transfer: decreasing viscosity and surface tension, increasing the entrainment.

Reference	α	β	γ	π
Gater and L' Ecuyer [15]	1.5	2	1	1
Nigmatulin et al. [16]	1	1	-	-
Karabeyoglu [13]	1-1.5	-	$> \pi$	$< \gamma$

Table 2.1: Entrainment exponent values from literature.

2.4.2 Extended hybrid theory

The classical Marxman's theory for hybrid boundary layer combustion has been modified, including the entrainment phenomenon. It leads to three major variation in the classical theory:

- The effective heat of gasification is reduced, due to the fact that the evaporation energy required for the fuel mass transfer from the surface is partially avoided by the entrainment of the liquid. The enthalpy difference between the flame and the surface is also reduced due to the fact that some of the reactants are now in liquid phase. In this way the ratio between the enthalpy differece and the effective heat of gasification $\frac{\Delta h}{h_v}$ is changed.
- The presence of two-phase flow causes an alteration in the blocking factor $\frac{C_h}{C_{h0}}$. It can now be expressed as a function of the evaporization blowing parameter: $\frac{C_h}{C_{h0}} = f(B_v)$
- The ripples formed on the liquid layer surface increase the surface roughness and the heat transfer from the flame front to the surface.

The total regression rate can be written as the sum of evaporation regression rate $\dot{r}_v$, caused by the vaporization of the liquid, and the contribution due to the entrainment that is related to the mass transfer from the liquid surface:

$$\dot{r}_f = \dot{r}_v + \dot{r}_{ent} \tag{2.37}$$

The entrainment regression rate con be written in terms of mass flux G in the port and total regression rate $\dot{r}$:

$$\dot{r}_{ent} = a_{ent} \frac{G^{2\alpha}}{r^{\beta}} \tag{2.38}$$

Where a_{ent} is the entrainment parameter and it depends on the properties of the selected propellant. Equations 2.37 and 2.38 with the energy balance at the liquid-gas interface and the correction of the blocking factor, form a non-linear set of equation that can be solved to find the total regression rate as a function of mass flux and axial location.

The entrainment term produces a great enhancement in the total regression rate value, giving values of total regression rate $3 \div 5$ times higher than HTPB.

Chapter 3

Viscosity Models and Measurement Methods

Viscosity describes the physical property of a fluid to resist shear induced flows. Except for the super-fluids, all other fluids are viscous. A fluid that has no resistence to shear stress is an ideal or inviscid fuel.
Viscosity is a function of different parameters. It depends on chemical properties of the fluid and on its temperature and shear rate. Generally, increasing temperature the viscosity decreases. It could depend also on pressure, shear history and on electrical field.

The behavior of an ideal fluid under the influence of stresses is described by Isaac Newton's law of viscometry, that links the shear stress τ and the shear rate $\dot{\gamma}$:

$$\tau = \eta \cdot \dot{\gamma} \tag{3.1}$$

where η is the *dynamic viscosity* of the fluid.
The shear stress is defined as the ratio between the force tangentially applied and the area of material wich is parallel to the applied force vector, $\tau = \frac{F}{A}$. It is generally measured in Pascal (Pa). The shear rate represents the speed drop across the gap size $\dot{\gamma} = \frac{dv}{dy}$ and it is measured in s^{-1}. The dynamic viscosity is typically measured in Pascal-second ($Pa \cdot s$) in the S.I. unit.
The *kinematic viscosity* instead is defined as the ratio between the dynamic viscosity η and the density of the fluid ρ. It is typically measured in S.I. unit with m^2/s.

Newton's constitutive equation is the simplest equation that can be used for viscous liquids. Newton's law is an approximation that holds some materials and fails in others. In general it describes the rheological behavior of low molecular weight liquids and even high polymers at very slow rates of deformation. However viscosity can be a strong function of the rate of deformation for polymeric liquids, emulsions and concentrated suspensions.

3.1 Newtonian and non-Newtonian fluids

A fluid is said to be *Newtonian* if the shear stress is proportional to the shear rate. In other words, the voscosity of a Newtonian fluid is constant (Figure 3.2) so it does

not depend on the velocity gradient. Due to the linear relation between the shear stress and the velocity gradient, the true viscosity and the apparent viscosity are the same. In this case the viscosity can be defined as the tangent of the slope angle of the flow curve $\tau - \dot{\gamma}$.

A *non-Newtonian* fluid is a fluid whose flow behavior departs from that of a Newtonian fluid, so that the rate of shear is not proportional to the corrisponding stress. Usually the viscosity of a non-Newtonian fluid depends on shear rate or shear rate history.
Generally the relation between shear rate and shear sress in non-Newtonian fluids is not linear and it could be time-dependent, therefore a constant coefficient of viscosity can not be defined. Different viscosity values with different velocity gradients can be defined, as can be seen in Figure 3.1 [17].

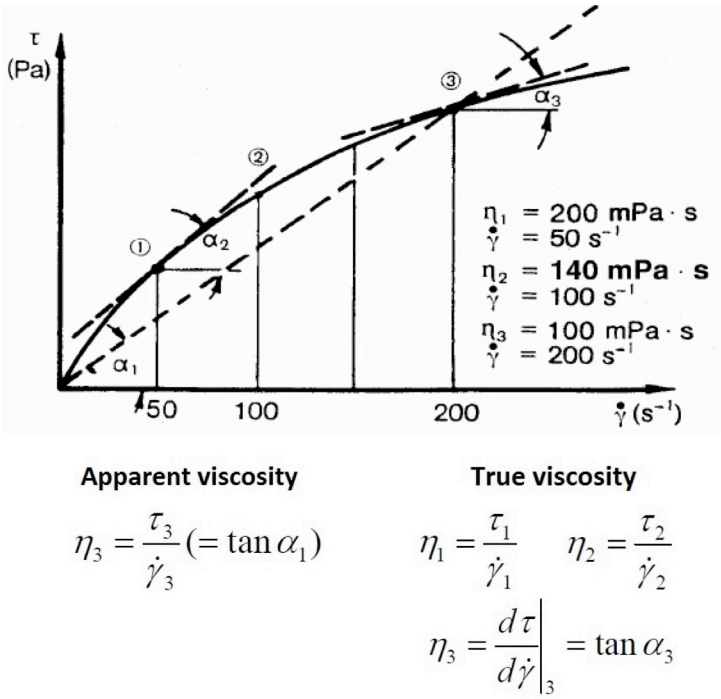

Figure 3.1: Example of true viscosity and apparent viscosity.

Non-Newtonian fluids can be classified as *Shear Thinning* or *Shear Thickening*. The general behavior of viscosity of shear thinning and shear thickening fluids with respect to shear rate is shown in Figure 3.2, while in Figure 3.3 the behavior of those kind of fluids is shown in term of shear stress with respect to shear rate.

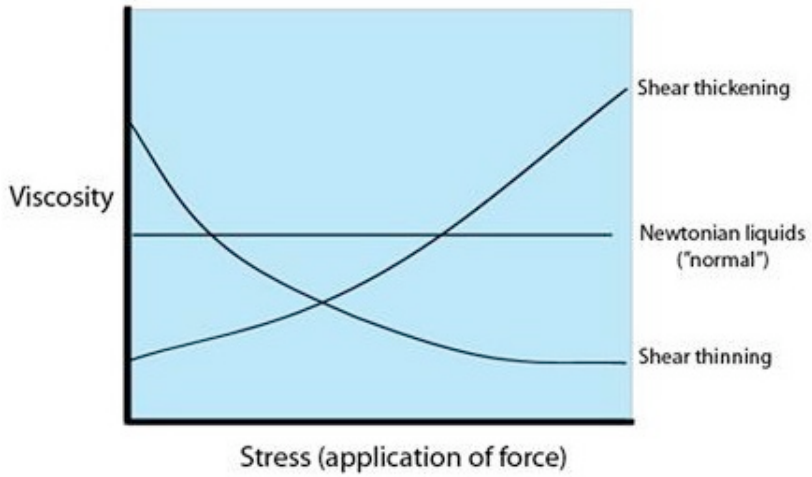

Figure 3.2: Viscosity vs shear rate for Newtonian, shear thinning and shear thickening fluids.

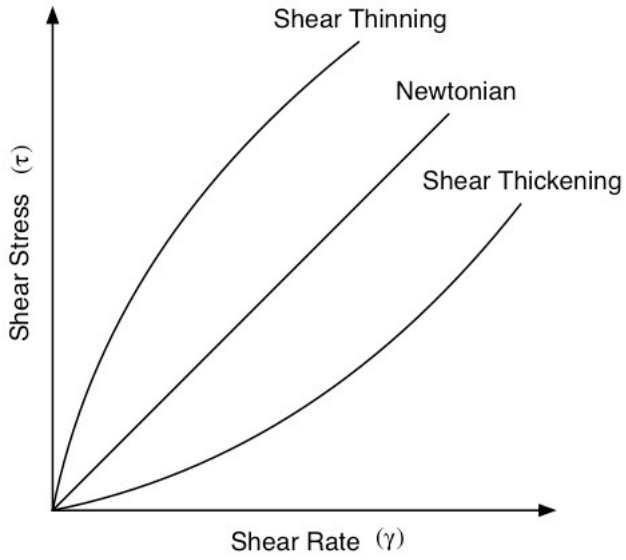

Figure 3.3: Shear stress vs shear rate for Newtonian, shear thinning and shear thickening fluids.

In shear thinning fluids the viscosity decreases increasing the shear rate. This is a non-linear phenomenon that is especially pronounced in polymer melts and in concentrated polymer solutions.

Shear thickening behavior shows an increase of the the viscosity increasing the shear rate. this is due to the fact that the system crystallizes if a stress is applied, and it behaves more alike a solid than a solution.

Some non-newtonian fluids have a time-dependent viscosity behavior. They could

be thixiotropic or rheopectic fluids. The first type shows shear thinning properties, it is very viscous under static conditions but it flows over time when shaken, agitated, or otherwise stressed. The longer the fluid undergoes the shear stress, the lower is its viscosity. Rheopectic fluids have the opposite behavior, they show a time-dependent increase in viscosity. They become more viscous or solidify when shaken. The longer the fluid undergoes the shearing force, the higher is its viscosity. Another type of non-Newtonian fluid is the so called Bingham plastic. This kind of material behaves like a rigid body if the stress applied is under the yield stress, above that the material flows with a nearly Newtonian behavior.

3.1.1 Viscous models

To describe the viscosity behavior of non-Newtonian fluids, a large number of models that depend on rate of deformation have been developed. Here few of them are presented.

Power law

The power law is the most used form of the general viscous consitutive law. For a steady shear the power law is:

$$\eta = m\dot{\gamma}^{k-1} \tag{3.2}$$

Where m and k are two constants experimentally determined. In general m is a function of temperature and, for shear thinning behavior $k < 1$, while for shear thickening materials $k > 1$. In the processing range of many polymeric liquids and dispersions, the power law is a good approximation to the data from viscosity versus shear rate. For high shear rate the power law fits data well but it fails to describe the low shear rate region.

Cross model

It is observed that viscosity becomes nearly newtonian at very high shear rate for many suspensions and dilute polymer solutions. Cross model has been developed to give newtonian regions both at high and low shear rate:

$$(\eta - \eta_\infty) \simeq (\eta_0 - \eta_\infty) m\dot{\gamma}^{k-1} \tag{3.3}$$

at very high shear rates the right-hand side term becomes very small and the viscosity goes to a high shear rate newtonian limit [18].

Plastic model

This model can describe Bingham plastic materials, in which there is no motion under the yield stress τ_y, and above this value the material starts flow as a Newtonian fluid:

$$\begin{cases} \dot{\gamma} = 0 & \text{for } \tau < \tau_y \\ \tau = \eta\dot{\gamma} + \tau_y & \text{for } \tau \geq \tau_y \end{cases} \tag{3.4}$$

3.2 Measurement methods

Common materials have very large viscosity range, for this reason different instruments are required to mesure over this range. The most versatile device used to measure viscosity is the rheometer. Two kind of rheometer are aveilable: rotational rheometer that controls the applied shear stress or shear strain, and the extensional rheometer which applies extensional stress or extensional strain.
Extensional rheometers development encountered some difficulties due to the problems associeted with generating an homogeneous extensional flow. They are commonly used with materials that are subjected to a tensile deformation. In this work extensional rheometers will not be used, only the rotational rheometers will be considered.

3.2.1 Rotational Rheometer

The first practical rotational rheometer was a concentric cylinder instrument made by Maurice Couette in 1890. The same design concept is used by a lot of today's instruments. In this kind of device the fluid is placed within the annulus of two concentric cyliders, one cylinder rotates at a set and known speed. The fluid drags the other cylinder round, and it exerts a torque on the cylinder that can be measured and converted in a shear stress. It has some advantages thanks to the fact that the shear rate is nearly constant for large radii and it is ideally suitable for pourable liquids. However it needs a large sample volume (typically between 3 and 30 g) and there is no way to load high viscosity polymer melts [19].

In other types of rheometers, known as capillary rheometers, the liquid is forced through a tube of constant cross-section and precisely known dimensions, under conditions of laminar flow. Pressure is generated on the fluid by gravity, compressed gas or a piston. Either the flow-rate or the pressure drop is fixed and the other is measured. Knowing the dimensions, the flow-rate can be converted into a value of shear rate and the pressure drop into a value of shear stress. Varying one of these two parameters, the flow curve can be determined. For non-Newtonian fluids that have shear thinning or shear thickening behavior the pressure drop versus flow rate is not linear and data must be analyzed with Weissenberg-Rabinowitch-Mooney equation.

Another kind of rotational rheometer is cone and plate geometry. This kind of geometry is probably the most popular rotational geometry to study non-Newtonian effects. The fluid is placed in an horizontal gap between a plate and a shallow cone. The cone is rotated and the resistence to rotation caused by the fluid is mesured. this kind of geometry is easy to load and clean, its shear rate distribution is uniform and it requires a small sample size.

The parallel disk rheometer is similar to the cone-plate one, it has two plates instead of one cone and one plate and it works in the same way. However in cotrast to cone and plate, in this case the flow between parallel disks is not homogeneous [18].

Most devices are designed to allow the use of both plates geometries as the one used at DLR to perform viscosity tests.

3.2.2 Plate selection

Different kind of plates are available to perform the tests, all plates range of application are given in the Instruction Manual of the Rheometer.

Parallel Plate Starting from the equation of motion and assuming a steady, laminar and isothermal flow, negligible body effect, cylindrical edge and considering the upper disk rotating at Ω and the lower one steady, the tangential velocity v_θ depends on the disk radius r and vertical position z:

$$v_\theta(r, z) = \frac{r\Omega z}{h} \tag{3.5}$$

where h is the thickness of the sampling material that fills the gap between the two plates.
And thus the shear rate $\dot{\gamma}$:

$$\dot{\gamma}(r) = \frac{r\Omega}{h} \tag{3.6}$$

It is noticeable that the shear rate depends on the radial position and in this way the flow between the parallel plates is not homogeneous.

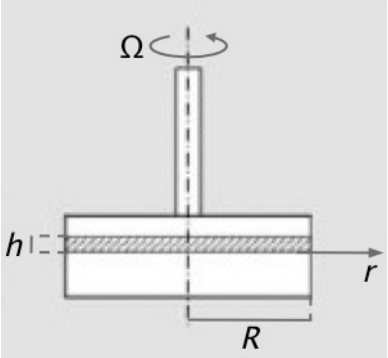

Figure 3.4: Scheme of parallel-plate sensor system.

Cone Plate Assuming a steady laminar and isothermal flow, spherical liquid boundary, neglecting the body affect and considering the upper plate rotating at Ω, the velocity profile can be approximated as:

$$v_\theta = \Omega r \frac{(\pi/2) - \theta}{\beta} \tag{3.7}$$

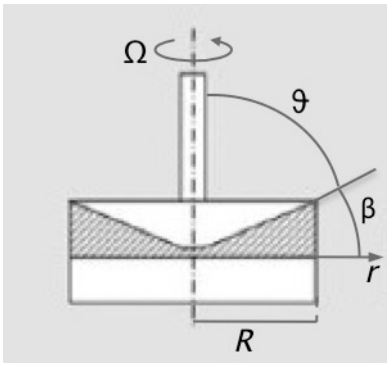

Figure 3.5: Scheme of cone-plate sensor system.

In the formulation of velocity $\beta < 6°$.
The shear rate results:

$$\dot{\gamma} = \frac{\Omega}{\beta}\left(1 + \beta^2 + \frac{\beta^4}{3}\right) \approx \frac{\Omega}{\beta} \tag{3.8}$$

In this case the shear rate does not depend on the position and so the flow between the two plates can be considered homogeneous.

Chapter 4

Paraffin wax

Paraffin wax is a mixture of normal alkanes with general formula C_nH_{2n+2}. Its molecules contain long carbon chains with more than 20 carbon atoms ($n > 20$). It is characterized by low melting point, between 46°C and 68°C, variable oil content, and density of about 900 kg/m^3. It is a white, oderless, tasteless waxy solid at room temperature and it is not soluble in water but soluble in ether, benzene, and certain esters. Paraffin is unaffected by most common chemical reagents but it burns readily.

4.1 Normal alkanes as hybrid rocket fuels

The homologous series of normal alkanes are a group of fully saturated, sraight chain hydrocarbons. Each member of the series is identified by the carbon number n, that ranges from 1 (methane) to very large numbers as for the High Density Polyethylene (HDPE). A large fraction of liquefying hybrid fuels is composed by pure normal alkanes, as pentane, or mixture of n-alkanes, as paraffin waxes. In fact their high heat of combustion, low cost, availability and chemical inertness characteristics make n-alkanes ideal fules for combustion systems.

The relations to predict and determine the properties of alkanes are presented by Marano and Holder [20]. These asymptotic behavior correlations (ABCs) allow the properties of higher carbon-number homologs to be estimated by extrapolation from known property values of their lower carbon-number relatives. The general formula for an ABC is:

$$Y = Y_\infty - \Delta Y_0 \exp(-\beta(n \pm n_0)^\gamma) \tag{4.1}$$

$$Y_\infty = Y_{\infty,0} + \Delta Y_\infty (n - n_0) \tag{4.2}$$

Where n is the carbon number, Y represents the general property value and the subscriptions ∞ and 0 are for the carbon number approaches to infinity and for effective carbon number of zero respectively.
Two kinds of properties have been indentified: type I and type II properties. Type I properties approach a finite value for large carbon numbers. Normal melting and boiling points and mass-based properties belong to this category. The limit for type II properties is instead linear with carbon number, the properties that show this kind

of behavior are for example molar volume, enthalpy, entropy and related properties of state.
Considering the equations 4.1 and 4.2 for type I properties, Y_∞ is a constant, so $\Delta Y_\infty = 0$ and $\Delta Y_0 = Y_\infty - Y_0$. There are then five adjustable parameters: n_0, Y_0, Y_∞, β and γ. For type II properties there are six adjustable parameters: n_0, ΔY_0, ΔY_∞, $Y_{\infty,0}$, β and γ. This is due to the fact that the asymptote Y_∞ is linear with carbon number n. These adjustable parameters are determined by minimizing the error between the predicted and reported values of the property studied.

It is interesting to notice the behavior of critical properties. In general in a system containing liquid and gaseous phases, it exists a special combination of pressure and temperature, the so-called critical point, at which the transition between liquid and gas becomes a second-order transition. In the subcritical phase the surface temperature is determined by a physical process controlled by the phase change, while in the supercritical phase the process depends on pyrolysis.
For n-alkanes the critical pressure decreases with increasing carbon number (Figure 4.1). In fact critical pressure is a type I property and the limit for an infinite carbon number is predicted to be zero [21]. This means that most hybrid systems using paraffin-based fuels are operating in the supercritical regime [22].
Also the critical temperature is a type I property, but it increases monotonically increasing molecular weight and the limit for infinite carbon number is $1020.7K$ (Figure 4.2).

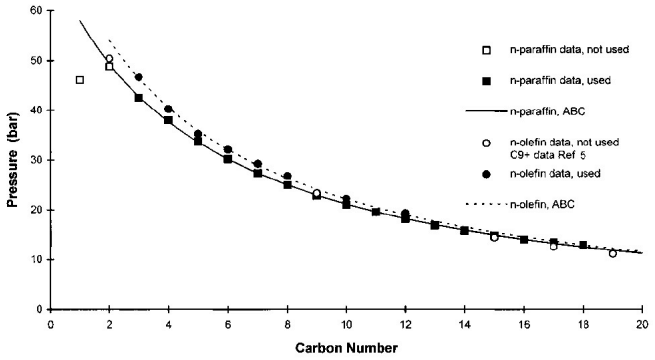

Figure 4.1: Critical pressure as function of carbon number.

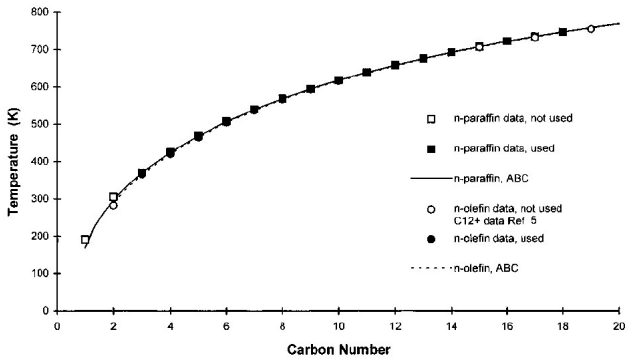

Figure 4.2: Critical temperature as function of carbon number.

One of the most important parameter that influences the regression rate of a liquefying hybrid fuel is the viscosity. Using the ABC method the viscosity can be calculated using the relations:

$$Y = Y_{\infty,0} - \Delta Y_{\infty}(n - n_0) - \Delta Y_0 \exp(-\beta(n - n_0)^{\gamma}) \tag{4.3}$$

$$\Delta Y_0 = A_0 + \frac{B_0}{T} + C_0 \ln T + D_0 T^2 + \frac{E_0}{T^2} \tag{4.4}$$

$$\Delta Y_{\infty} = A_{\infty} + \frac{B_{\infty}}{T} + C_{\infty} \ln T + D_{\infty} T^2 + \frac{E_{\infty}}{T^2} \tag{4.5}$$

and

$$\eta_l = \exp(Y) \tag{4.6}$$

Since the logarithm of viscosity is a type II property, it is expected that the property is linear with the carbon number for high value of n. However it is demostrated that there is a critical carbon number at which a transition occurs in polymer melts behavior. The critical carbon number is identified to be 286. Below the critical carbon number the solutions show the typical Newtonian behavior, while above the critical carbon number a shear thinning behavior is shown. This transition can be explained with chain entanglement. Increasing the carbon number, the molecules become more and more entwined. This means that a long range motion requires cooperative motion of other molecules, increasing viscosity. The transition occurs due to a changing in the mechanism of viscous transport: below the critical carbon number bulk flow is mostly due to the motion of individual molecules, above it is due predominantly to entangled chains motion [23].

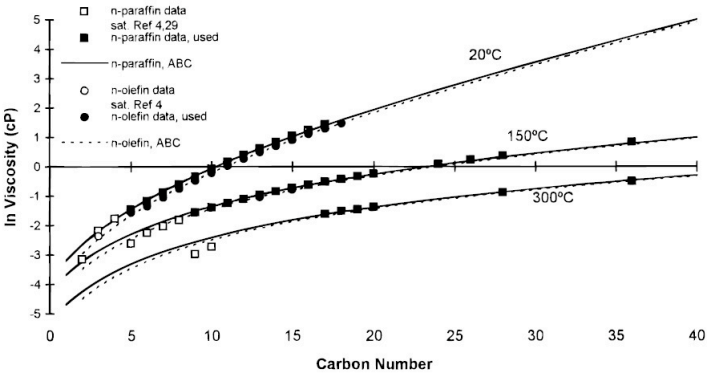

Figure 4.3: Viscosity as function of carbon number.

This method is inaccurate for carbon number lower than 11. The accuracy reduces also with increasing the molecular weight for carbon number larger than 70. It exists another method to evaluate the viscosity of compounds with large n-alkanes molecules at a specified temperature T. This method has been reported by Bicerano [24] and it predicts a critical molecular weight of 3552.5 g/mol that corresponds to a carbon number of 254. At this carbon number the viscosity behavior with increasing carbon number changes dramatically. This is due to the extra restrictions on the molecular

motion induced by the entanglement of long molecules. The rate of viscosity increases with decreasing carbon number above the entanglement molecular weight. The liquid also shows a shear thinning behavior.

4.1.1 Mixtures of n-alkanes

Many paraffinic fuel systems are not composed by only one type of n-alkane molecules, they are usually a mixture of straight chain molecules. The estimation of the properties of a mixture of n-alkanes is very complex. It requires the knowledge of the details of the molecular weight distribution, which is not readly available for most materials. This problem can be overcome by evaluating the material properties at the number averaged carbon number (n).
It will become important at this point the concept of polydispersity (PD) which is defined as the ratio of the weight averaged carbon number to the number averaged carbon number. In general it represents the broadness of the molecular weight distribution in the mixture. For a pure n-alkane $PD = 1$ and it increases as the distribution of the molecular weight in the mixture becomes wider. Only two quantities are now adequate to describe a mixture: PD and n.

For an accurate estimation of the regresion rate, it is important to evaluate the material properties at a representative temperature for the layer. To do this three temperatures must be identified: ambient temperature, melting temperature and surface temperature.

Ambient temperature is the bulk temperature of the solid fuel grain. The selection of the ambient temperature is somewhat arbitrary, in general as long as the melting temperature is higher than $298K$, setting the ambient temperature at $298K$ is a reasonable selection.

Melting temperature can be estimated with the ABC method as:

$$Y = Y_\infty - (Y_\infty - Y_0)\exp(-\beta(n - n_0)^\gamma) \tag{4.7}$$

With $T_m = Y$. Melting temperature behaves like a type I property and the value for $T_{m\infty}$ predicted by the ABC method is 144.9°C [21].

Surface temperature determines the effective melt layer temperature at wich the fuel properties should be evaluated. Most important properties to be evaluated are the viscosity and the density of the fuel. These are key-properties for the entrainment phenomenon due to the fact that they rule the liquid layer stability. If the partial pressure of the fuel is less than the critical pressure, the surface temperature is determined by the evaporation process. This behavior is expected for fuels with high critical pressure or for moderate carbon numbered fuels if the chamber pressure is very low.
If the partial pressure at the surface is larger than the critical pressure, there is no thermodynamic distinction between the liquid and the gas phases. The surface temperature is now defined as the temperature for which an arbitrary ammount of fuel is thermally decomposed into smaller molecules.

To evaluate the surface temperature in the first case, it can be used the concept of the *kinetic theory*. As said before, if the partial pressure of the vapor is less than the critical pressure of the fuel, the surface temperature will be determined by the evaporation process. A formula for the surface temperature in terms of the properties of the fuel and operational parameters of the motor could be derived in this case [22]. However it is not of interest for this work because fuel systems with high carbon numebers will operate in the supercritical regime for which the surface temperature is

not determined by the evaporation process. Therefore for carbon numbers higher than 20, as for the paraffin waxes, the surface temperature prediction is not significant.

In the supercritical case, assuming that the relevant surface phenomenon is governed by pyrolysis, a *thermal analysis* should be carried out to determine the surface temperature. In this case the fuel slab can be divided into three zones: pyrolysis zone, liquid zone and solid zone. In the solid and liquid zones there are no reactions. The pyrolysis zone is a thin layer next to the surface in which the pyrolysis reactions take place. The temperature varies from the temperature at which the pyrolysis starts to the surface temperature. Due to the thermal cracking of the n-alkanes molecules, the mass fraction of the fuel reduces from one to a low value. If the activation energies are high, the radiation zone will be small. The radiative term can be also neglected in the two extreme cases of very large and very small absorbivity. The discussion of the thermal analysis and its analytical results are presented by Karabeyoglu et al. [22]. It is found out that for a fixed regression rate value, the surface temperature increases slightly with decreasing fuel mass fraction at the surface.

In the same article results of motor tests to evaluate the regression rate are presented. They tested two different polyethylene waxes, one paraffin wax and HDPE. All formulations have the same flux exponent and the regression rate is only determined by the mass flux coefficient. The paraffin wax burns more than 5 times faster than the HDPE as can be seen in Figure 4.4.

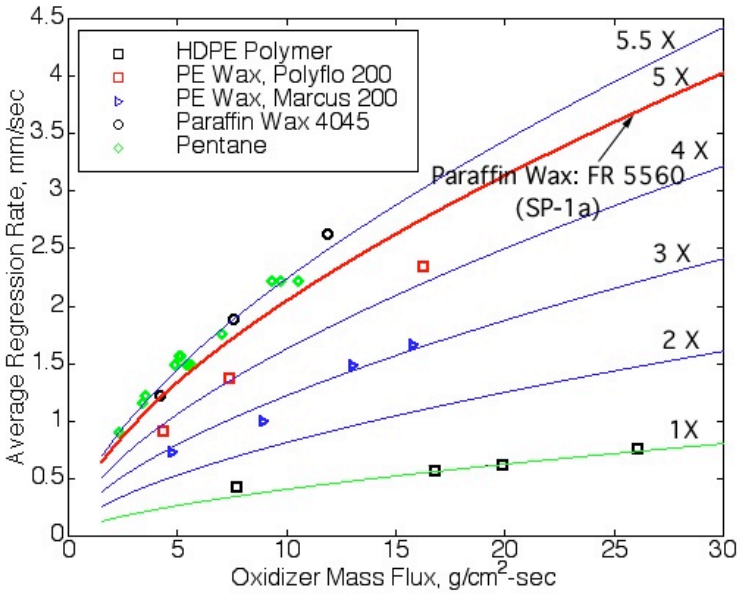

Figure 4.4: Regression rate of some n-alkanes vs. G_{ox}.

Heat of gasification increases in the subcritical region and it has a jump at the critical carbon number, then it declines slowly to an asymptotic value. This change in heat of gasification affects the blowing parameter. Its value decreases from 13 in the subcritical region to a value of about 5 in the supercritical region (Figure 4.5). The blowing parameter influences both the classical regression rate and the entrainment parameter (chapter 2.3).

The entrainment parameter depends on the properties of the fluid layer evaluated at the effective melt layer temperature. The entrainment parameter is low in the subcritical region mainly due to the high value of the blowing parameter. It jumps to a high value reaching the critical carbon number and then it starts to decrease with increasing carbon number. This decreasing trend in the supercritical region, is due to the increase in the melt layer viscosity. This shows the important influence that viscosity has on the regression rate.

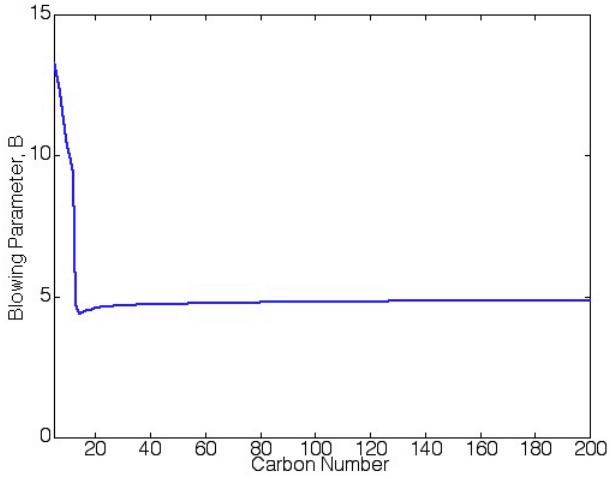

Figure 4.5: Blowing parameter as a function of carbon number.

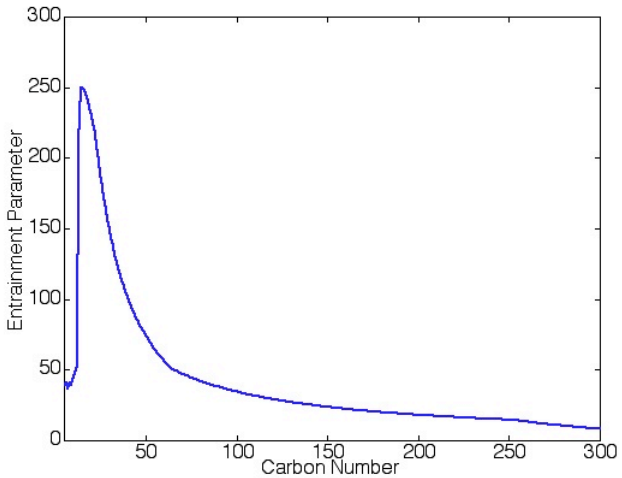

Figure 4.6: Entrainment parameter as a function of carbon number.

The change of blowing parameter also affects the regression rate. The classical regression rate in fact decreases from the subcritical to the supercritical regime. The entrainment regression rate behaves like the entrainment parameter. It is low in the

subcritical region, it jumps to high values at the critical point and starts to decrease with increasing carbon number in the supercrtical zone. The total regression rate values are very close to the entrainment regression rate values. It means that changes in the vaporization part are small compared to the entrainment component.

Another parameter that influences the regression rate is the polydispersity. As can be seen in Figure 4.7, increasing PD the improvement in the regression rate over the polymer is compromised. For this reason the best hybrid fuel with specified melting point is the one with the narrowest molecular weight distribution.

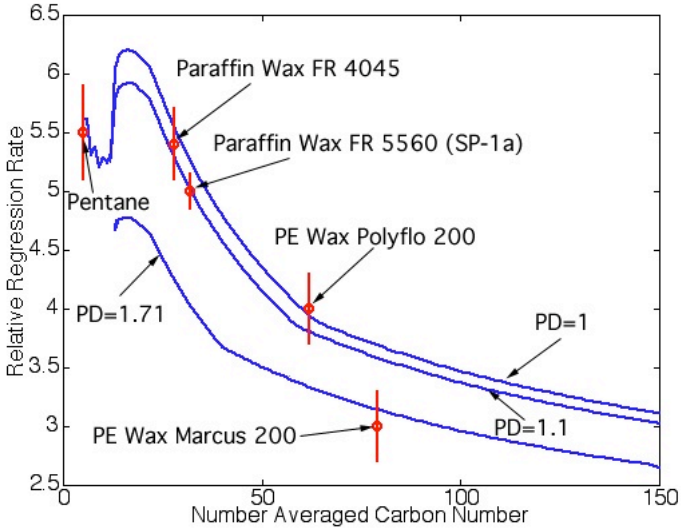

Figure 4.7: Regression rate as a function of carbon number at different values of polydispersity.

4.2 Fuel tested

In the frame of this work five different waxes have been tested in order to measure their viscosity and their regression rate. Every wax has been tested both pure and with different additives in order to change its rheological, mechanical and burning properties. Waxes properties as declared by the manufacturer are listed in table 4.1. Three of them (Sasolwax 6003, 6805 and Carlo Erba wax) are paraffin waxes. They are characterized by low molecular mass, low viscosity and low congealing point [25] [26]. Sasolwax 0907 is a microcrystalline wax. In general this type of wax shows plasticity stickiness in comparison with other paraffin waxes. Mycrocristalline waxes contain higher percentage of isoparanic hydrocarbons and naphthenic hydrocarbons than paraffin waxes. They have higher molecular weight and melting point. They also have a more branched structure. Sasolwax 1276 is a wax-based mixture with additives inserted by the manufacturer in order to increase its mechanical properties.

Additives

Different additives have been used to change waxes properties.

Wax	Melting point [°C]	Congealing point [°C]	Oil content [%]	Penetration at 25°C $[1/10mm]$	Viscosity at at 100°C $[mm^2/s]$
Sasolwax 0907	-	83-94	0-1	4-10	14-18
Sasolwax 1276	-	64-68	-	8-13	880-920
Sasolwax 6003	-	60-62	0-0.5	17-20	-
Sasolwax 6805	-	66-70	0-1	16-20	6-8
Carlo Erba wax	58-60	-	-	-	-

Table 4.1: Wax properties declared by the manufacturer.

Stearic acid Stearic acid is one of the most common saturated fatty acid with 18 carbon chains and its IUPAC name is octadecanoic acid. Its chemical formula is $CH_3(CH_2)_{16}CO_2H$. It looks like white solid grains at ambient temperature.
For its production, some animal and vegetable fats and oils are treated with water at high pressure and temperature. This leads to the hydrolysis of triglycerides and then the resulting mixture is distilled [27]. Stearic acid is commonly used in production of detergents, soaps and cosmetics. It is also a classic component for candle-making and it could be used as a hardener in candies.
It is added to paraffin to improve the mechanical properties of the mixture.

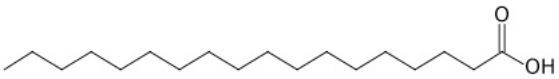

Figure 4.8: Chemical structure of stearic acid.

Molar mass $[g/mol]$	284.5
Density $[g/cm^3]$ at 70°C	0.85
Melting point [°C]	70
Boiling point [°C]	382

Table 4.2: Stearic acid properties.

Carbon black Carbon Black is a pigment produced by the incomplete combustion of heavy petroleum products, mainly from fluid catalytic cracking tar, coal tar, ethylene cracking tar. It is a form of paracrystalline carbon that has a high surface-area-to-volume ratio and its common use is as pigment and reinforcing phase in automobile tires. It can also helps to take heat away from the tread and belt area of the tire, reducing thermal damage.
Added to waxes it decreases the amount of radiant energy transmitted from the flame to the grain surface, in order to decrease the decay of the mechanical properties of the grain.

Micro-aluminum Light metals are often used to enhance solid fuel performances, due to their high developed enthalpy of combustion per unit mass. However their use can produce some problems due the fact that their ingnition is difficult, their combustion can be incomplete and they could lead to a two-phase flux due to the presence of condensed combustion products. Aluminum is the most used metallic additive due to its good performances and relative low cost. It can be introduced in the mixture with different granulometries, typically nano and micro-sized. The most important parameter is its specific surface, measured with BET technique [3]. The surface coating can be natural (aluminum oxide) or artificial. Micro-aluminum influences the theoretic specific impulse, but it also increases the drop between the real specific impulse value and the ideal one. Due to the fact that the micro-sized aluminum has a lower specific surface and a higher ignition temperature than nano-aluminum, it is less reactive. For this reason its contribution to regression rate increase is mainly due to higher contribution of radiation from soot and condensed combustion products from the flame zone toward the solid fuel grain [28].

In this work it has been used a micro-sized aluminum powder, Aluminum -325 mesh. "Mesh" is a U.S. measure that indicates the measure of the particles, it describes the number of openings per inch in a screen. There is no truly accurate conversion from mesh size to microns, because the wire thickness in screens varies all over the place. 325 mesh is approximately equal to 44 microns [29].

Chapter 5

Viscosity Measurement Results

5.1 Experimental apparatus

To measure the viscosity of a general fluid it is used a rheometer, in this case the HAAKE RheoStress 6000 Rotational Rheometer (Figure 5.1). It consists of a measuring plate (where test substance is positioned) situated on a measuring table that controls the temperature, and a rotor with shaft and quick-fit coupling. Technical data of the rheometer used are reported in table 5.1. Two softwares have been used to set up tests, to acquire and to elaborate the data, HAAKE RheoWin 4 Job Manager and HAAKE RheoWin Data Manager.

Torque range	200 nNm - 200 mNm
Speed range (constant shear)	$10^{-7} - 1500\ min^{-1}$
Speed range (constant rotation)	$10^{-7} - 1500\ min^{-1}$ (4500 min^{-1} optional)
Frequency range	$10^{-5} - 100\ Hz$
Normal force	$0.01 - 50\ N$
Min. lift speed	$0.2\ \mu m/sec$
Max. lift speed	$7\ mm/sec$
Temperature range	$-60°C$ to $+400°C$
Dimensions	15.6 x 15.6 x 30.4 $in.$ (40 x 40 x 78 cm)
Weight	42 kg

Table 5.1: HAAKE RheoStress 6000 Rotational Rheometer technical data.

Figure 5.1: HAAKE RheoStress 6000 Rotational Rheometer.

The plates used for different kind of fluid have been selected according to theory in chapter 3.2.2. The best choice to test paraffin wax is the combination with a lower plate and cone upper plate, due to the fact that the shear rate does not depend on the position. The chosen plate is the C60 2°Ti that has a cone angle of 2° and its radius is 30 mm.

However if the fluid has particles inside the cone plate can not be used otherwise it will be scratched and it could be not used anymore. For this reason, when particles are added to the paraffin, tests have been performed using both upper and lower parallel plate plates. The plate used is the PP35 Ti having 17.5 mm radius.

5.1.1 Calibration test

To be sure that the Rheometer works in the proper way a calibration test has been performed using the chosen plate.
After putting the calibration fluid E2000 on the measuring plate, a test that measures the viscosity with respect to the shear rate, at 20°C has been performed. Knowing that the viscosity of the calibration fluid is 1.930 Pa s, and comparing it with the test results, it can be determined if the Rheometer is calibrated or not.
In Table 5.2 the found values are shown. It can be noticed that increasing the shear rate the viscosity value becomes closer to the expected one. In general the test values are not so different from the theoretical one, so the Rheomter can be consider calibrated.

Shear Rate [s^{-1}]	Viscosity [Pa s]
0.0100	1.967
11.200	1.950
22.297	1.943
33.402	1.937
44.494	1.939
55.599	1.937
66.698	1.931
77.804	1.930
88.892	1.9285
100.001	1.930

Table 5.2: Results of calibration test using E2000 fluid.

5.2 Tests results

For each kind of mixture the viscosity has been investigated at first as a function of the shear rate. It is expected from the theory that the fluid has an almost plate trend due to the fact that paraffins should behave like a Newtonian fluid.
After that the viscosity behavior has been investatigated with respect to the temperature: increasing temperature the viscosity should decrease.

All tests performed are resumed in table 5.3.
For each kind of test at least two tests have been performed to ensure the repeatability of the results. All curves shown in paragraphs below are averaged on all tests performed for each type.

Table 5.3: Viscosity test set up data.

Formulation	Shear Rate [s^{-1}]	Temperature [°C]	Plate
0907 Pure	0.001-3300	120	C60 2°Ti
0907 Pure	50	190-90	C60 2°Ti
0907 + 10% S.A.	0.001-3300	120	C60 2°Ti
0907 + 10% S.A.	100	190-90	C60 2°Ti
0907 + 10% Al	0.001-3300	120	PP35 Ti
0907 + 10% Al	100	190-90	PP35 Ti
0907 + 1.5% C.B.	0.001-3300	120	PP35 Ti
0907 + 1.5% C.B	0.001-3300	190	PP35 Ti
0907 + 1.8% C.B.	0.001-3300	120	PP35 Ti
0907 + 1.8% C.B.	0.001-3300	190	PP35 Ti
0907 + 1.8% C.B.	100	190-95	PP35 Ti
0907 + 1.8% C.B.	500	190-95	PP35 Ti
0907 + 1.8% C.B.	1000	190-95	PP35 Ti
0907 + 2% C.B.	0.001-3300	100	PP35 Ti
0907 + 2% C.B.	0.001-3300	120	PP35 Ti
0907 + 2% C.B.	0.001-3300	150	PP35 Ti
0907 + 2% C.B.	100	190-95	PP35 Ti

Table 5.3: Continues in the next page

Table 5.3: Continues from previous page

Formulation	Shear Rate [s^{-1}]	Temperature [°C]	Plate
0907 + 2% C.B.	500	190-95	PP35 Ti
0907 + 2% C.B.	1000	190-95	PP35 Ti
0907 + 3% C.B.	0.001-3300	150	PP35 Ti
0907 + 3% C.B.	0.001-3300	190	PP35 Ti
0907 + 3% C.B.	100	190-95	PP35 Ti
0907 + 3% C.B.	500	190-95	PP35 Ti
0907 + 3% C.B.	1000	190-95	PP35 Ti
0907 + 10% S.A. +2% C.B.	0.001-3300	120	PP35 Ti
0907 + 10% S.A. +2% C.B.	0.001-3300	150	PP35 Ti
0907 + 10% S.A. +2% C.B.	300	190-90	PP35 Ti
0907 + 10% S.A. +2% C.B.	500	190-90	PP35 Ti
0907 + 10% S.A. +2% C.B.	700	190-90	PP35 Ti
0907 + 10% S.A. +2% C.B.	1000	190-90	PP35 Ti
1276 Pure	0.001-3300	120	C60 2°Ti
1276 Pure	50	190-70	C60 2°Ti
1276 + 10% S.A.	0.001-3300	120	C60 2°Ti
1276 + 10% S.A.	100	190-70	C60 2°Ti
1276 + 10% Al	0.001-3300	120	PP35 Ti
1276 + 10% Al	100	190-70	PP35 Ti
1276 + 10% S.A. +2% C.B.	0.001-3300	120	PP35 Ti
1276 + 10% S.A. +2% C.B.	0.001-3300	150	PP35 Ti
1276 + 10% S.A. +2% C.B.	300	190-70	PP35 Ti
1276 + 10%S.A +2% C.B	500	190-70	PP35 Ti
1276 + 10% S.A +2% C.B.	1000	190-70	PP35 Ti
6003 Pure	0.001-3300	120	C60 2°Ti
6003 Pure	50	190-70	C60 2°Ti
6003 + 10% S.A.	0.001-3300	120	C60 2°Ti
6003 + 10% S.A.	100	190-70	C60 2°Ti
6003 + 10% Al	0.001-3300	120	PP35 Ti
6003 + 10% Al	100	190-70	PP35 Ti
6003 + 10% S.A. +2% C.B.	0.001-3300	120	PP35 Ti
6003 + 10% S.A. +2% C.B.	0.001-3300	150	PP35 Ti
6003 + 10% S.A. +2% C.B.	300	190-70	PP35 Ti
6003 + 10% S.A. +2% C.B.	500	190-70	PP35 Ti
6003 + 10% S.A. +2% C.B.	1000	190-70	PP35 Ti
6805 Pure	0.001-3300	120	C60 2°Ti
6805 Pure	50	190-70	C60 2°Ti
6805 + 10% S.A.	0.001-3300	120	C60 2°Ti
6805 + 10% S.A.	100	190-70	C60 2°Ti
6805 + 10% Al	0.001-3300	120	PP35 Ti
6805 + 10% Al	150	190-70	PP35 Ti
6805 + 10% S.A. +2% C.B.	0.001-3300	120	PP35 Ti
6805 + 10% S.A. +2% C.B.	0.001-3300	150	PP35 Ti
6805 + 10% S.A. +2% C.B.	300	190-70	PP35 Ti
6805 + 10% S.A. +2% C.B.	500	190-70	PP35 Ti

Table 5.3: Continues in the next page

Table 5.3: Continues from previous page

Formulation	Shear Rate [s^{-1}]	Temperature [°C]	Plate
6805 + 10% S.A. +2% C.B.	1000	190-70	PP35 Ti
C.E. Pure	0.001-3300	120	C60 2°Ti
C.E. Pure	100	190-70	C60 2°Ti
C.E. + 10% S.A. +2% C.B.	0.001-3300	120	PP35 Ti
C.E. + 10% S.A. +2% C.B.	0.001-3300	150	PP35 Ti
C.E. + 10% S.A. +2% C.B.	300	190-70	PP35 Ti
C.E. + 10% S.A. +2% C.B.	500	190-70	PP35 Ti
C.E. + 10% S.A. +2% C.B.	1000	190-70	PP35 Ti

5.2.1 Pure waxes

At first pure waxes have been tested. First the viscosity is found with respect to the shear rate, the results for Sasolwax 0907, Sasolwax 1276, Sasolwax 6003 and Sasolwax 6805 are shown in Figure 5.2. To quantify the difference between the viscosity values, Sasolwax 6003 is taken as reference, due to the fact that it is the one with the lowest viscosity.
The values of viscosity at $T = 120°C$ and $\dot{\gamma} = 50\ s^{-1}$ are reported in the table 5.4. In same table are also shown the average differences between the Sasolwax 6003 curve and the others.

Paraffin	Viscosity [Pa s]	Difference from Sasolwax 6003 [%]
Sasolwax 0907	0.0078	175.06
Sasolwax 1276	0.4136	144907.2
Sasolwax 6003	0.0028	-
Sasolwax 6805	0.0034	19.07

Table 5.4: Viscosity at T = 120°C and $\dot{\gamma} = 50\ s^{-1}$ of each wax and average difference in percentage from Sasolwax 6003 value.

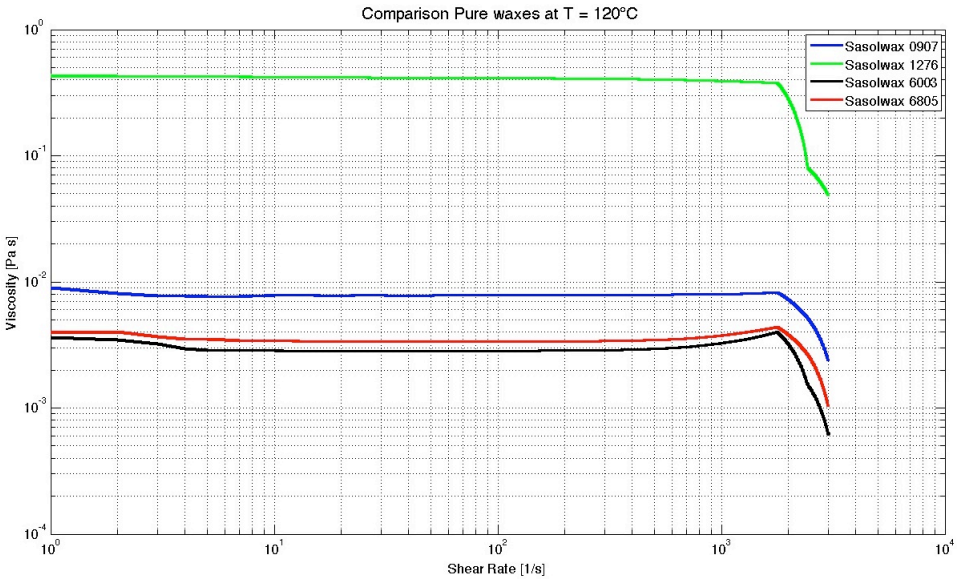

Figure 5.2: Behavior of the viscosity vs. shear rate of the Sasol waxes at 120°C.

As expected from the theory all the curves show an almost plate behavior, pure waxes behave as Newtonian fluids. The sudden decrease of all curves at shear rate higher than 10^3 s^{-1} is due to the fact that for very high velocity of the shaft, the wax spreads out from the measuring plate and the rheometer can not measure the right viscosity.
In the plate range of the curve, changing the shear rate value the viscosity does not change. The curve with respect to the temperature is the same for every value of shear rate. So, to determine the viscosity vs. temperature curves, the value of shear rate at which the test is performed is not demanding, it has only to be in the plate range. The shear rate value chosen is $\dot{\gamma} = 50$ s^{-1}.

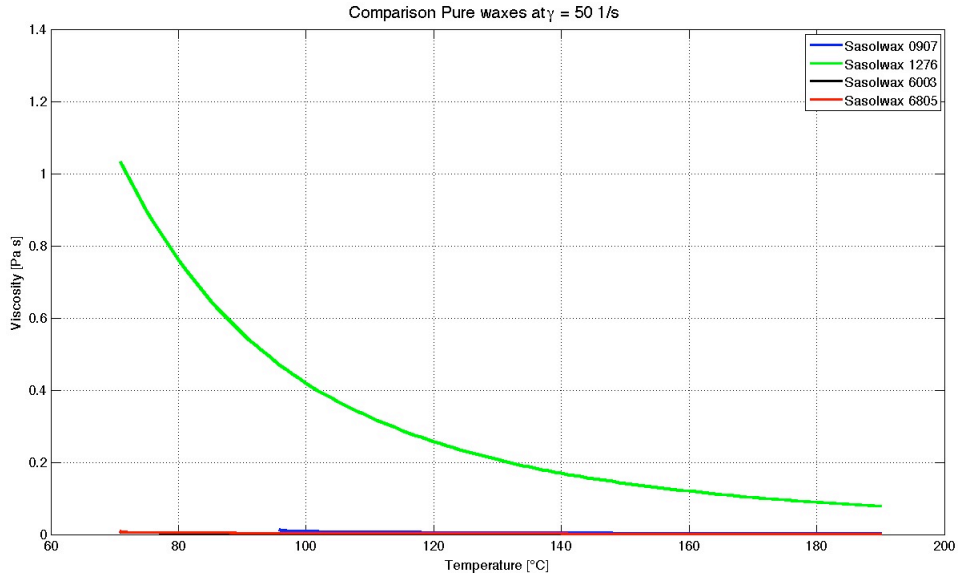

Figure 5.3: Behavior of the viscosity vs. temperature of the Sasol waxes at $\dot{\gamma} = 50\ s^{-1}$.

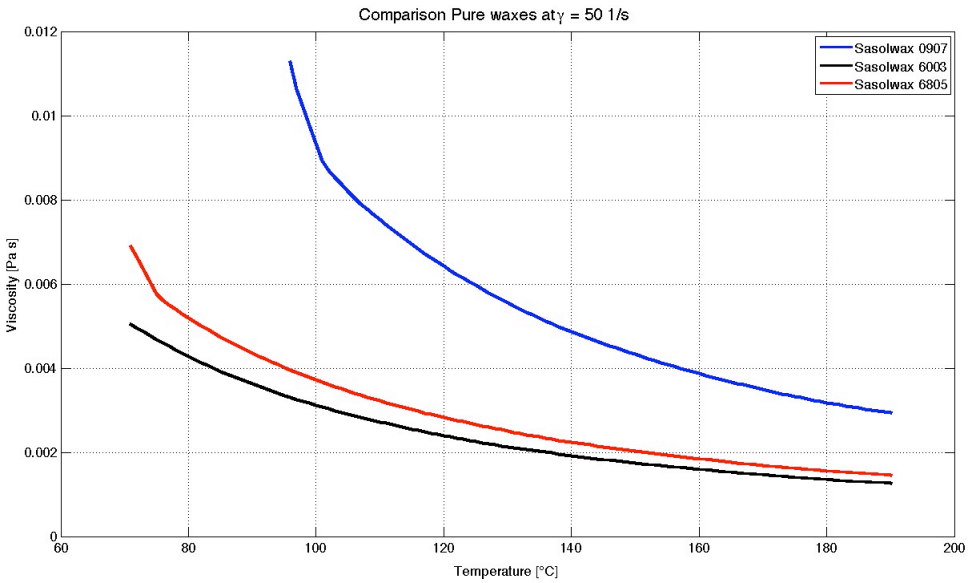

Figure 5.4: Behavior of the viscosity vs. temperature of the Sasol waxes at $\dot{\gamma} = 50\ s^{-1}$. Sasolwax 1276 curve is not included.

From Figure 5.3 it can be noticed that the viscosity of Sasolwax 1276 is two orders of magnitude higher than the others. This is due to the fact that it is not a pure wax, but it is a mixture with different additives inserted directly by the manufacturer, as said in paragraph 4.2.
In Figure 5.4 it is shown the behavior of Sasolwax 0907, 6003 and 6805 with respect to temperature that can not be appreciated in Figure 5.3 because of the too big difference

between Sasolwax 1276 values and the others.
Viscosity of Sasolwax 0907 is higher than the other two because it is a microcrystalline wax. Microcrystalline waxes have thinner crystals and higher molecular weight and melting point than paraffin waxes. They also have a more branched structure, these non-straight chain components counteract the flow and this leads to higher viscosity.

The average difference between each curve with respect to temperature and reference curve of Sasolwax 6003 is shown in table 5.5.

Paraffin	Difference from Sasolwax 6003 [%]
Sasolwax 0907	104.0
Sasolwax 1276	87046.3
Sasolwax 6805	14.21

Table 5.5: Average percentage differences from Sasolwax 6003 viscosity curve with respect to temperature.

Same type of tests has also been done on Carlo Erba wax. Results are shown in Figure 5.5 and Figure 5.6 with respect to shear rate and temperature respectively. It is compared with the two Sasolwax paraffins (6003 and 6805) that have similar values of viscosity. Carlo Erba wax is a paraffin wax, and its behavior is very close to the other two. Its viscosity at $T = 120°C$ and $\gamma = 50\ s^{-1}$ is about 4.3% lower than the one of Sasolwax 6003.
In Figure 5.6 the value of shear rate at which the test is performed is 100 s^{-1}. As said before, the value is not demanding, but it has to belong to the plate range. Once in that range, the viscosity does not change changing the shear rate. For this reason it is possible to compare the Carlo Erba curve with the other two curves even if they are at a different shear rate value.

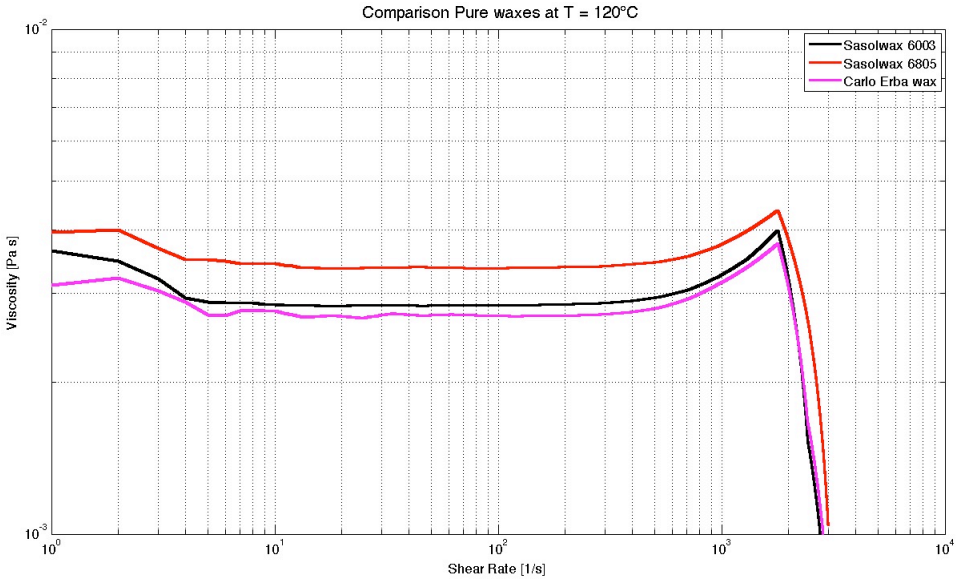

Figure 5.5: Comparison between the viscosity vs. shear rate of Carlo Erba wax and the viscosity of Sasolwax 6003 and Sasolwax 6805 at 120°C.

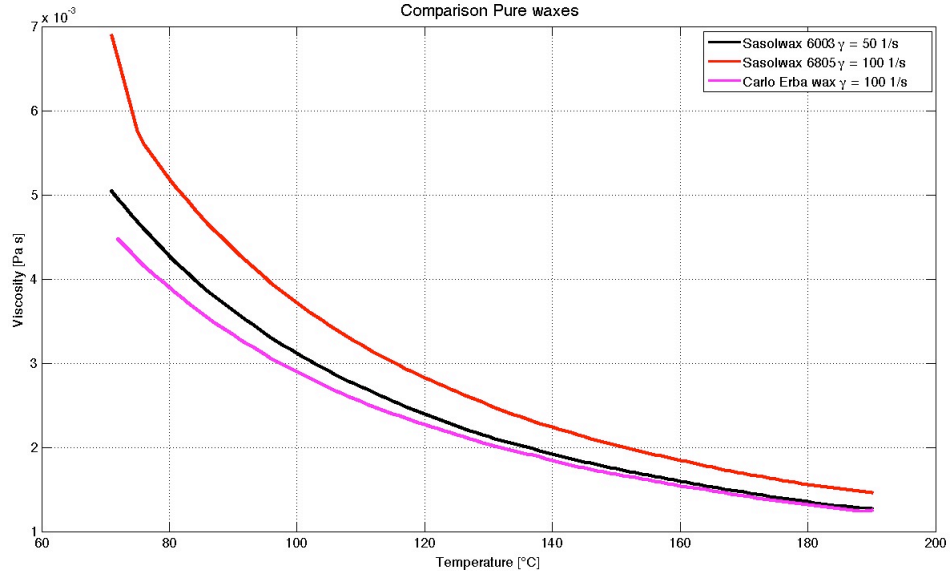

Figure 5.6: Comparison between the viscosity vs. temperature of Carlo Erba wax and the viscosity of Sasolwax 6003 and Sasolwax 6805.

5.2.2 Mixtures of wax and aluminum

Aluminum is often added to solid fuels to enhance their performances. In this work it has been tested mixtures of 90% wax and 10% micro-aluminum. Due to the strong

correlation between viscosity and regression rate, some measurements have been done to characterize the viscosity behavior of metallized wax.
It has been used the plate-plate configuration of the rheometer, because the presence of particles could scratch the cone plate. Each mixture tested is compared with the corresponding pure wax.
As done for the pure waxes, first the viscosity has been determined with respect to the shear rate. In Figure 5.7 and Figure 5.8 the red curve represents the mixture with aluminum and the blue one is the pure wax. Despite the presence of particles the mixture shows a Newtonian behavior with its typical plate trend. Viscosity values of mixtures at $T = 120°C$ and $\dot{\gamma} = 100\ s^{-1}$ are presented in table 5.6.

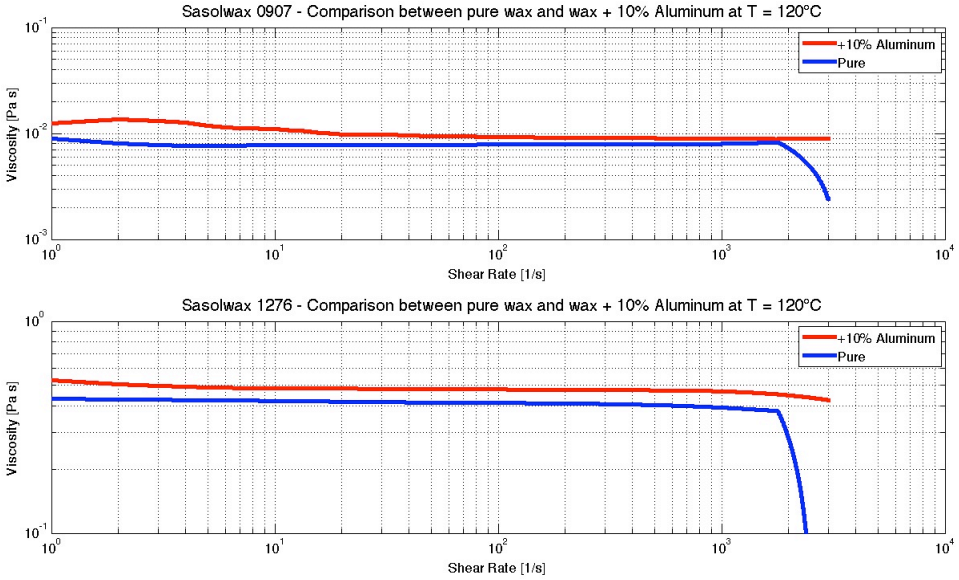

Figure 5.7: Comparison between the viscosity vs. shear rate of mixture with 10% Al and the viscosity of pure wax for Sasolwax 0907 and Sasolwax 1276.

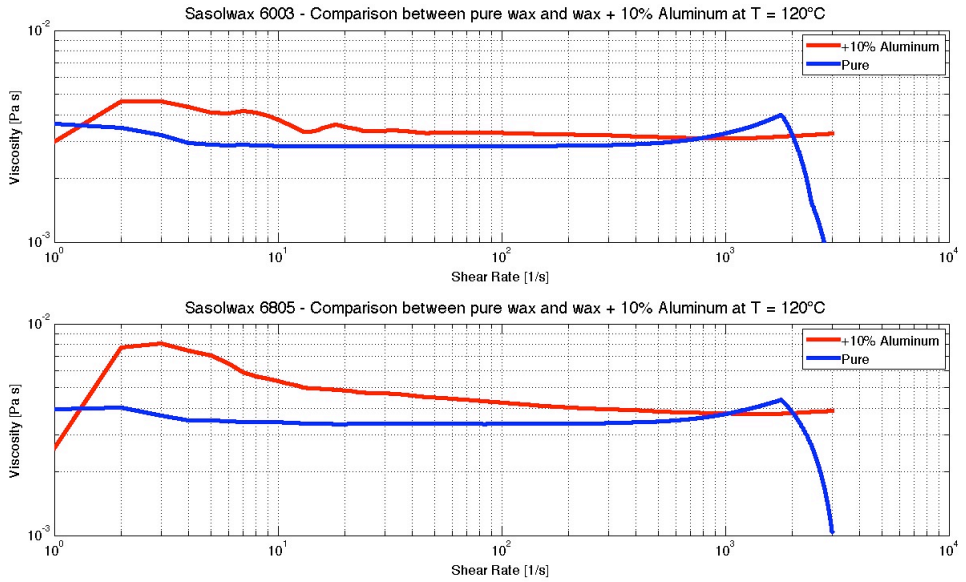

Figure 5.8: Comparison between the viscosity vs. shear rate of mixture with 10% Al and the viscosity of pure wax for Sasolwax 6003 and Sasolwax 6805.

Mixture	Viscosity [Pa s]
0907 +10% Al	0.0093
1276 +10% Al	0.4769
6003 +10% Al	0.0033
6805 +10% Al	0.0042

Table 5.6: Viscosity at T = 120°C and $\dot{\gamma} = 100\ s^{-1}$ of each mixture of 90% wax and 10% aluminum.

As said for pure waxes, in the Newtonian range the viscosity does not change changing the shear rate value. This allows to evaluate the curve of viscosity vs. temperature at an arbitrarily chosen shear rate value. Sasolwax 0907, 1276 and 6003 have been tested at a shear rate value of $100s^{-1}$, while the shear rate chosen for Sasolwax 6805 is $150s^{-1}$. The different shear rate value of 6805 is due to the quite different behavior of the viscosity vs. shear rate curve. It starts to have a plate trend at about $130s^{-1}$. Results are compared with the pure wax behavior. Even if the two curves are at different shear rate, they can be compared thanks to the Newtonian behavior of both fluids. The little oscillating behavior of the mixture curves (Figure 5.9, 5.11 and 5.12) is due to the presence of particles in the mixtures.

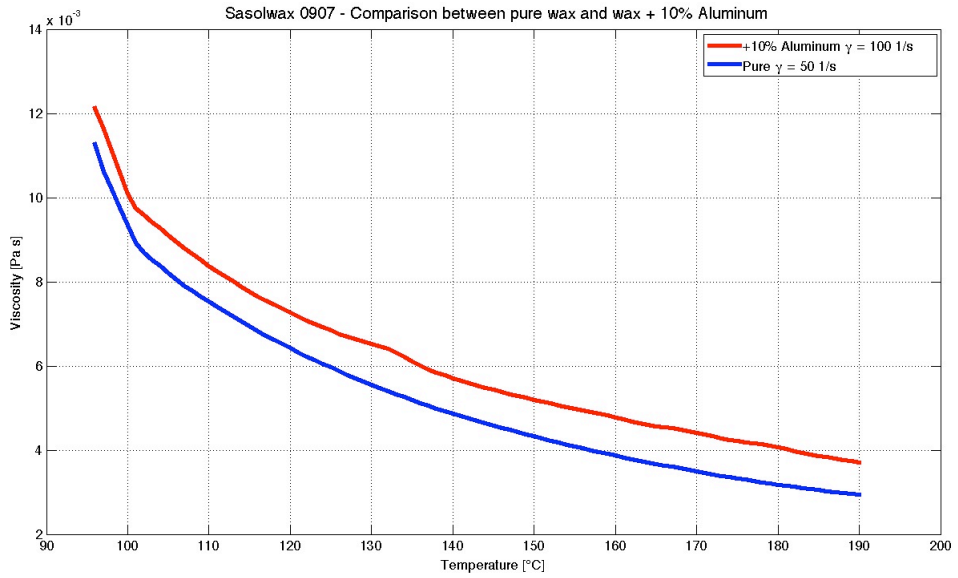

Figure 5.9: Comparison between the viscosity vs. temperature of mixture with 10% Al and the viscosity of pure wax for Sasolwax 0907.

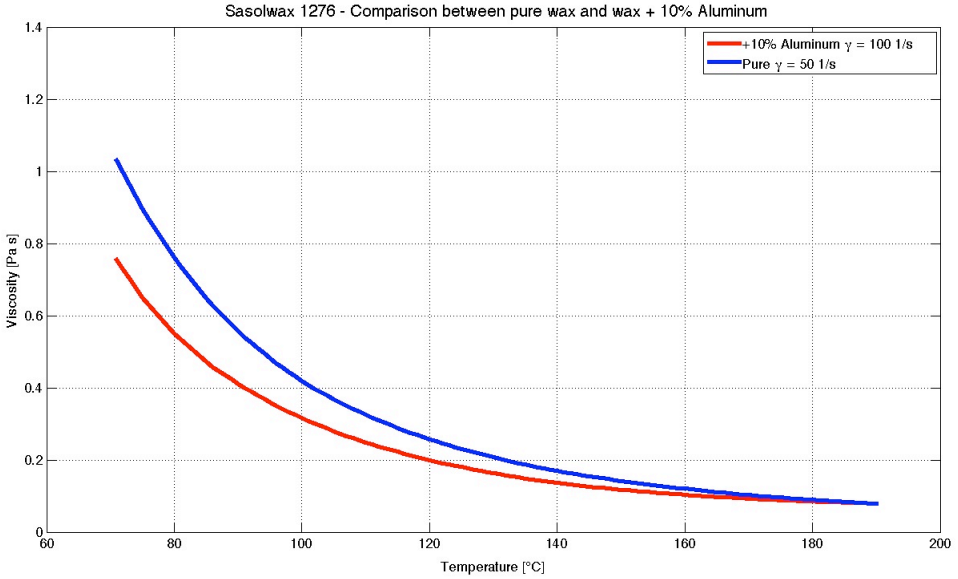

Figure 5.10: Comparison between the viscosity vs. temperature of mixture with 10% Al and the viscosity of pure wax for Sasolwax 1276.

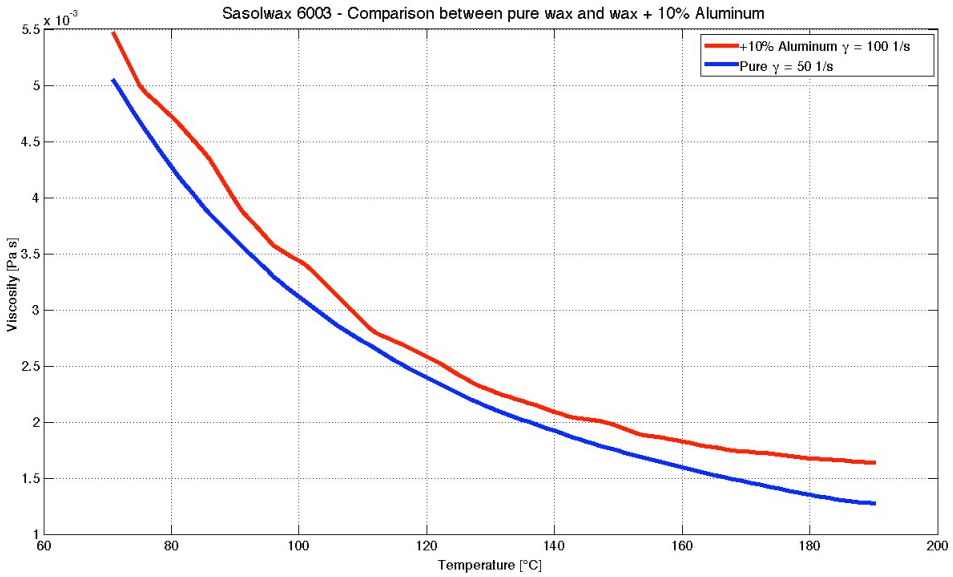

Figure 5.11: Comparison between the viscosity vs. temperature of mixture with 10% Al and the viscosity of pure wax for Sasolwax 6003.

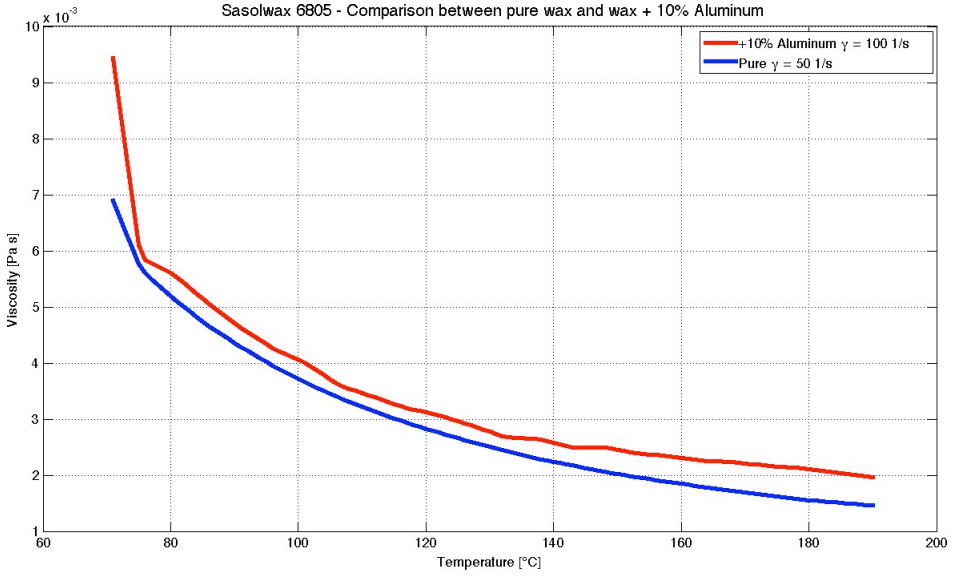

Figure 5.12: Comparison between the viscosity vs. temperature of mixture with 10% Al and the viscosity of pure wax for Sasolwax 6805.

The average values of the difference between the mixtures curves and pure waxes curves are reported in Table 5.7. The average difference is evalueted between $10s^{-1}$ and $1000s^{-1}$ for the viscosity vs. shear rate curves and between $90°C$ and $190°C$ for viscosity vs. temperature curves.
In general adding aluminum powder seems to affect more the waxes that have higher

viscosity. Mixture with Sasolwax 1276 shows an higher changing in viscosity values from the pure wax. Moreover at low temperature the two curves are quite different (-26.75% at 71°C), while the difference becomes very small for high temperature (0.79% at 190°C). 1276 is also the only one that shows a decrease in viscosity adding micro-aluminum powder. For the other waxes the difference between the pure and the mixture curves is almost constant and the viscosity of the mixture is higher than the viscosity of pure wax.

Mixture	Difference from pure w.r.t. shear rate [%]	Difference from pure w.r.t. temperature [%]
Sasolwax 0907 + 10% Al	14.6	16.7
Sasolwax 1276 + 10% Al	17.35	−20.6
Sasolwax 6003 + 10% Al	6.2	11.45
Sasolwax 6805 + 10% Al	12.8	15.68

Table 5.7: Average differences in percentage between mixture and pure wax viscosity curves with respect to shear rate and temperature.

5.2.3 Mixtures of wax and stearic acid

Stearic acid is added to waxes in order to improve their mechanical properties. Mixtures with 90% wax and 10% stearic acid have been tested to characterized their viscosity behavior. The results for each mixture are compared with the corresponding pure wax curves.
Tests have been performed using a cone-plate configuration according to theory of paragraph 3.2.2.

The viscosity has been first determined with respect to the shear rate. Results are reported in Figure 5.13 and 5.14. As done before, the red curve is the mixture while the blue curve represents the pure wax. The sudden decrase of the curves for $\dot{\gamma} > 10^3 s^{-1}$ is due to the fact that, at high shear rates the fluid spreads out from the plate and the rheometer can not perform the right measumernt.
Mixtures curves show the plate trend that is typical for Newtonian fluids. For paraffin waxes (Sasolwax 6003 and 6805) the viscosity increases adding the stearic acid. Sasolwax 6003 seems to be more affected by the presence of the additive. Mixture with Sasolwax 0907 has almost the same viscosity as the pure wax, while the mixture with 1276 shows a decrease in viscosity adding stearic acid. Values of viscosity for each mixture at $T = 120°C$ and $\dot{\gamma} = 100 s^{-1}$ are reported in table 5.8.

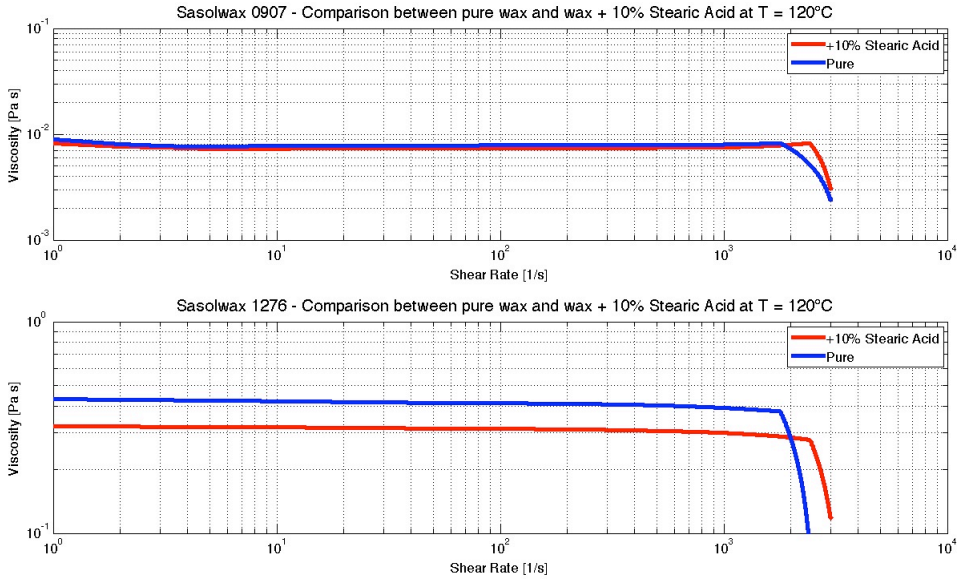

Figure 5.13: Comparison between the viscosity vs. shear rate of mixture with 10% Stearic Acid and the viscosity of pure wax for Sasolwax 0907 and Sasolwax 1276.

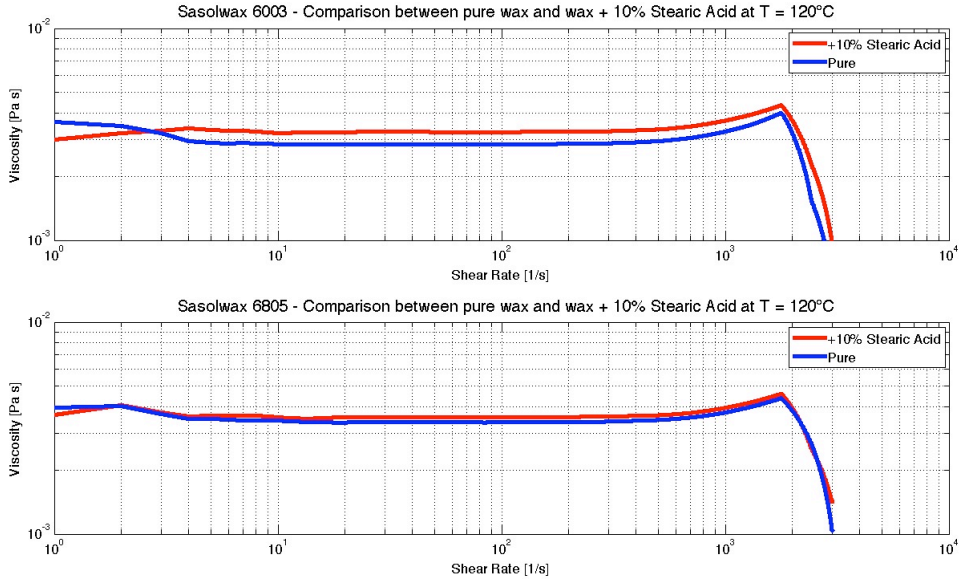

Figure 5.14: Comparison between the viscosity vs. shear rate of mixture with 10% Stearic Acid and the viscosity of pure wax for Sasolwax 6003 and Sasolwax 6805.

Due to the Newtonian behavior, the viscosity does not change changing the shear rate. To determine the curve of viscosty vs. temperature, the value of shear rate at which the test is performed is not demanding, the only constraint is that it belongs to the plate range. The shear rate value has been arbitrarily set at 100 $1/s$. Resulting curves are compared with corresponding pure one. They can be compared even if they

Mixture	Viscosity [Pa s]
Sasolwax 0907 + 10% Stearic Acid	0.0074
Sasolwax 1276 + 10% Stearic Acid	0.3112
Sasolwax 6003 + 10% Stearic Acid	0.0032
Sasolwax 6805 + 10% Stearic Acid	0.0036

Table 5.8: Viscosity at $T = 120°C$ and $\dot{\gamma} = 100\ s^{-1}$ of each mixture with stearic acid.

are at different shear rate values, thanks to the Newtonian behavior of both fluids.

These tests show the same behavior of the previous one. In mixtures with Sasolwax 6003 and 6805 the viscosity increases adding stearic acid, while for the other two the viscosity decreases. In particular the viscosity of the mixture with 0907 is very close to the pure one. Adding stearic acid in Sasolwax 1276 the viscosity decreases by more than 10%.
In table 5.9 the average percentage differences between mixture and pure curves are reported both with respect to shear rate and temperature. The differences are evalueted between 10 and $1000 s^{-1}$ for the viscosity vs. shear rate curves, and between $90°C$ and $190°C$ for viscosity vs. temperature curves.

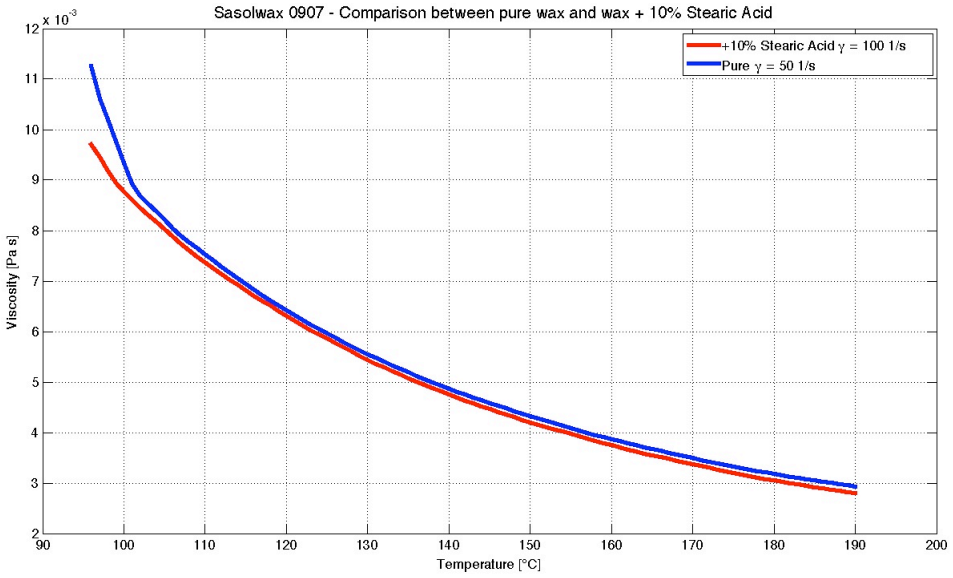

Figure 5.15: Comparison between the viscosity vs. temperature of mixture with 10% Stearic Acid and the viscosity of pure wax for Sasolwax 0907.

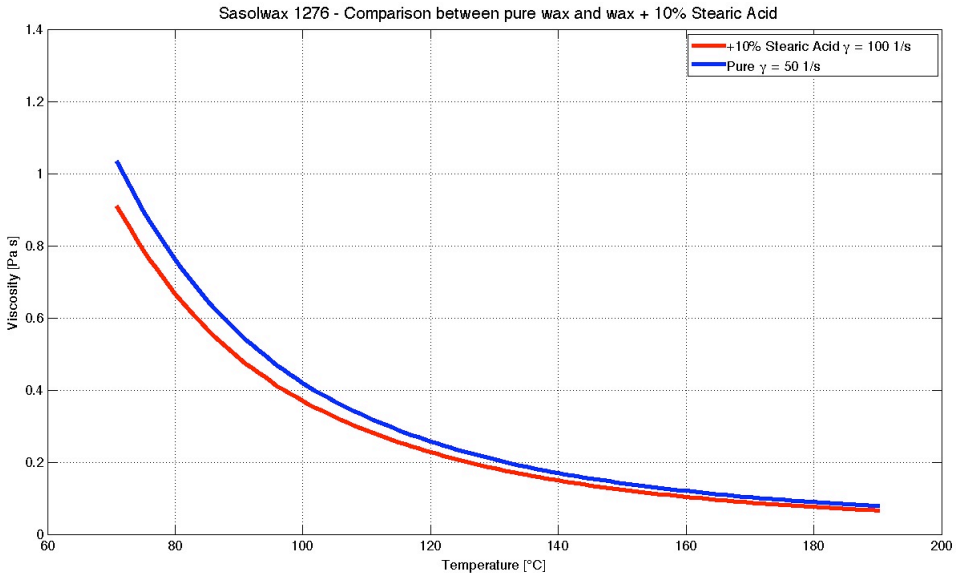

Figure 5.16: Comparison between the viscosity vs. temperature of mixture with 10% Stearic Acid and the viscosity of pure wax for Sasolwax 1276.

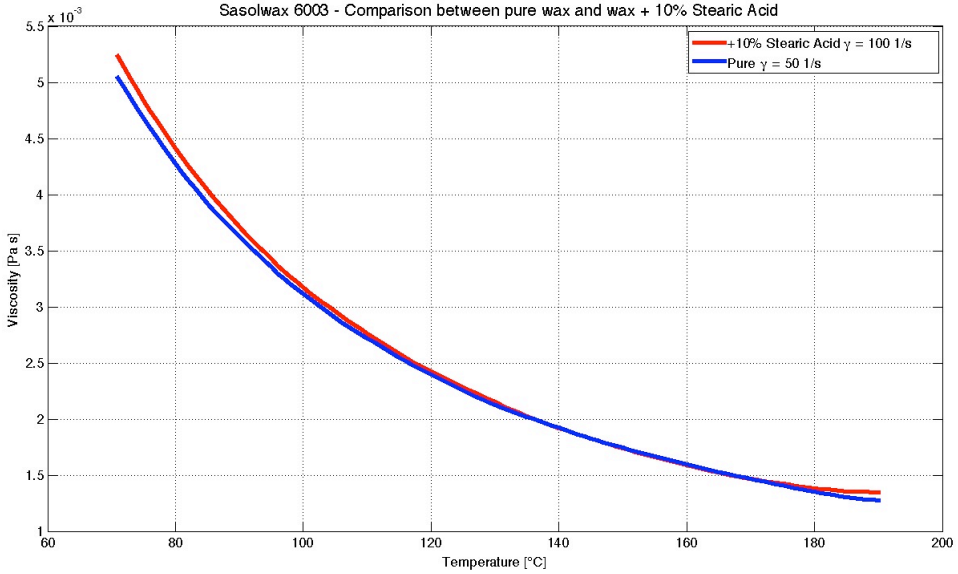

Figure 5.17: Comparison between the viscosity vs. temperature of mixture with 10% Stearic Acid and the viscosity of pure wax for Sasolwax 6003.

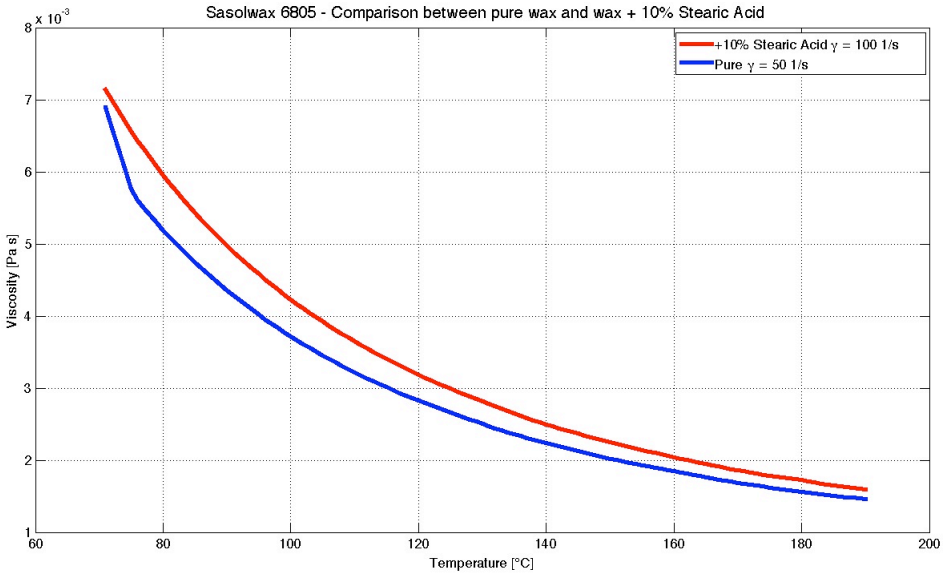

Figure 5.18: Comparison between the viscosity vs. temperature of mixture with 10% Stearic Acid and the viscosity of pure wax for Sasolwax 6805.

Mixture	Difference from pure w.r.t. shear rate [%]	Difference from pure w.r.t. temperature [%]
Sasolwax 0907+10% Stearic Acid	−5.98	−3.35
Sasolwax 1276+10% Stearic Acid	−24.18	−12.39
Sasolwax 6003+10% Stearic Acid	13.58	1.21
Sasolwax 6805+10% Stearic Acid	5.33	12.23

Table 5.9: Average differences in percentage between mixtures with 10% stearic acid and pure wax viscosity curves with respect to shear rate and temperature.

5.2.4 Mixtures of wax and carbon black

Adding carbon black to wax produces a decrease in the amount of radiant energy transmitted from the flame to the grain surface, and this leads to a decrease in the decay of mechanical properties of the fuel grain. A mixture with 98% Sasolwax 0907 and 2% carbon black has been tested in order to determine its rheological behavior. Studies performed at SPlab of Politecnico di Milano, show that 2% of carbon black is the best compromise between the decrease of radiative energy wanted and the decay in regression rate causes by additive insertion.
Performing rheological tests, it is noticed that this kind of mixture has non-Newtonian behavior as shown in Figure 5.19. The fluid has a descending trend, that means that it behaves like a shear thinning fluid. In shear thinning fluids the viscosity decreases increasing the shear rate (see paragraph 3.1).

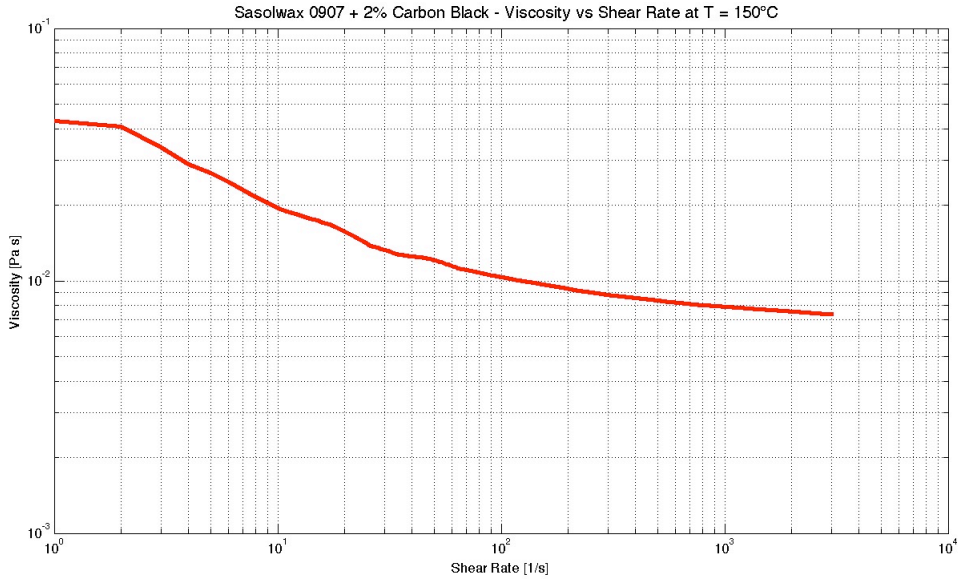

Figure 5.19: Viscosity vs. shear rate of Sasolwax 0907 + 2% Carbon Black, at T=150°C.

To investigate the phenomenon, mixtures with different carbon black percentage have been tested:

- Sasolwax 0907 + 1.5% Carbon Black
- Sasolwax 0907 + 1.8% Carbon Black
- Sasolwax 0907 + 2% Carbon Black
- Sasolwax 0907 + 3% Carbon Black

Starting from the mixture with lower percentange of carbon black, the rheological behaviour with respect to shear rate has been determined at different temperatures. The mixture with 1.5% and the one with 1.8% of carbon black have been tested at $T = 120°C$ and at $T = 190°C$. The mixture with 1.5% carbon black shows an almost Newtonian behavior (Figure 5.20). For higher percentage of carbon black, viscosity vs. shear rate curve starts to show the shear thinning behavior, in fact it does not have the plate trend of Newtonian fluid, but it decreases monotonically (Figure 5.21). Mixture with 2% carbon black has been tested at $100°C$, $120°C$ and $150°C$ while mixture with 3% carbon black has been tested at $150°C$ and $190°C$. In general the higher is the temperature, the lower is the viscosity, but the slope angle of the curves does not change linearly with temperature (Figure 5.22 and 5.23).

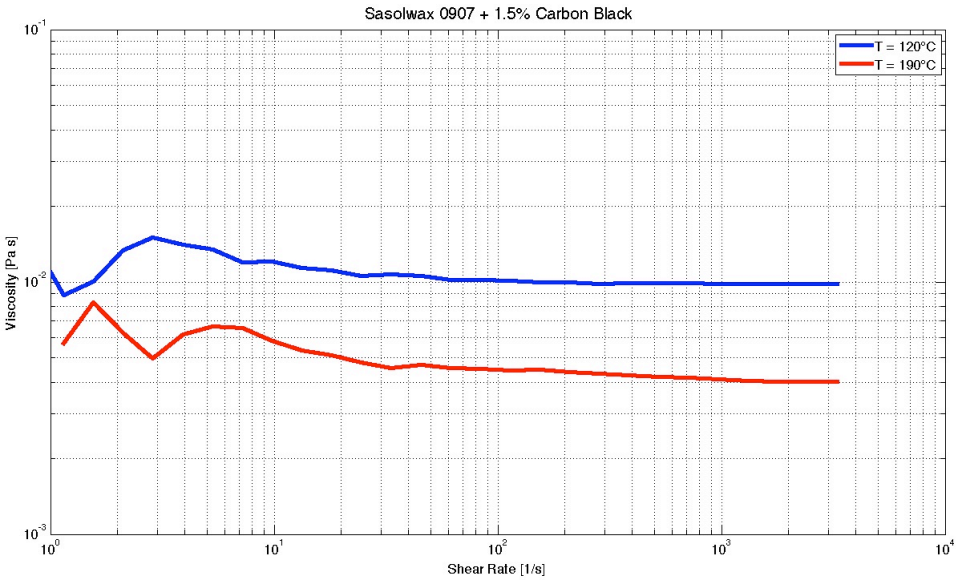

Figure 5.20: Viscosity vs. shear rate of Sasolwax 0907 + 1.5% Carbon Black, at diferrent temperatures.

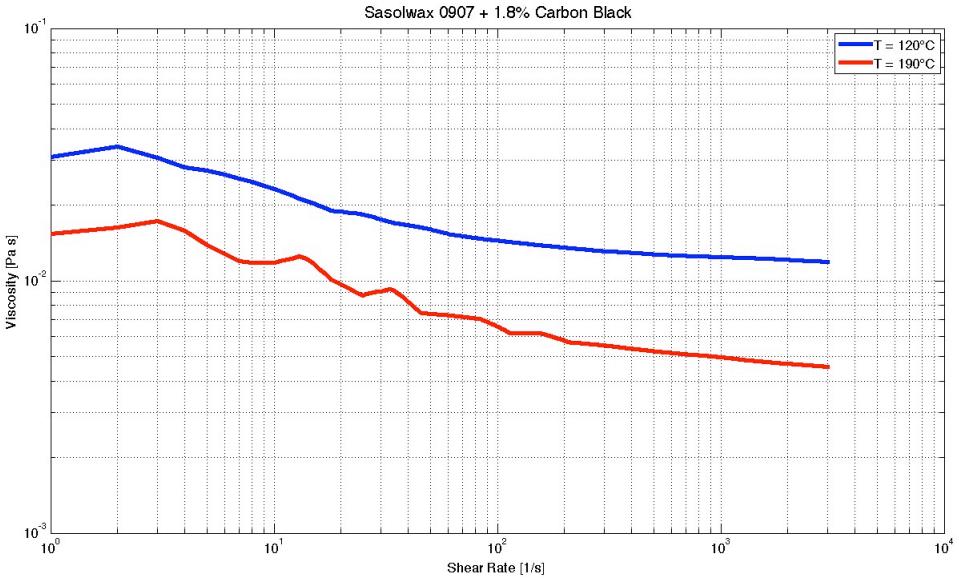

Figure 5.21: Viscosity vs. shear rate of Sasolwax 0907 + 1.8% Carbon Black, at different temperatures.

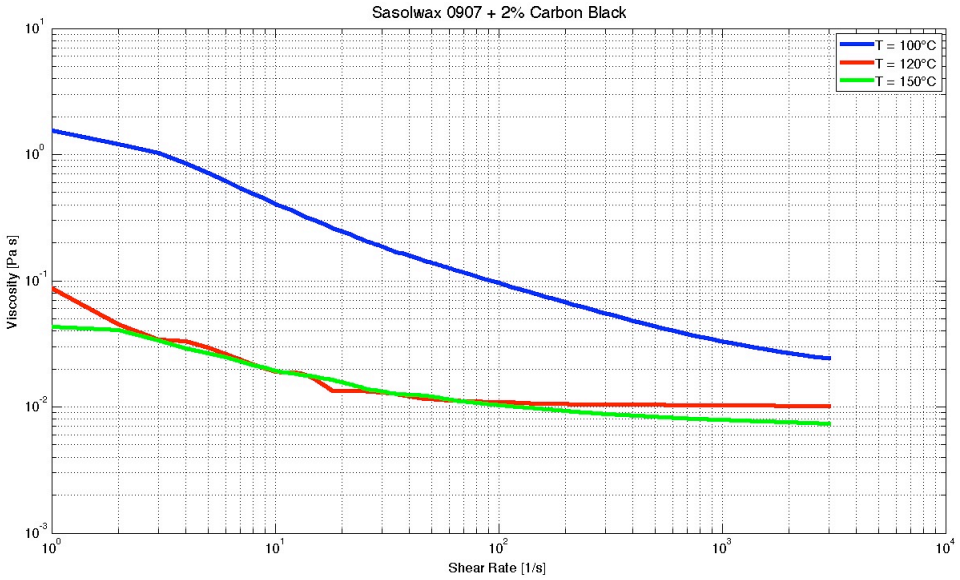

Figure 5.22: Viscosity vs. shear rate of Sasolwax 0907 + 2% Carbon Black, at different temperatures.

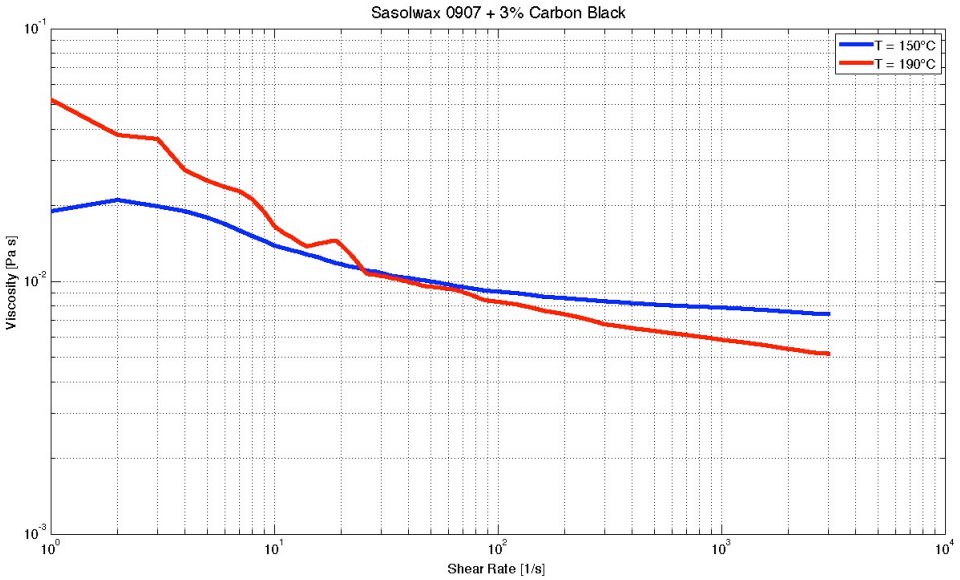

Figure 5.23: Viscosity vs. shear rate of Sasolwax 0907 + 3% Carbon Black, at different temperatures.

Higher is the percentage of carbon black, higher is the viscosity and so the difference between the mixture value and the pure wax value. Comparison between the mixtures with different percentage of carbon black and pure wax (dashed line) at $T = 120°C$ is shown in Figure 5.24. Contrary to how is expected, mixture with 1.8% carbon black has the highest viscosity. Mixture with 3% carbon black is not reported in the comparison

because no tests at $T = 120°C$ have been performed for that mixture.

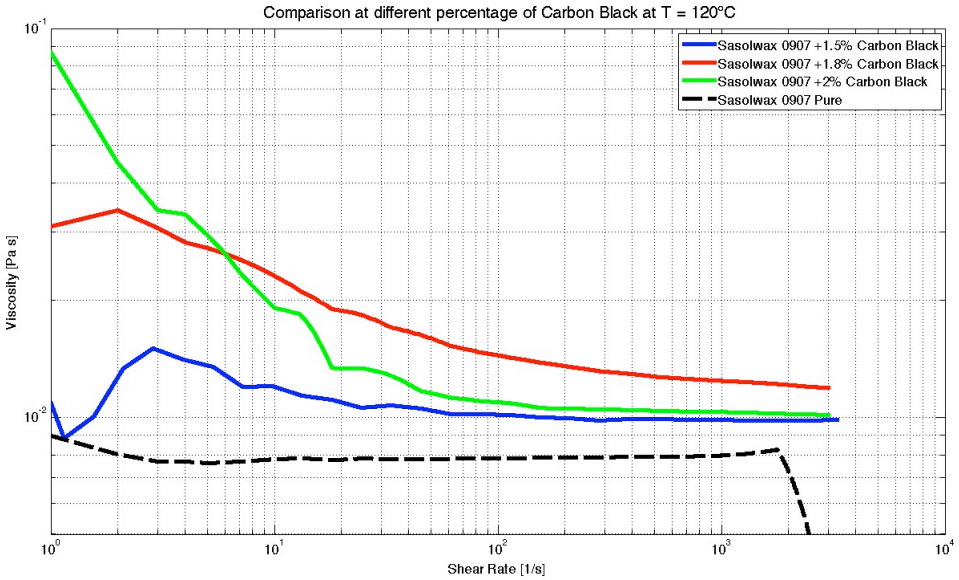

Figure 5.24: Comparison between mixture of Sasolwax 0907 and carbon black in different percentage at T = 120°C.

With non-Newtonian fluids the viscosity is not constant changing the shear rate. So in this case it is not possible to have a unique viscosity vs. temperature curve, for each value of shear rate the curve is different. For this reason the investigation of the viscosity behavior with respect to temperature has been done at three different shear rates: $\dot{\gamma} = 100s^{-1}$, $\dot{\gamma} = 500s^{-1}$ and $\dot{\gamma} = 1000s^{-1}$. Due to the shear thinning behavior, it is expected that higher is the shear rate lower is the viscosity. Mixtures with 2% and 3% of carbon black show this kind of behavior (Figure 5.26 and 5.27). Mixture with 1.8% carbon black shows a strange behavior due to the fact that it seems that the viscosity at $\dot{\gamma} = 1000s^{-1}$ is higher than the one at $\dot{\gamma} = 500s^{-1}$ as can be seen in Figure 5.25.
In each case the viscosity of the mixture is higher than the pure wax one.

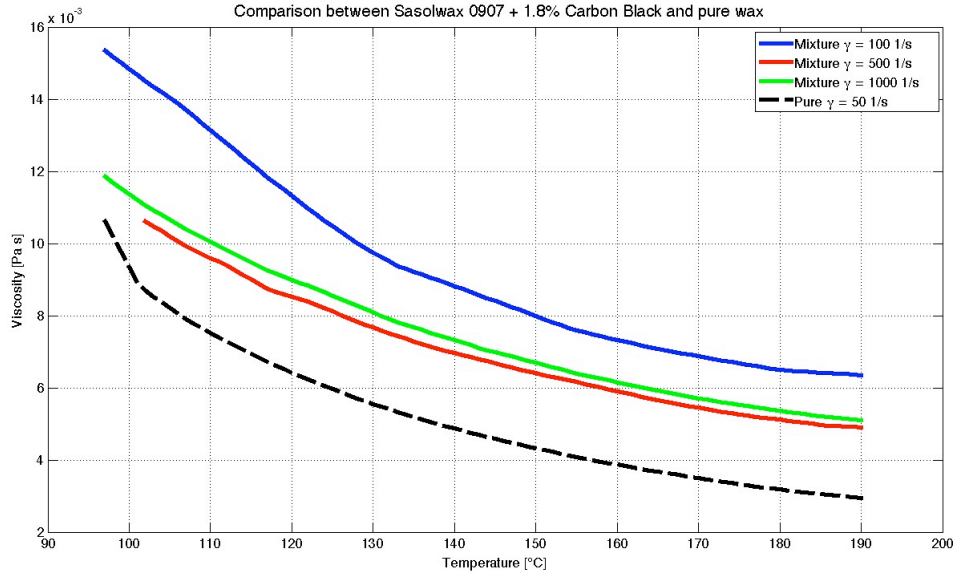

Figure 5.25: Comparison between mixture of Sasolwax 0907 + 1.8% carbon black at different shear rate and the pure wax.

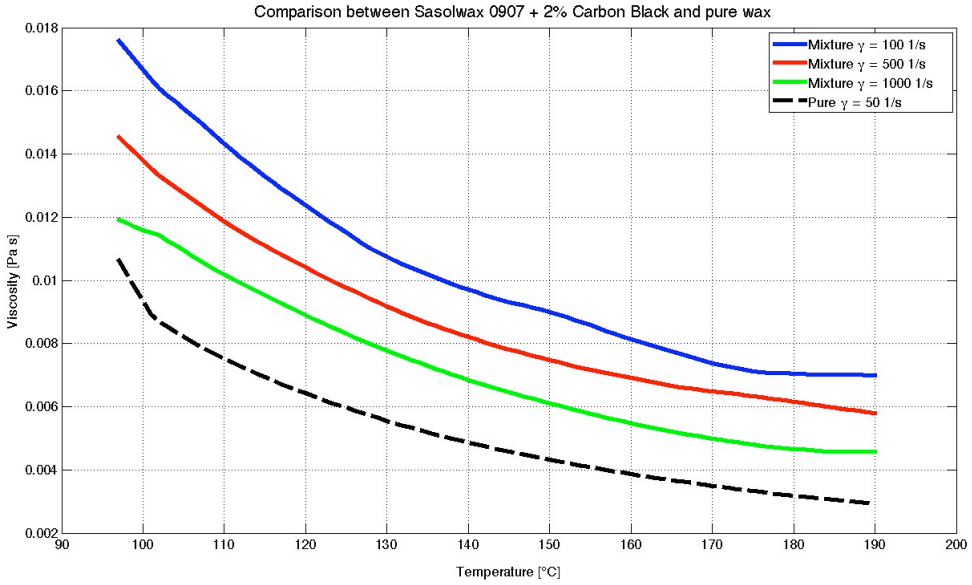

Figure 5.26: Comparison between mixture of Sasolwax 0907 + 2% carbon black at different shear rate and the pure wax.

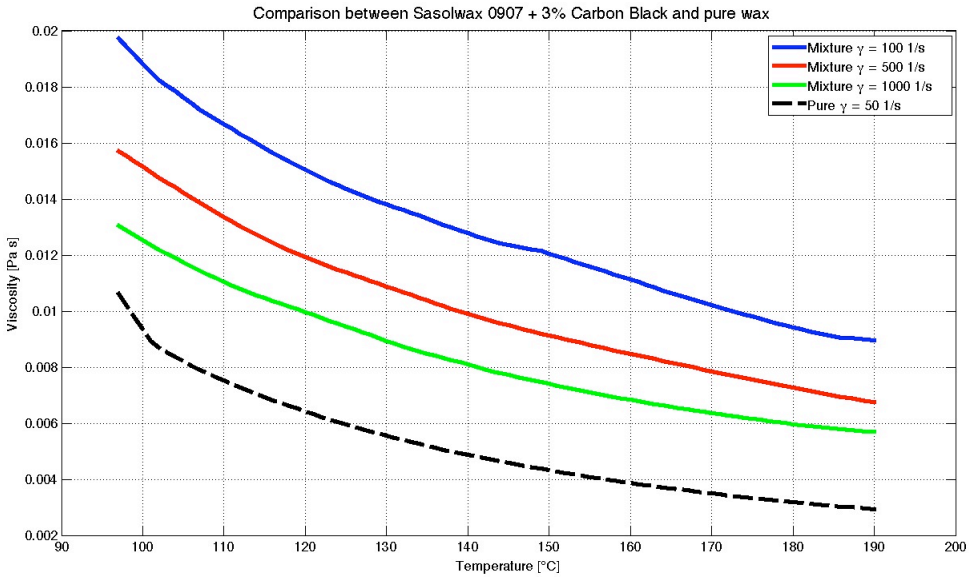

Figure 5.27: Comparison between mixture of Sasolwax 0907 + 3% carbon black at different shear rate and the pure wax.

Using collected data, it has been tried to implement a power law type model (paragraph 3.1.1) for the non-Newtonian behavior of the mixtures. The model has been based on the equation 3.2. In this case however, it has been found out that the two constants m and k depend both on shear rate and temperature. For every value of shear rate both the constants change and they have to be determined every time. In this way the model loses its predictive function and it is useless.

5.2.5 Mixtures of wax, stearic acid and carbon black

Mixtures with 88% wax, 2% carbon black and 10% stearic acid are investigated using all waxes. Stearic acid increases the mechanical properties of the fuel grain and carbon black decreases the ammount of radiant energy transmitted to the grain surface. Both these additives decrease the possibility of collapse of the fuel grain. Due to the strong correlation between viscosity and regression rate, the mixtures have been tested to determine their rheological behavior.
This kind of mixture is expected to be non-Newtonian due to the percentage of carbon black, as discussed in the previous paragraph.

Tests to determine the rheological behavior with respect to shear rate have been performed at two different temperature for each mixture: $T = 120°C$ and $T = 150°C$. The comparison between the mixture and the corresponding pure wax is made at $T = 120°C$. The difference between mixture and pure wax is high at low shear rate but it becomes very small for shear rates higher than $10^3 s^{-1}$. Mixture with Sasolwax 0907 shows the biggest difference from pure wax. Difference in percentage at $T = 120°C$ and $\dot{\gamma} = 100 s^{-1}$ is about 135%. For paraffin waxes the difference is a bit lower: 128% for 6003 and 109% for 6805. The viscosity of mixture with sasolwax 1276 at $T = 120°C$ does not change so much from the pure wax value (about 6% at $\dot{\gamma} = 100 s^{-1}$).

Comparing the curves at different temperatures it is clear that higher is the temper-

ature, lower is the viscosity. For Sasolwax 0907 and 6003 the two curves have more or less the same slope angle, as can be seen in Figure 5.28 and 5.30. 1276 curves also show the same slope angle but only for $\dot{\gamma} > 10s^{-1}$. It has also the biggest difference between the curve at $120°C$ and the one at $150°C$ (Figure 5.29). Mixture with Sasolwax 6805 shows the same behavior only for shear rate higher than $10^2 s^{-1}$, before this value the curve at higher temperature shows also higher viscosity (Figure 5.31).
In Figure 5.32 it is shown that Carlo Erba wax has the opposite behavior. The higher is the temperature the higher is the viscosity. The difference between the two curves is high for low shear rates and it becomes very small for high shear rate values.

In table 5.10 values of viscosity for the mixtures at $T = 120°C$ and $\dot{\gamma} = 100s^{-1}$ are reported. In the same table are also presented the average percentage differences between mixtures curves and the corresponding pure wax curve at $T = 120°C$. The average differences are evaluated between $10s^{-1}$ and $1000s^{-1}$.

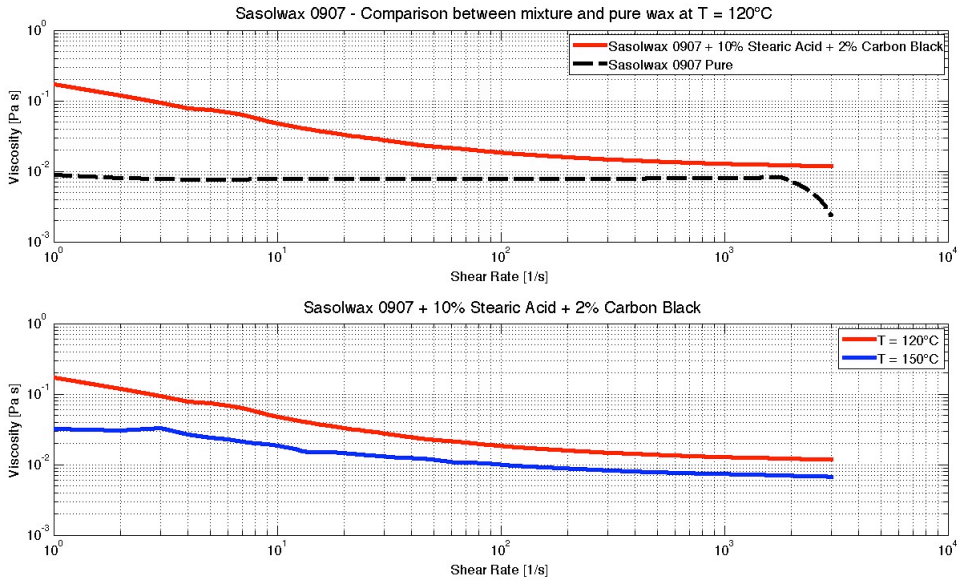

Figure 5.28: Comparison between mixture of Sasolwax 0907 with 2% carbon black and 10% stearic acid and pure wax at T = 120°C and comparison of viscosity behaviour of the mixture at different temperature.

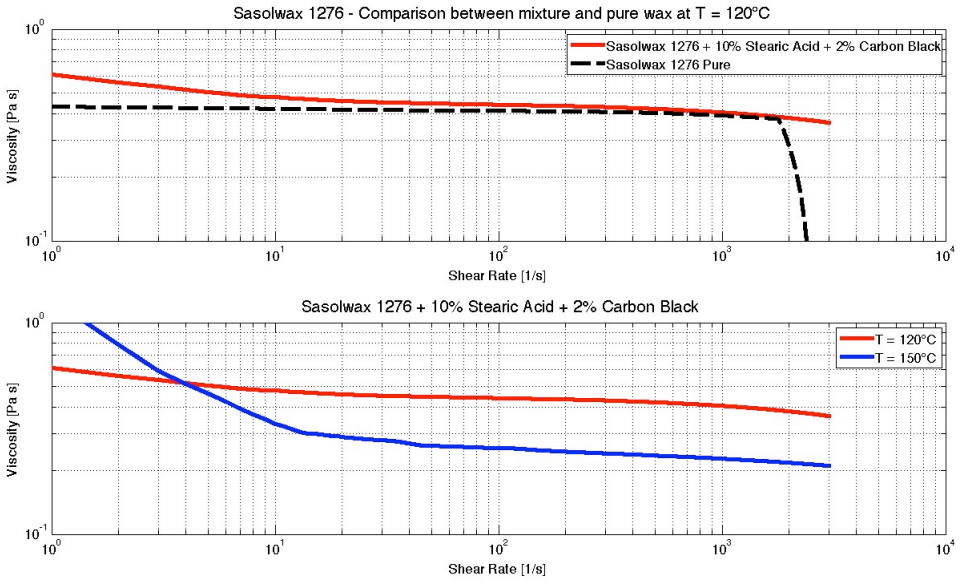

Figure 5.29: Comparison between mixture of Sasolwax 1276 with 2% carbon black and 10% stearic acid and pure wax at T = 120°C and comparison of viscosity behavior of the mixture at different temperature.

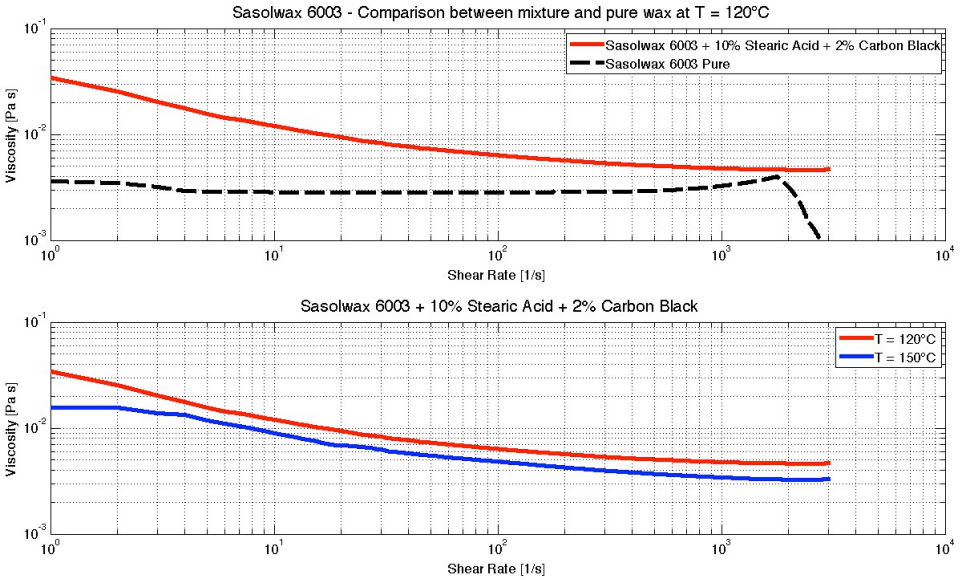

Figure 5.30: Comparison between mixture of Sasolwax 6003 with 2% carbon black and 10% stearic acid and pure wax at T = 120°C and comparison of viscosity behavior of the mixture at different temperature.

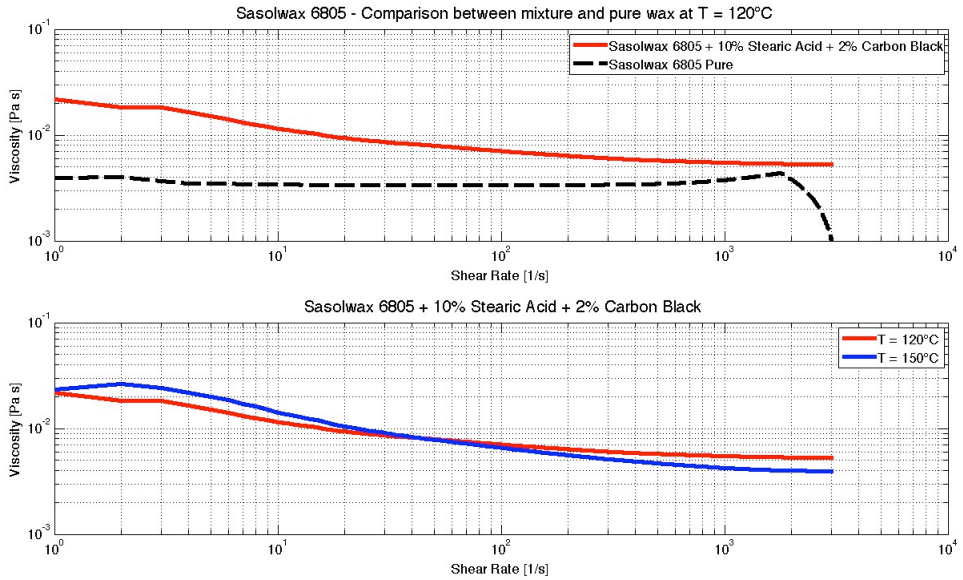

Figure 5.31: Comparison between mixture of Sasolwax 6805 with 2% carbon black and 10% stearic acid and pure wax at T = 120°C and comparison of viscosity behavior of the mixture at different temperature.

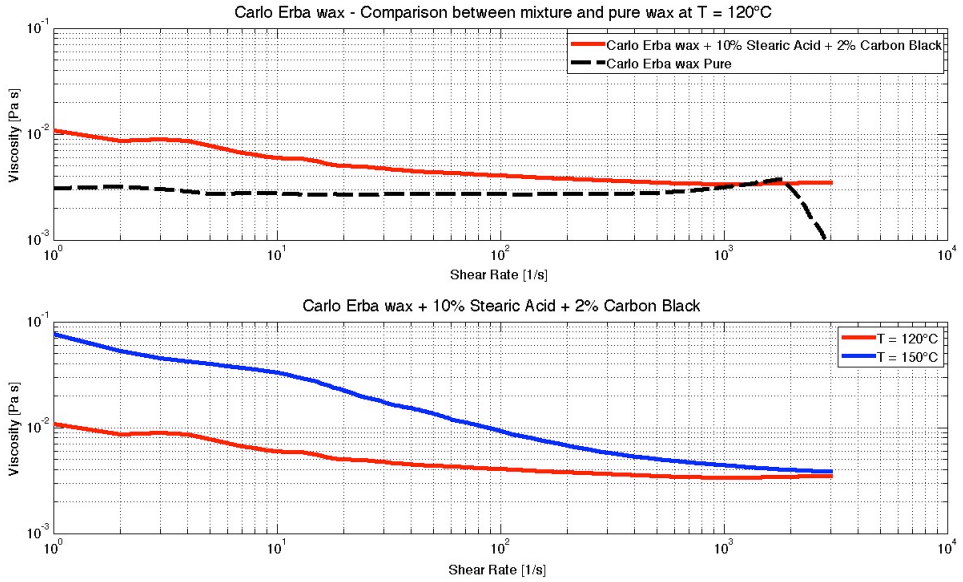

Figure 5.32: Comparison between mixture of Carlo Erba wax + 2% carbon black and 10% stearic acid and pure wax at T = 120°C and comparison of viscosity behavior of the mixture at different temperature.

Viscosity of the mixtures has been investigated also with respect to the temperature. Due to their non-Newtonian behavior, viscosity vs. temperature curves are not unique. The curves change changing the shear rate at which the test is performed.

Mixture	Value of viscosity [Pa s]	Difference from pure [%] at T=120°
0907 +2%C.B. +10%S.A.	0.0184	89.40
1276 +2%C.B. +10%S.A.	0.4397	4.91
6003 +2%C.B. +10%S.A.	0.0064	80.37
6805 +2%C.B. +10%S.A.	0.0071	73.06
Carlo Erba +2%C.B. +10%S.A.	0.0041	27.18

Table 5.10: Viscosity at T = 120°C and $\dot{\gamma} = 100\ s^{-1}$ of each mixture and average difference in percentage from pure wax with respect to shear rate.

For this reason viscosity with respect to temperature curves have been evaluated at three different values of shear rate: $300s^{-1}$, $500s^{-1}$ and $1000s^{-1}$. For each mixture the results of the three types of test are compared and they are also compared with the respective pure wax curve.

For every mixture the viscosity is higher than the pure wax viscosity. Sasolwax 1276-based mixture shows the lowest change changing the shear rate (Figure 5.34), the curves are almost overlapping. 0907-based mixture has its lowest viscosity at $\dot{\gamma} = 1000s^{-1}$ as expected. The other two curves show the opposite behavior than the expected: at $500s^{-1}$ it has higher viscosity than at $300s^{-1}$, but the difference between these two curves is small (Figure 5.33). Mixture with 6003 shows the expected behavior only for $T > 150°C$. Before this value the curve at $500s^{-1}$ is higher than the one at $300s^{-1}$. The curve at $\dot{\gamma} = 1000s^{-1}$ has very strange behavior, it has a jump around $100°C$ that brings the viscosity to its maximum value. Before and after this jump the curve is the lowest between the three curves of this mixture (Figure 5.35). This jump could be due to agglomerated carbon black particles, but because it is present in all tests done, a more in-depth investigation should be done to understand the phenomenon. 6805-based mixture shows the same behavior of 0907-based one. At $\dot{\gamma} = 500s^{-1}$ it has the higher viscosity and at $\dot{\gamma} = 1000s^{-1}$ it has the lowest viscosity(Figure 5.36).
Carlo Erba-based mixture shows a different behavior also in the viscosity vs. temperature curves. The highest curve is the one at $\dot{\gamma} = 300s^{-1}$ as expected, but the lowest one is the curve at $\dot{\gamma} = 500s^{-1}$. The curve at lowest shear rate lies in between the other two.

In table 5.11 average percentage differences between the mixtures' viscosity vs. temperature curves and corresponding pure wax curve are presented. Average differences are evaluated in temperature range $90° - 190°C$.

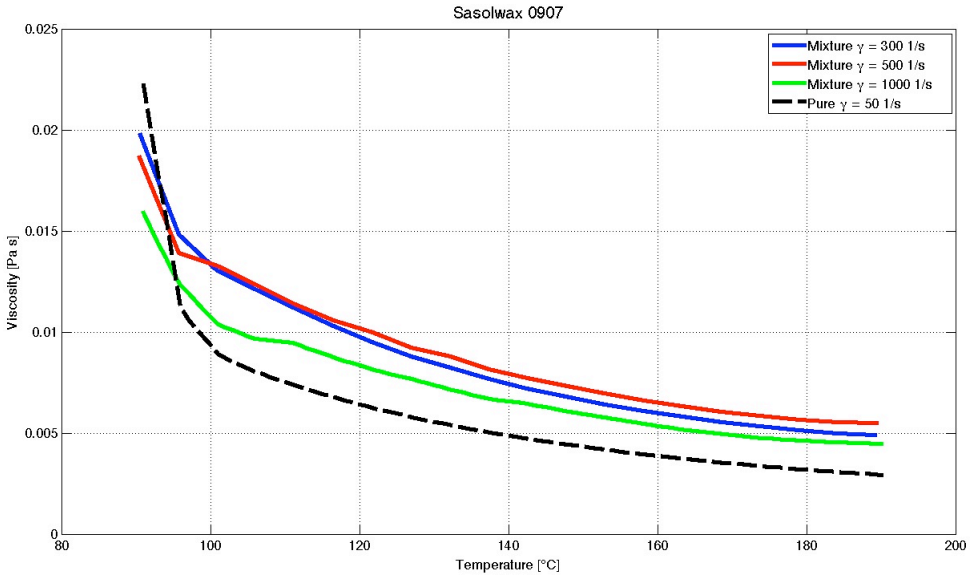

Figure 5.33: Viscosity vs. temperature of Sasolwax 0907-based mixture at different shear rate and comparison with pure wax viscosity.

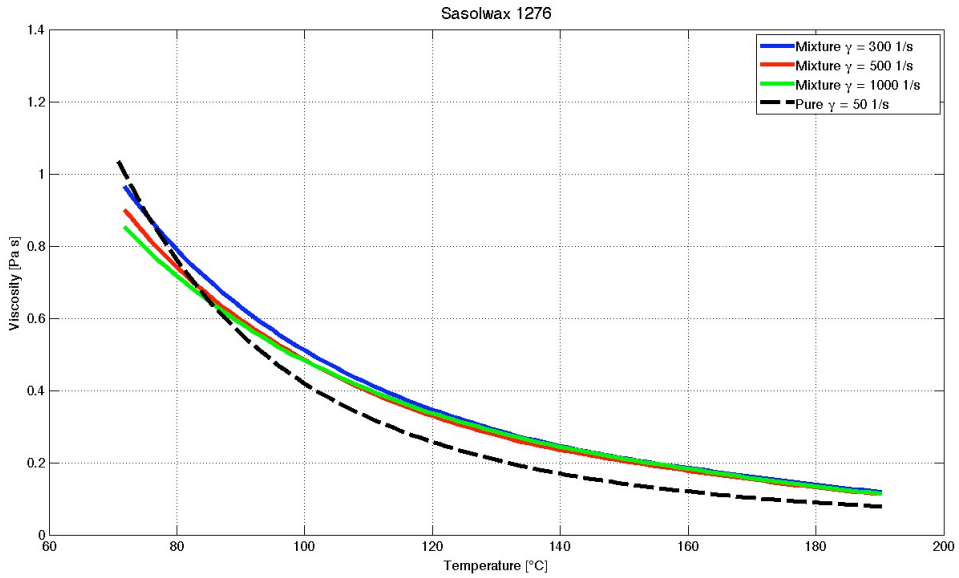

Figure 5.34: Viscosity vs. temperature of Sasolwax 1276-based mixture at different shear rate and comparison with pure wax viscosity.

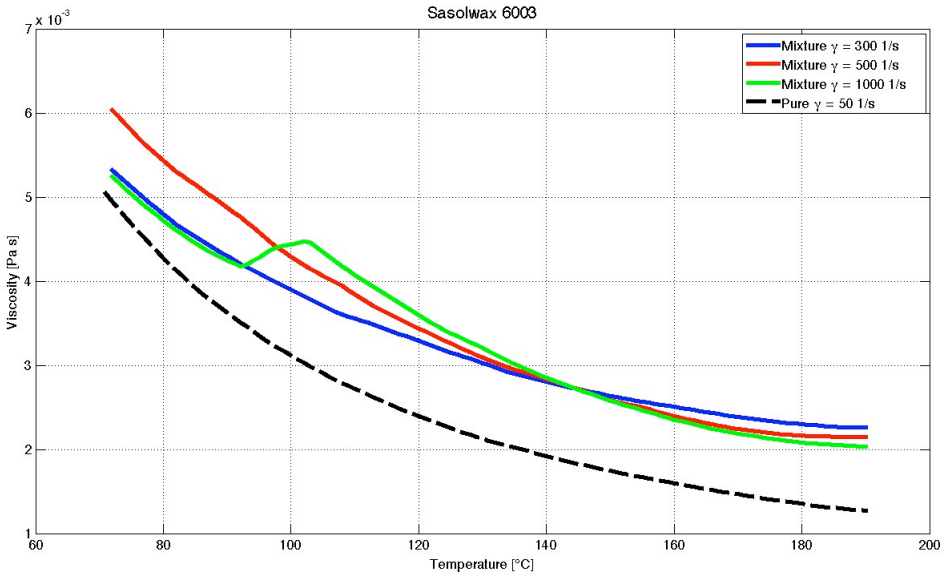

Figure 5.35: Viscosity vs. temperature of Sasolwax 6003-based mixture at different shear rate and comparison with pure wax viscosity.

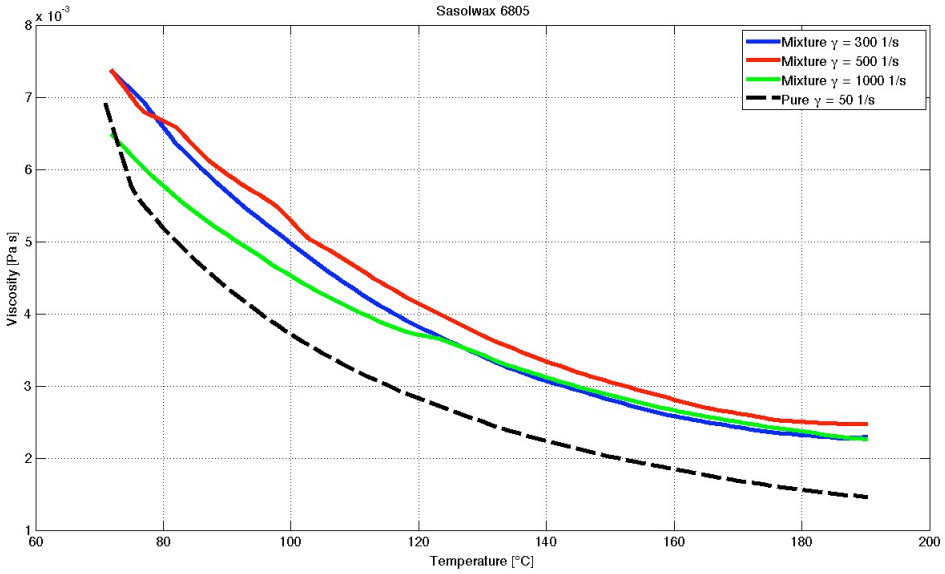

Figure 5.36: Viscosity vs. temperature of Sasolwax 6805-based mixture at different shear rate and comparison with pure wax viscosity.

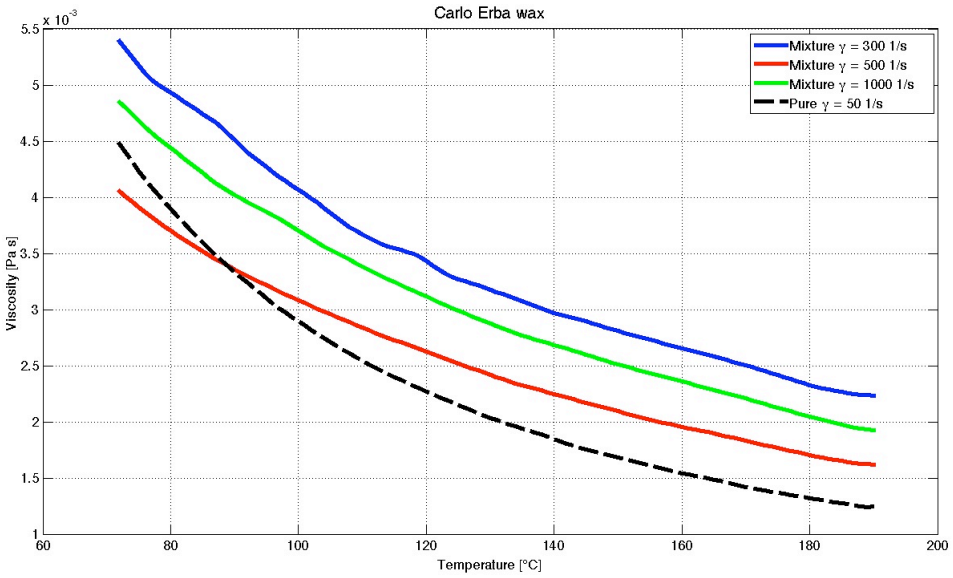

Figure 5.37: Viscosity vs. temperature of Carlo Erba wax-based mixture at different shear rate and comparison with pure wax viscosity.

Mixture	Difference from pure [%] at $\dot{\gamma} = 300\ s^{-1}$	Difference from pure [%] at $\dot{\gamma} = 500\ s^{-1}$	Difference from pure [%] at $\dot{\gamma} = 1000\ s^{-1}$
0907 mixture	44.25	52.18	27.30
1276 mixture	34.24	27.70	29.70
6003 mixture	42.11	45.66	46.11
6805 mixture	37.48	48.10	34.17
Carlo Erba mixture	56.06	17.32	40.37

Table 5.11: Average differences in percentage between mixtures and pure waxes with respect to temperature at different shear rate values.

5.2.6 Comparison with previous data

Same kind of tests has already been performed at DLR Lampoldshausen, using different rheometer set up. For this set of tests plates chosen for the rheometer were different, it has been used a plate-plate configuration using the PP35 Ti plate for all tests, moreover for the pure waxes it has also been used a rough lower plate. No cone-plate configuration has been used.
The shear rate range in which the curves of viscosity vs. shear rate have been determined is the same, while for the determination of curves of viscosity vs. temperature, the range of temperature is quite different. For this work the temperature range chosen is $190° - 90°C$ for Sasolwax 0907 and $190° - 70°C$ for all other waxes. In the set of previous measurements the temperature range chosen is $200° - 75°C$ for Sasolwax 1276 and 6805, $200° - 70°C$ for 6003 and $200° - 85°C$ for 0907. This difference in range does

not affect the measurements or the comparison. Previous tests have been performed on all Sasol waxes both pure and with some additives [30]:

- wax + 1% Poly Ethylene Co Vinyl Acetate
- wax + 5% Poly Ethylene Co Vinyl Acetate
- wax + 10% Poly Ethylene Co Vinyl Acetate
- wax + 10% Poly Ethylene Glykol
- wax + 5% Stearic Acid
- wax + 10% Stearic Acid
- wax + 5% Sasolwax 1276
- wax + 10% Sasolwax 1276
- wax + 1% Carbon Black
- wax + 10% Aluminum
- wax + 40% Aluminum

Due to the fact that some mixtures are equal to the one considered in this work, comparison between some of previous and actual results can be done.

Pure waxes show the same trend in both sets of tests: Sasolwax 1276 has the highest viscosity, than the 0907, 6805 and 6003. However values are different. Actual curves are higher than previous one for Sasolwax 0907 and 1276, while for 6003 the previous curve is higher and for 6805 the two curves cross each other at about $140°C$. As can be seen in Figure 5.38. Sasolwax 0907 shows the highest difference between the two sets of data. 1276 curve is not reported due to its too big viscosity that makes other curves not visible.

Values of vscosity at $T = 120°C$ and $\dot{\gamma} = 50s^{-1}$ of previous set of data are reported in table 5.12. In the same table also the average and maximum differences between the two types of curves for each wax are reported.

Sasolwax	η [Pa s] at $T = 120°C$ and at $\dot{\gamma} = 50\ s^{-1}$	Mean $\Delta\eta$ w.r.t. temperature [%]	Max $\Delta\eta$ w.r.t. shear rate [%]
0907	0.0072	−30.89	−40.12
1276	0.3886	−16.43	−22.66
6003	0.0030	7.47	15.01
6805	0.0041	7.61	−21.54

Table 5.12: Value of viscosity at T=120°C and $\dot{\gamma} = 50\ s^{-1}$ of previous set of data for pure waxes, and average and maximum percentage differences from actual data curves of pure waxes

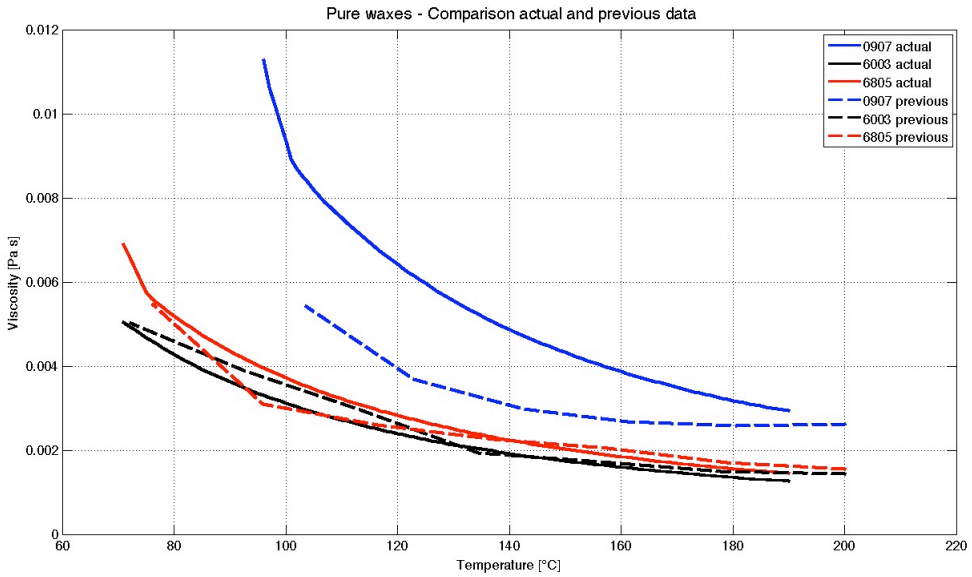

Figure 5.38: Comparison between actual and previous curves (dashed lines) of viscosity vs. temperature for pure waxes.

It has been also compared the data for mixture with 10% stearic acid and with 10% aluminum. The mixture with carbon black can not be compared due to the fact that the percentage of carbon black is different.
For mixture of 90% wax and 10% aluminum previous curves are all above the actual one, except from the 1276 curve that is lower. The differences between the two type of curves are very high, expecially for the paraffin waxes that show average differences higher than 100%.
Previous data set for the mixture with 90% Sasolwax 6003 and 10% stearic acid shows higher value of viscosity than the actual data set, while the same kind of mixture based on Sasolwax 1276 shows higher values in the actual data set.
0907-based and 6805-based mixtures with stearic acid show similar behaviors. The previous and actual curves cross each other at 130°C for 6805 and at 155°for 0907. Before that point both actual curves are higher than the previous.

In table 5.13 they are reported average and maximum differences between the curves of viscosity vs. temperature for all mixtures compared. In the same table it is also shown the value of viscosity at $T = 120°C$ and $\dot{\gamma} = 100s^{-1}$ for the set of tests previous performed at DLR.

The differences in the two data sets are due to the fact that for this work the viscosity has been sampled every 5°C, while in the previous set it was sampled every 20°C. That means that the actual data are more accurate and the curves have a more smooth behavior.
Another reason for the difference between the two sets of data is that, doing the previous tests, it was chosen a different type of plate that did not fit as best the requirements of the measurements. In fact in the plate-plate configuration of the rheometer, the shear rate is a function of the radial position (see paragraph 3.2.2). Furthermore the lower rough plate should be used paired with the upper rough plate. They are usually used to measure the viscosity of special types of liquids that, when subjected to shear rate,

Mixture	η [Pa s] at $T = 120°C$ and at $\dot{\gamma} = 100\ s^{-1}$	Mean $\Delta\eta$ w.r.t. temperature [%]	Max $\Delta\eta$ w.r.t. shear rate [%]
0907 +10%Al	0.0102	13.87	22.31
1276 +10%Al	0.3482	−22.38	−34.79
6003 +10%Al	0.0051	115.20	128.86
6805 +10%Al	0.0065	204.57	273.28
0907 +10% S.A.	0.0068	0.98	73.29
1276 +10% S.A.	0.2924	−36.96	−47.86
6003 +10% S.A.	0.0028	22.12	36.91
6805 +10% S.A.	0.0041	5.98	23.06

Table 5.13: Value of viscosity at T=120°C and $\dot{\gamma} = 100\ s^{-1}$ of the previous set of data for waxes with additives, and average and maximum percentage differences from actual data curves of mixture with 10% aluminum and 10% stearic acid.

originate a layer with very low viscosity on their surface. In this case using a normal plate-plate configuration leads to errors in measurements because the true viscosity of the fluid is not measured. Waxes do not belog to this type of fluids.

Chapter 6

Combustion Tests

6.1 Experimental apparatus

Combustion tests have been performed at DLR Lampoldshausen at test complex M11 [31].
The test bench is composed by a combustion chamber (Figure 6.2), the supply systems, the remote control system and a video recording system.
Combustion chamber is already existing, used in the past to investigate the combustion of solid fuel ramjets [32], and adjusted to perform the test campaign. It has rectangular cross section of 150 mm width and 45 mm height. A 20 mm height flame holding step is positioned in the front.
The oxidizer enters in the first part and assumes an homogeneous flow passing two flow straighteners. The solid fuel slab is glued on a steel plate and it is inserted from the bottom of the combustion chamber.
The ignition system is allocated under the flame holding step and it starts burn a mixture of gaseous hydrogen and oxygen.
On the lateral surfaces of the combustion chamber two windows are installed, one for each side, in order to enable different optical diagnostics. An high speed camera recordes every test from one of the lateral windows.
Three supply systems are used to feed the combustion system. The first one is for hydrogen and oxygen needed for the ignition, the second one for the oxidizer needed during the combustion and the last one is for the nitrogen that keeps clean the lateral windows during the combustion. The nitrogen is also used to cool down and clean the combustion chamber after each test.
The whole system is controlled from the neighboring control room by means of a remote control system.

Figure 6.1: Test bench at M11 complex at DLR Lampoldshausen.

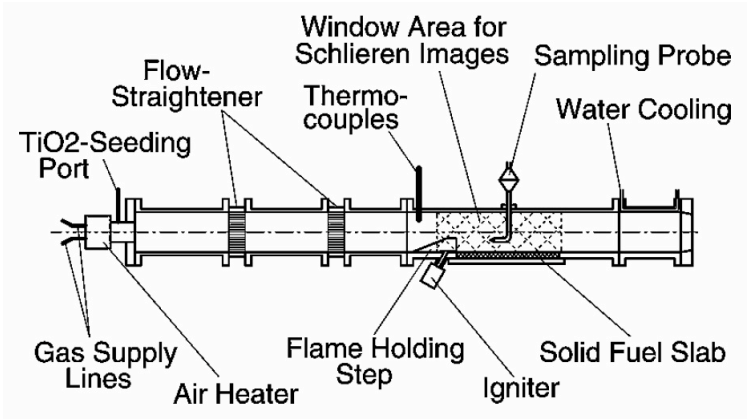

Figure 6.2: Combustion chamber scheme.

6.2 Fuel compositions and experimental conditions

Not all waxes presented in paragraph 4.2 have been tested in combustion chamber. It has been used Sasolwax 0907, 1276, 6003 and 6805. Carlo Erba wax has not been tested. Burning tests have been performed on pure waxes and mixture of 88% wax, 10% stearic acid and 2% carbon black.

All combustion tests have been performed at ambient pressure (1 bar) and with steady-state oxydizer mass flow of about 53 g/s. All tests have a duration of about 6 seconds. The oxidizer mass flow is adjusted by a flow control valve. It is measured with

a Coriolis flowmeter with an accuracy better than 0.35% and a repeatability better than 0.2% of the flow rate. Mass flow rate data are aquired in Labview via a digital protocol.

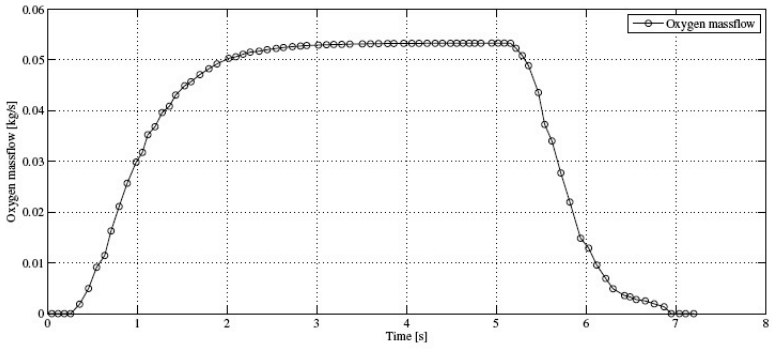

Figure 6.3: Typical oxidizer mass flow rate (Test 107).

Test sequence is programmed before the test and it is run automatically by the test bench control system. All tests have been done with the same settings shown in table 6.1.

For redundancy a separate measurement system is used for data aquisition during the tests. An ADwin measurement system by Jager Messtechnik is used for this purpose. Data aquisition on this measurement system was programmed by the proprietary software named ADbasic. All raw data is low-pass filtered via Dewetron signal amplifiers before the data aquisition. Depending on the sensor type that is used a gain can be set to the signal if needed. The measured data is then routed from ADwin via ethernet to a second PC which handles the data saving routines by a Labview program [33].

Time [s]	Action
T−30	Start of sequence
T−29	Commanding control valve
T−15	Set dome regulator pressures
T−03	Start of data acquisition
T−1	Start spark plug
T−0.2	Open ignition valve
T0	Open oxidizer main valve, start High-speed camera
T+0.5	Close ignition valve
T+5	Close oxidizer main valve, start nitrogen purge
T+10	End of sequence

Table 6.1: Automatic test sequence [33].

Manufacture of solid fuel slab

Solid fuel slabs have been created with a simple procedure in the chemical laboratory of DLR Lampoldshausen. First desired quantities of wax, stearic acid and carbon black

are weighed with a precision balance. Then wax is introduced in a glass baker and it is put on a hotplate. The hotplate temperature is set above the wax melting temperature but it has not to be too high, otherwise the wax properties will decay. Once it is totally melted, the additives (if they are necessary for the mixture) are added to the melted wax. The mixture is mixed with a steel spoon. It is then casted in a steel casing and then wait for its natural cooling. When the mixture is totally solidified the casing is removed.

In order to have a good O/F value, slab of two different dimensions have been tested. The fuel slab dimensions are shown in table 6.2.

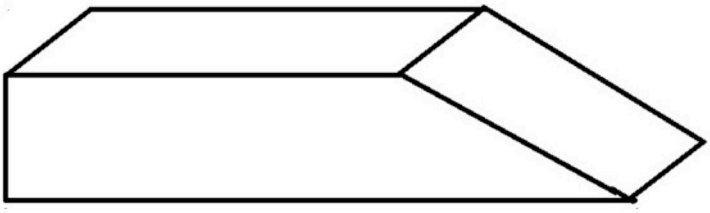

Figure 6.4: Sketch of the fuel slab used in combustion tests.

slab type	length [mm]	width [mm]	height [mm]
small slab	100	70	14
big slab	180	90	18

Table 6.2: Dimensions of slabs used for the combustion tests.

6.3 Regression rate measurements

The regression rate is strongly dependent on the mass flux. However the evaluation of the total mass flux inside the combustion chamber is not so simple due to the blowing phenomenon. To evercome this problem, as explained in chapter 2, it is usually used a simple empirical equation to theoretically evaluate the regression rate:

$$\dot{r}_f = a_0 G_{ox}^{n_r} \tag{6.1}$$

In this equation it is considered only the oxidizer mass flux, that can be easily measured. Constants a_0 and n_r are experimentally determined and they change with the fuel used. However values for these constants found in literature are related to cylindrical geometry.

In the frame of this work the measure of the regresion rate is quite difficult because the slab does not burn only on the upper surface, but also on lateral surfaces. For this reason it is not possible to measure it directly. Besides values of the regression rate for the slab are not comparable directly with the theoretical values that are calculated for a cylindrical fuel grain because the convective and radiative flux are different. In slab configuration much more heat is lost to the surroundings like the quartz glass windows and the upper metallic surface of the combustion chamber. Thus less heat is transfered

to the fuel and the regression rates measured are lower than with cylindrical fuel grains [33].

The regression rate is then calculated using the mass flow from solid fuel to the combustion zone $\dot{m}_f$ that is proportional to the density of the fuel ρ_f, its surface A_s and the regression rate:

$$\dot{m}_f = \rho_f A_s \dot{r}_f \tag{6.2}$$

The mass flow $\dot{m}_f$ is calculated dividing the mass burned by the test duration, the surface considered is the total surface of the slab that is invested by the oxidizer mass flow and the density of the wax is known. Values found in this way are time and space averaged.
It must take also into account that some measurement uncertanties are present in the results presented below. Uncertanties are due to the fact that during the test some wax flows down from the slab to the bottom of the combustion chamber and does not burn. After each test, this wax is collected if possible and it is taken into account to calculate the mass loss.

Temperaure in the combustion chamber changes changing the O/F value. Tests have been performed at constant oxidizer mass flow, under this condition the only way to change the O/F value is to change the surface of the slab. For this reason slabs with two different dimensions have been tested for pure waxes. Mixtures of wax, stearic acid and carbon black have been tested only using the big slab. Number of tests performed are reported in table 6.3.

The comparison between the small slab and big slab tests results are shown in Figure 6.5 and Figure 6.6. The regression rate value using the big slab is in general higher that the one for the small slab, this is due to the fact that, change dimensions of the slab means change O/F. In particular increase the ammount of fuel means decrease the O/F value. For the big slab O/F is between 5 and 15, while for the small slab O/F is higher up to 70. Karabeyoglu et al. proposes a correction for this effect based on the regression rate constants and the O/F ratio [11] [34].

Fuel and Slab type	Number of tests performed
0907 pure - Small	2
0907 pure - Big	4
1276 pure - Small	3
1276 pure - Big	3
6003 pure - Small	8
6003 pure - Big	2
6805 pure - Small	1
6805 pure - Big	4
0907 +10%S.A. +2%C.B. - Big	10
1276 +10%S.A. +2%C.B. - Big	3
6003 +10%S.A. +2%C.B. - Big	4
6805 +10%S.A. +2%C.B. - Big	5

Table 6.3: Number of tests performed for each fuel type.

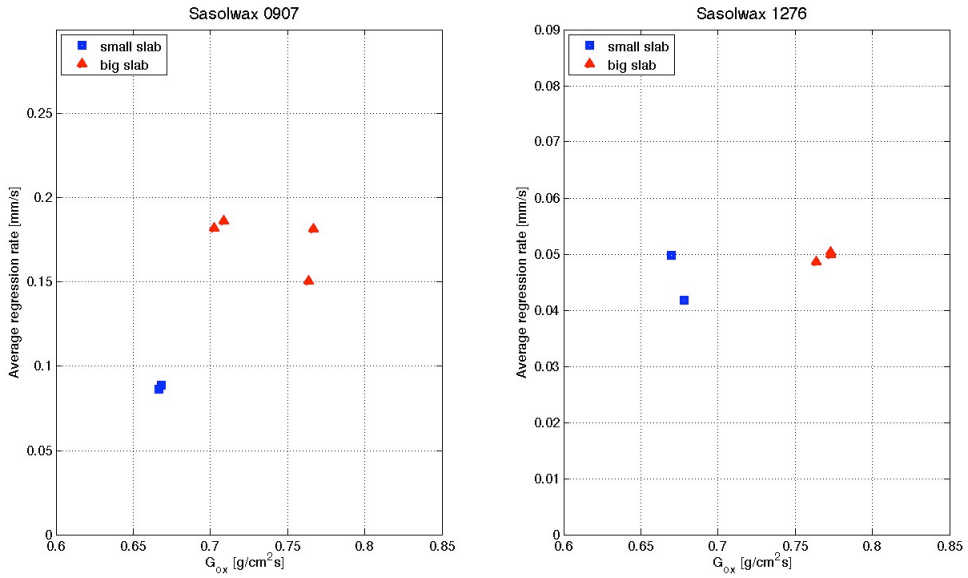

Figure 6.5: Comparison between regression rate values of small and big slab for Sasolwax 0907 (left) and Sasolwax 1276 (right).

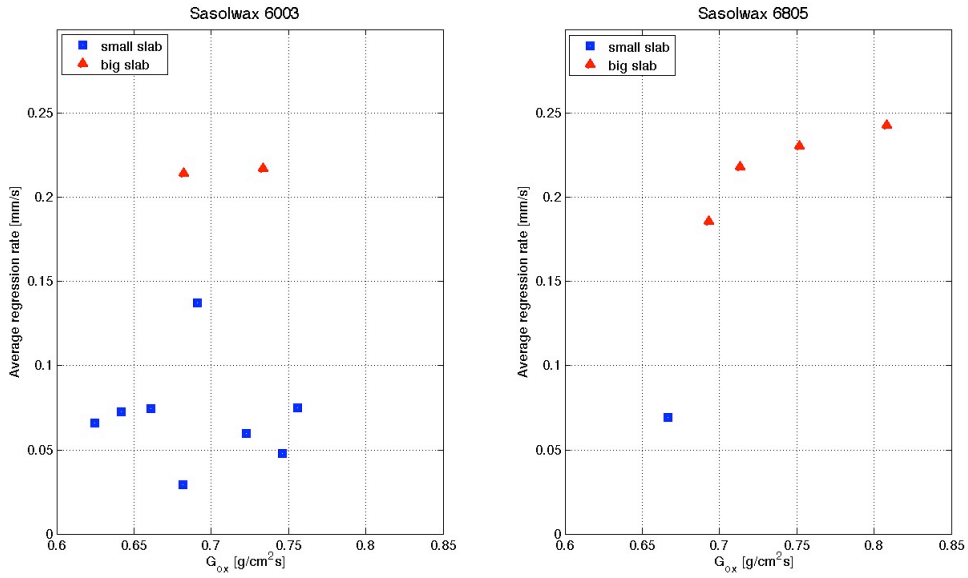

Figure 6.6: Comparison between regression rate values of small and big slab for Sasolwax 6003 (left) and Sasolwax 6805 (right).

An overview of all tests using big slabs is presented in Figure 6.7 for pure waxes and in Figure 6.8 for the mixtures. In general Sasolwax 1276 has the lowest regression rate, both pure and mixture, while the highest regression rates are shown by Sasolwax 6003 and Sasolwax 6805.

The comparison between pure waxes and mixtures is presented in Figure 6.9 by

using the mean value of all tests for each kind of wax. Average values of regression rate both for pure waxes and mixtures are shown in table 6.4, in the table are also shown the percentage differences between the regression rate values of mixtures and corresponding pure wax.

The results shown have a correspondence with the viscosity values described in chapter 5.2. The entrainment of the liquid layer is higher for fuels with lower viscosity. This leads to an increase in the entrainment phenomenon, as explained by equation 2.36, thus resulting in higher regression rate. Paraffin waxes have a less branched molecular structure, this means that their viscosity is lower, it follows that their regression rate is higher.

Due to the presence of additives the mixtures have lower regression rates than the pure waxes. The decay in regression rate value is more emphatic in Sasolwax 0907, regression rate for this mixture is 41.5% lower than the regression rate of the pure wax. For paraffin waxes (6805 and 6003) the decay is smaller: 26.2% for 6805 and only 5.5% for 6003. It seems that the decay of regression rate between mixtures and pure waxes is lower for lower values of viscosity. The only exception is Sasolwax 1276 that seems to increase its regression rate values using additives. Maybe this is due to fact that adding stearic acid the viscosity of the mixture is lower than the pure one.

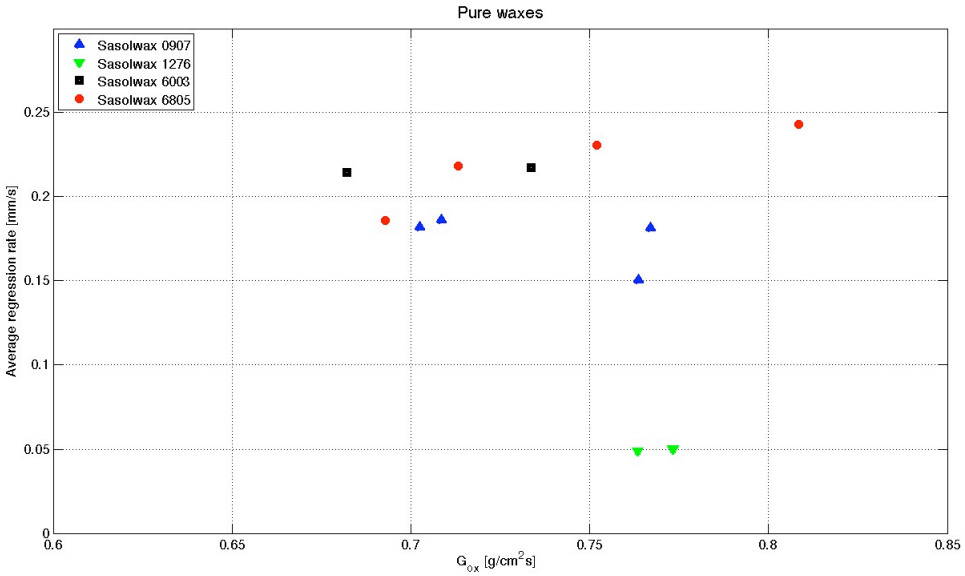

Figure 6.7: All regression rate values found for pure waxes.

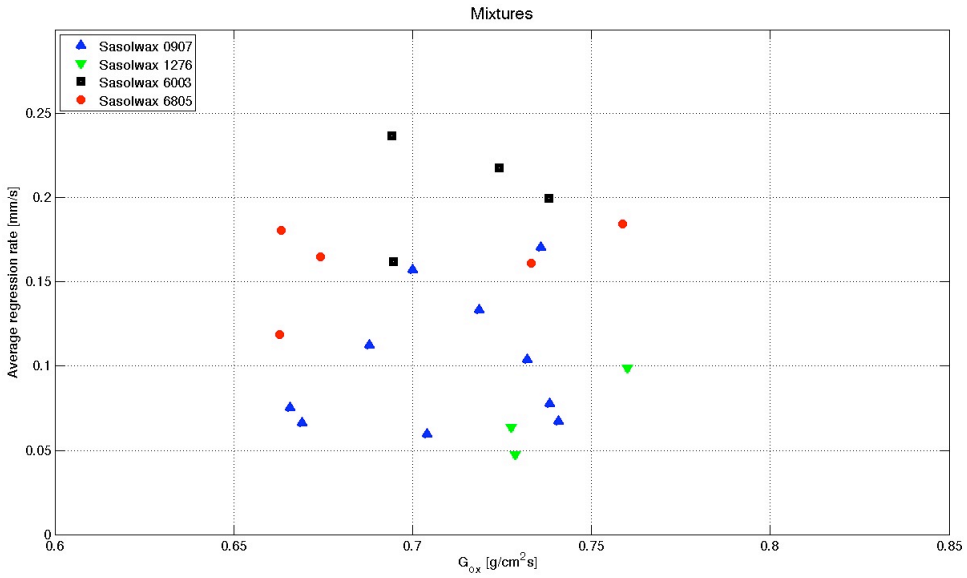

Figure 6.8: All regression rate values found for mixtures.

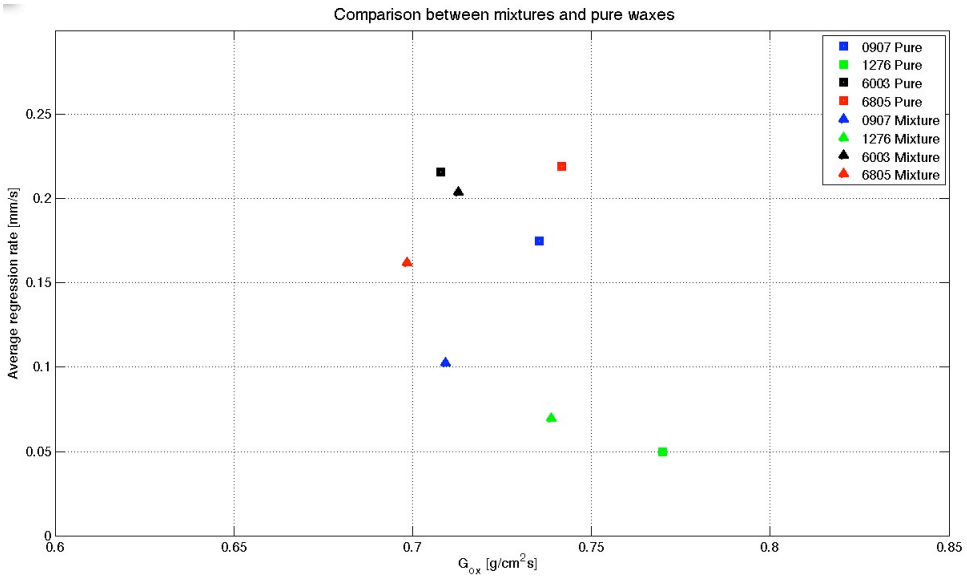

Figure 6.9: Comparison between regression rate average values of pure waxes and mixtures.

Wax	Average $\dot{r}$ mean value [mm/s]	Difference from pure [%]
0907 Pure	0.175	-
1276 Pure	0.050	-
6003 Pure	0.22	-
6805 Pure	0.22	-
0907 Mixture	0.10	−41.5
1276 Mixture	0.07	40.85
6003 Mixture	0.20	−5.5
6805 Mixture	0.16	−26.2

Table 6.4: Average values of regression rate for waxes tested, both pure and +10% stearic acid +2% carbon black. Values calculated for big slab tests.

Table 6.5: Results of successful burning tests. Regression rate and G_{ox} values are time and space averaged.

Test n°	Fuel	Test duration [s]	G_{ox} $[g/cm^2s]$	$\dot{r}_f$ $[mm/s]$
32	1276 Pure - Small	6.59	0.68	0.0418
35	1276 Pure - Small	6.61	0.67	0.0498
36	1276 Pure - Small	6.86	0.87	0.0640
44	6003 Pure - Small	6.55	0.69	0.1375
45	6003 Pure - Small	6.56	0.68	0.0294
46	6003 Pure - Small	6.35	0.66	0.0744
49	6805 Pure - Small	6.65	0.67	0.0691
52	0907 Pure - Small	6.74	0.67	0.0865
53	0907 Pure - Small	6.62	0.67	0.0888
56	6003 Pure - Small	6.62	0.64	0.0724
58	6003 Pure - Small	6.58	0.62	0.0658
59	6003 Pure - Small	6.67	0.75	0.0477
60	6003 Pure - Small	6.56	0.76	0.0748
61	6003 Pure - Small	6.62	0.72	0.0600
62	0907+10%C.B.+2%S.A.-Big	6.46	0.73	0.1042
63	0907+10%C.B.+2%S.A.-Big	6.62	0.74	0.0779
65	0907+10%C.B.+2%S.A.-Big	6.54	0.74	0.0672
66	0907+10%C.B.+2%S.A.-Big	6.50	0.70	0.0596
67	0907+10%C.B.+2%S.A.-Big	6.66	0.67	0.0755
68	0907+10%C.B.+2%S.A.-Big	6.70	0.67	0.0662
70	0907 Pure - Big	6.53	0.77	0.1815
74	0907 Pure - Big	6.54	0.76	0.1506
80	0907 Pure - Big	6.69	0.71	0.1866
81	0907 Pure - Big	6.52	0.70	0.1820
83	6805+10%C.B.+2%S.A.-Big	6.59	0.76	0.1845
84	6805+10%C.B.+2%S.A.-Big	6.65	0.73	0.1611
85	6805+10%C.B.+2%S.A.-Big	6.60	0.66	0.1806
90	1276+10%C.B.+2%S.A.-Big	6.56	0.76	0.0990
92	1276+10%C.B.+2%S.A.-Big	6.71	0.73	0.0473

Table 6.5: Continues in the next page

Table 6.5: Continues from previous page

Test n°	Fuel	Test duration [s]	G_{ox} $[g/cm^2s]$	$\dot{r}_f$ $[mm/s]$
93	1276+10%C.B.+2%S.A.-Big	6.55	0.73	0.0637
95	6003+10%C.B.+2%S.A.-Big	6.00	0.69	0.2371
96	6003+10%C.B.+2%S.A.-Big	6.74	0.72	0.2178
97	0907+10%C.B.+2%S.A.-Big	6.56	0.74	0.1707
98	0907+10%C.B.+2%S.A.-Big	6.58	0.72	0.1334
105	0907+10%C.B.+2%S.A.-Big	6.66	0.70	0.1574
106	6805 Pure - Big	6.62	0.81	0.2430
107	6805 Pure - Big	6.69	0.75	0.2306
108	6805 Pure - Big	6.69	0.71	0.2184
109	1276 Pure - Big	6.73	0.76	0.0487
112	1276 Pure - Big	6.61	0.77	0.0500
113	1276 Pure - Big	6.54	0.77	0.0504
114	6805+10%C.B.+2%S.A.-Big	6.60	0.67	0.1650
117	6003+10%C.B.+2%S.A.-Big	6.57	0.74	0.1996
122	6003+10%C.B.+2%S.A.-Big	6.24	0.69	0.1620
123	6805+10%C.B.+2%S.A.-Big	6.27	0.66	0.1187
124	6805 Pure - Big	6.25	0.69	0.1859
126	6003 Pure - Big	6.3	0.73	0.2175
128	6003 Pure - Big	6.29	0.68	0.2145
132	0907+10%C.B.+2%S.A.-Big	6.47	0.69	0.1125

6.4 Combustion Temperature

An investigation on how the combustion chamber temperature changes changing the O/F ratio has been done using CEA software. First the mixture of Sasolwax 0907, 10% stearic acid and 2% carbon black has been investigated. Chemical formula and heat of formation of the wax and stearic acid are presented in table 6.6. Values for carbon black were already implemented in the software and it was only necessary to choose the right component from the built-in list of reagents. The temperature has been calculated for values of O/F between 1 and 70. Results are shown in Figure 6.10. Then the same kind of investigation has been carried out on pure 0907. Because the behavior is expected to be the same, the range of O/F evaluated is narrower: between 1 and 14. Results are comperad with the previous in Figure 6.11.
Mixture temperature reaches its maximum ($3110K$) at $O/F = 2.8$ and then it decreases rapidly. The pure wax shows very close behavior, its maximum temperature is a bit higher ($3111.8K$) and it is reached for $O/F = 3$.
The rapid decrease of temperature after its maximum means that increasing O/F the heath transferred to the solid grain decreases. Accordingly the regression rate decreases. This phenomenon can also be seen in the comparison between small and big slab Figure 6.5 and Figure 6.6 where the small slab has a lower regression rate due to the higher O/F ratio.

Component	Chemical formula	Heat of formation [kj/mol]
Sasolwax 0907	$C_{50}H_{102}$	-1438
Stearic Acid	$C_{18}H_{36}O_2$	-948

Table 6.6: Chemical formula and heat of formation of Sasolwax 0907 and stearic acid.

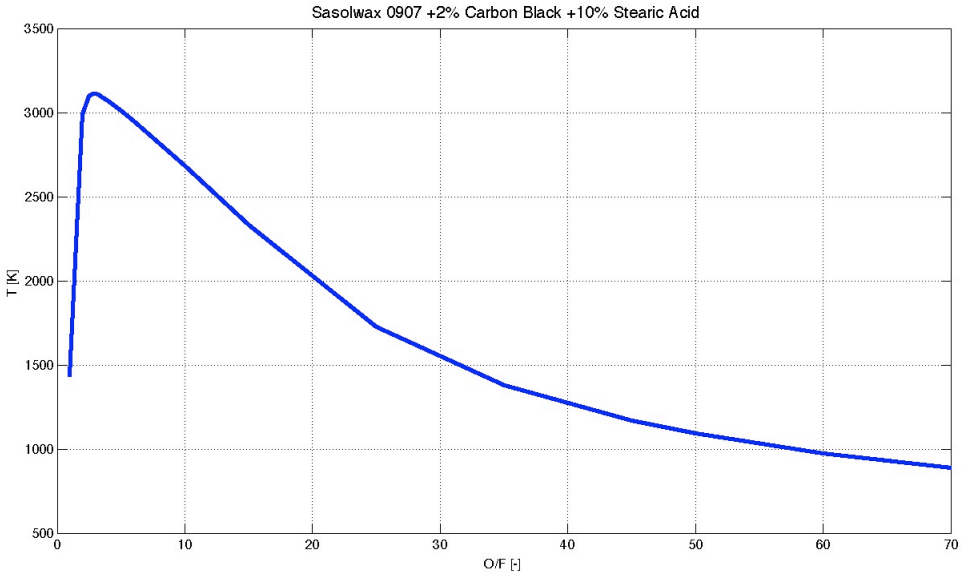

Figure 6.10: Combustion temperature vs. O/F for Sasolwax 0907 +10% stearic acid +2% carbon black.

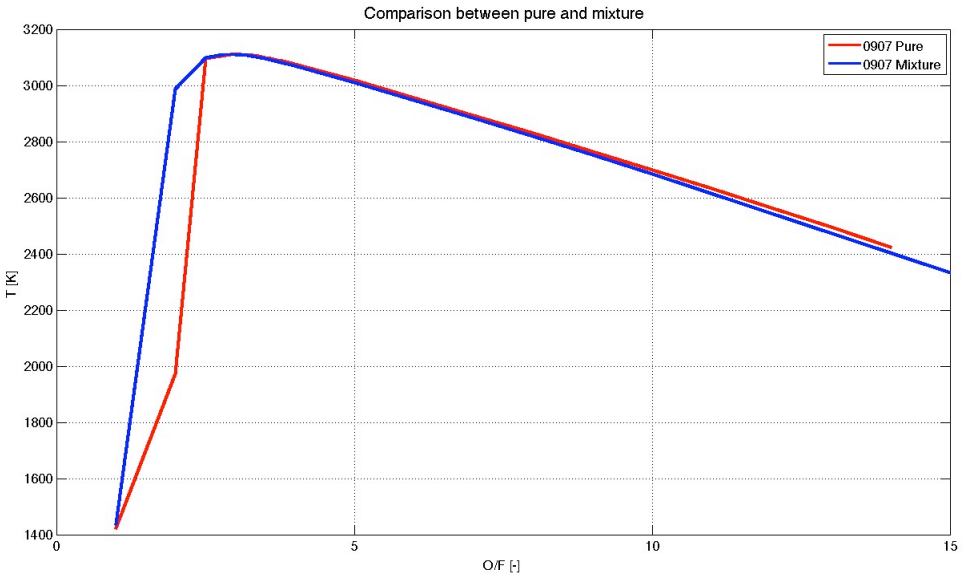

Figure 6.11: Combustion temperature vs. O/F for Sasolwax 0907 pure and with additives.

6.5 Comparison with SPLab data

Tests to investigate the regression rate of the same wax-based mixtures tested at DLR have been done at SPLab of Politecnico di Milano. Tests have been performed in a 2D radial micro-burner at reference conditions of 16 *bar* chamber pressure and 210 Nl/min oxidizer flow rate. Gaseous oxygen has been used as oxidizer. To ensure quasi-steady operation conditions, pressure and oxidizer mass flow have been maintained constant during the combustion. The internal cooling of the chamber is achieved using air with low oxygen content mixture or nitrogen. Values of regression rate found at SPLab are presented in table 6.7. Values presented are instantaneous. Comparing these values with reference values of HTPB baseline, the difference results to be higher than 150%. The only exception is Sasolwax 1276 in which the increase in regression rate is at least 41% [35].

G_{ox} $kg/(m^2s)$	HTPB baseline $\dot{r}[mm/s]$	Cerlo Erba mixture $\dot{r}[mm/s]$	0907 mixture $\dot{r}[mm/s]$	1276 mixture $\dot{r}[mm/s]$	6003 mixture $\dot{r}[mm/s]$	6805 mixture $\dot{r}[mm/s]$
120	0.520	1.646	1.214	0.773	1.511	1.439
150	0.589	1.841	1.441	0.776	1.761	1.611
200	0.645	2.225	1.691	0.853	2.258	1.940
230	0.691	2.515	1.870	0.906	2.645	2.184

Table 6.7: Regression rate values obtained by tests peformed at SPLab.

The geometry of tests performed at DLR is a 2D slab configuration, while at SPLab it has been used a 2D radial geometry. Moreover the operational conditions are different: at DLR the burning tests have been performed at 1 *bar* and with oxidizer mass flow of 53 g/s. While at SPLab tests have been performed at 16 *bar* and with oxidizer mass flow of 210 Nl/min ($\simeq$ 5 g/s). Also the oxidizer mass fluxes are different: between 5 and 35 g/cm^2s for SPLab tests and between 0.6 and 0.85 g/cm^2s for DLR tests.
Due to all these motivations the comparison between the two sets of data can be done only in a qualitative way. The two data sets show the same trend, Sasolwax 1276 is the one with lowest regression rate, than the 0907 and higher regression rate is achieved for 6805 and 6003. In SPLab also the Carlo Erba wax has been tested. This paraffin wax is resulted to have the highest regression rate. This is expected also from viscosity behavior, Carlo Erba wax in fact has the lowest viscosity.

Chapter 7

Conclusions and Future Work

Regression rate in liquefying hybrid propellants is strongly dependent on the viscosity of the melt layer. Decreasing viscosity leads to an increase in regression rate value. In this work, measurements of both these values have been performed on different waxes.

Viscosity measurements have been performed on five different waxes: three paraffin waxes (Sasolwax 6003, 6805 and Carlo Erba wax), one microcrystalline wax (Sasolwax 0907) and one wax with some additives already inserted by the manufacturer (Sasolwax 1276). All waxes have been tested both pure and with some additives like aluminum, stearic acid and carbon black.
Viscosity is strongly dependent on chemical structure of the molecules. Paraffin waxes show the lowest viscosity values due to their molecules with few branches. Microcrystalline wax has a more branched structure that counteracts the flow and leads to higher viscosity. Viscosity of wax with already added additives is two orders of magnitude higher than the others.
All pure waxes have Newtonian behavior, that means that the dynamic viscosity does not depend on the shear rate.

In general additives lead to an increase in viscosity, except for Sasolwax 1276 with stearic acid and with aluminum, that decreases its viscosity. Most of wax-based mixtures also show Newtonian behavior, the exception is for mixtures with carbon black. It shows shear thinning behavior in mixture with carbon black content higher than 1.8%. In this case viscosity decreases increasing the shear rate and a unique viscosity value can not be determined anymore.

Combustion tests have been perfomed only on Sasol waxes, both pure and in mixture with 10% stearic acid and 2% carbon black. Regression rate values change according to the wax type and the presence of additives. It is higher for waxes with lower viscosity. Lower viscosity leads to higher instability of melt layer, that means more remarked entrainment phenomenon.

CEA simulation of combustion chamber temperature shows that, after the stoichiometric value (around 3), temperature decreases and so the regression rate. This is also found experimentally by burning at two differents O/F: the regression rate is higher for lower O/F.

To extend the experimental database tests with higher burning time and at different

pressures in combustion chamber shall be done. Moreover the effect of other additives in wax-based hybrid fuels shall be investigated.
In addition further investigation should involve the mechanical properties of wax-based fuels to characterize the structural behavior.

Appendix A

Viscosity data

In this chapter the viscosity values of Newtonian mixtures tested are presented, they are sampled every $10°C$. Also the data for mixture with 88% wax 10% stearic acid and 2% carbon black are shown at three different shear rate values.

Pure waxes					
T $[°C]$	Viscosity $[Pa \cdot s]$				
	0907	1276	6003	6805	Carlo Erba
80	-	0.7603	$4.272 \cdot 10^{-3}$	$5.186 \cdot 10^{-3}$	$3.898 \cdot 10^{-3}$
90	$3.326 \cdot 10^{-2}$	0.5581	$3.623 \cdot 10^{-3}$	$4.355 \cdot 10^{-3}$	$3.335 \cdot 10^{-3}$
100	$9.344 \cdot 10^{-3}$	0.4199	$3.118 \cdot 10^{-3}$	$3.718 \cdot 10^{-3}$	$2.896 \cdot 10^{-3}$
110	$7.525 \cdot 10^{-3}$	0.3256	$2.721 \cdot 10^{-3}$	$3.220 \cdot 10^{-3}$	$2.545 \cdot 10^{-3}$
120	$6.421 \cdot 10^{-3}$	0.2572	$2.396 \cdot 10^{-3}$	$2.828 \cdot 10^{-3}$	$2.269 \cdot 10^{-3}$
130	$5.555 \cdot 10^{-3}$	0.2069	$2.126 \cdot 10^{-3}$	$2.504 \cdot 10^{-3}$	$2.035 \cdot 10^{-3}$
140	$4.869 \cdot 10^{-3}$	0.1698	$1.922 \cdot 10^{-3}$	$2.239 \cdot 10^{-3}$	$1.845 \cdot 10^{-3}$
150	$4.326 \cdot 10^{-3}$	0.1419	$1.743 \cdot 10^{-3}$	$2.021 \cdot 10^{-3}$	$1.680 \cdot 10^{-3}$
160	$3.867 \cdot 10^{-3}$	0.1200	$1.598 \cdot 10^{-3}$	$1.847 \cdot 10^{-3}$	$1.541 \cdot 10^{-3}$
170	$3.493 \cdot 10^{-3}$	0.1028	$1.468 \cdot 10^{-3}$	$1.687 \cdot 10^{-3}$	$1.421 \cdot 10^{-3}$
180	$3.180 \cdot 10^{-3}$	$0.8919 \cdot 10^{-1}$	$1.352 \cdot 10^{-3}$	$1.557 \cdot 10^{-3}$	$1.320 \cdot 10^{-3}$
190	$2.934 \cdot 10^{-3}$	$0.7877 \cdot 10^{-1}$	$1.272 \cdot 10^{-3}$	$1.464 \cdot 10^{-3}$	$1.249 \cdot 10^{-3}$

Table A.1: Viscosity data of pure waxes between $80°C$ and $190°C$, sampled every $10°C$.

90% Wax + 10% Aluminum				
T $[°C]$	Viscosity $[Pa \cdot s]$			
	0907	1276	6003	6805
80	-	0.5507	$4.724 \cdot 10^{-3}$	$5.603 \cdot 10^{-3}$
90	-	0.4104	$3.970 \cdot 10^{-3}$	$4.710 \cdot 10^{-3}$
100	$2.896 \cdot 10^{-3}$	0.3163	$3.437 \cdot 10^{-3}$	$4.061 \cdot 10^{-3}$
110	$2.545 \cdot 10^{-3}$	0.2488	$2.897 \cdot 10^{-3}$	$3.466 \cdot 10^{-3}$
120	$2.269 \cdot 10^{-3}$	0.1994	$2.582 \cdot 10^{-3}$	$3.119 \cdot 10^{-3}$
130	$2.035 \cdot 10^{-3}$	0.1633	$2.284 \cdot 10^{-3}$	$2.773 \cdot 10^{-3}$
140	$1.845 \cdot 10^{-3}$	0.1366	$2.092 \cdot 10^{-3}$	$2.576 \cdot 10^{-3}$
150	$1.680 \cdot 10^{-3}$	0.1175	$1.958 \cdot 10^{-3}$	$2.455 \cdot 10^{-3}$
160	$1.541 \cdot 10^{-3}$	0.1033	$1.827 \cdot 10^{-3}$	$2.309 \cdot 10^{-3}$
170	$1.421 \cdot 10^{-3}$	$0.9282 \cdot 10^{-1}$	$1.736 \cdot 10^{-3}$	$2.212 \cdot 10^{-3}$
180	$1.320 \cdot 10^{-3}$	$0.8500 \cdot 10^{-1}$	$1.675 \cdot 10^{-3}$	$2.110 \cdot 10^{-3}$
190	$1.249 \cdot 10^{-3}$	$0.7939 \cdot 10^{-1}$	$1.638 \cdot 10^{-3}$	$1.967 \cdot 10^{-3}$

Table A.2: Viscosity data of mixtures with 90% wax + 10% aluminum between $80°C$ and $190°C$, sampled every $10°C$.

90% Wax + 10% Stearic Acid				
T $[°C]$	Viscosity $[Pa \cdot s]$			
	0907	1276	6003	6805
80	-	0.6662	$4.409 \cdot 10^{-3}$	$5.950 \cdot 10^{-3}$
90	-	0.4879	$3.709 \cdot 10^{-3}$	$4.970 \cdot 10^{-3}$
100	$8.775 \cdot 10^{-3}$	0.3700	$3.176 \cdot 10^{-3}$	$4.233 \cdot 10^{-3}$
110	$7.370 \cdot 10^{-3}$	0.2875	$2.762 \cdot 10^{-3}$	$3.650 \cdot 10^{-3}$
120	$6.309 \cdot 10^{-3}$	0.2275	$2.425 \cdot 10^{-3}$	$3.185 \cdot 10^{-3}$
130	$5.440 \cdot 10^{-3}$	0.1828	$2.152 \cdot 10^{-3}$	$2.812 \cdot 10^{-3}$
140	$4.754 \cdot 10^{-3}$	0.1491	$1.920 \cdot 10^{-3}$	$2.498 \cdot 10^{-3}$
150	$4.205 \cdot 10^{-3}$	0.1236	$1.738 \cdot 10^{-3}$	$2.252 \cdot 10^{-3}$
160	$3.748 \cdot 10^{-3}$	0.1035	$1.591 \cdot 10^{-3}$	$2.041 \cdot 10^{-3}$
170	$3.372 \cdot 10^{-3}$	$0.8786 \cdot 10^{-1}$	$1.467 \cdot 10^{-3}$	$1.861 \cdot 10^{-3}$
180	$3.051 \cdot 10^{-3}$	$0.7567 \cdot 10^{-1}$	$1.384 \cdot 10^{-3}$	$1.723 \cdot 10^{-3}$
190	$2.797 \cdot 10^{-3}$	$0.6595 \cdot 10^{-1}$	$1.346 \cdot 10^{-3}$	$1.596 \cdot 10^{-3}$

Table A.3: Viscosity data of mixtures with 90% wax + 10% stearic acid between $80°C$ and $190°C$, sampled every $10°C$.

80% Wax + 10% Stearic Acid + 2% Carbon Black					
T $[°C]$	Viscosity $[Pa \cdot s]$ at $\dot{\gamma} = 300\ s^{-1}$				
	0907	1276	6003	6805	Carlo Erba
80	-	0.7901	$4.799 \cdot 10^{-3}$	$6.582 \cdot 10^{-3}$	$4.930 \cdot 10^{-3}$
90	$2.410 \cdot 10^{-2}$	0.6305	$4.297 \cdot 10^{-3}$	$5.683 \cdot 10^{-3}$	$4.507 \cdot 10^{-3}$
100	$1.335 \cdot 10^{-2}$	0.5115	$3.900 \cdot 10^{-3}$	$4.976 \cdot 10^{-3}$	$4.068 \cdot 10^{-3}$
110	$1.140 \cdot 10^{-2}$	0.419	$3.553 \cdot 10^{-3}$	$4.333 \cdot 10^{-3}$	$3.671 \cdot 10^{-3}$
120	$9.762 \cdot 10^{-3}$	0.3463	$3.287 \cdot 10^{-3}$	$3.820 \cdot 10^{-3}$	$3.430 \cdot 10^{-3}$
130	$8.472 \cdot 10^{-3}$	0.290	$3.027 \cdot 10^{-3}$	$3.409 \cdot 10^{-3}$	$3.178 \cdot 10^{-3}$
140	$7.434 \cdot 10^{-3}$	0.2462	$2.808 \cdot 10^{-3}$	$3.071 \cdot 10^{-3}$	$2.970 \cdot 10^{-3}$
150	$6.618 \cdot 10^{-3}$	0.212	$2.637 \cdot 10^{-3}$	$2.804 \cdot 10^{-3}$	$2.808 \cdot 10^{-3}$
160	$5.989 \cdot 10^{-3}$	0.1852	$2.507 \cdot 10^{-3}$	$2.578 \cdot 10^{-3}$	$2.652 \cdot 10^{-3}$
170	$5.499 \cdot 10^{-3}$	0.1614	$2.386 \cdot 10^{-3}$	$2.427 \cdot 10^{-3}$	$2.503 \cdot 10^{-3}$
180	$5.108 \cdot 10^{-3}$	0.1384	$2.299 \cdot 10^{-3}$	$2.321 \cdot 10^{-3}$	$2.328 \cdot 10^{-3}$
190	$4.903 \cdot 10^{-3}$	0.1198	$2.258 \cdot 10^{-3}$	$2.292 \cdot 10^{-3}$	$2.231 \cdot 10^{-3}$

Table A.4: Viscosity data of mixtures with 88% wax + 10% stearic acid + 2% carbon black at $\dot{\gamma} = 300\ s^{-1}$, between $80°C$ and $190°C$, sampled every $10°C$.

80% Wax + 10% Stearic Acid + 2% Carbon Black					
T $[°C]$	Viscosity $[Pa \cdot s]$ at $\dot{\gamma} = 500\ s^{-1}$				
	0907	1276	6003	6805	Carlo Erba
80	-	0.7422	$5.433 \cdot 10^{-3}$	$6.671 \cdot 10^{-3}$	$3.702 \cdot 10^{-3}$
90	$2.870 \cdot 10^{-2}$	0.5953	$4.873 \cdot 10^{-3}$	$5.933 \cdot 10^{-3}$	$3.560 \cdot 10^{-3}$
100	$1.337 \cdot 10^{-2}$	0.4852	$4.294 \cdot 10^{-3}$	$5.290 \cdot 10^{-3}$	$3.840 \cdot 10^{-3}$
110	$1.163 \cdot 10^{-2}$	0.3975	$3.846 \cdot 10^{-3}$	$4.660 \cdot 10^{-3}$	$2.839 \cdot 10^{-3}$
120	$1.018 \cdot 10^{-2}$	0.3283	$3.436 \cdot 10^{-3}$	$4.136 \cdot 10^{-3}$	$2.623 \cdot 10^{-3}$
130	$8.962 \cdot 10^{-3}$	0.2758	$3.093 \cdot 10^{-3}$	$3.699 \cdot 10^{-3}$	$2.419 \cdot 10^{-3}$
140	$7.944 \cdot 10^{-3}$	0.2353	$2.838 \cdot 10^{-3}$	$3.343 \cdot 10^{-3}$	$2.248 \cdot 10^{-3}$
150	$7.165 \cdot 10^{-3}$	0.2038	$2.583 \cdot 10^{-3}$	$3.055 \cdot 10^{-3}$	$2.094 \cdot 10^{-3}$
160	$6.515 \cdot 10^{-3}$	0.1775	$2.392 \cdot 10^{-3}$	$2.811 \cdot 10^{-3}$	$1.953 \cdot 10^{-3}$
170	$5.991 \cdot 10^{-3}$	0.1536	$2.241 \cdot 10^{-3}$	$2.620 \cdot 10^{-3}$	$1.832 \cdot 10^{-3}$
180	$5.645 \cdot 10^{-3}$	0.1315	$2.165 \cdot 10^{-3}$	$2.504 \cdot 10^{-3}$	$1.704 \cdot 10^{-3}$
190	$5.529 \cdot 10^{-3}$	0.1137	$2.147 \cdot 10^{-3}$	$2.475 \cdot 10^{-3}$	$1.616 \cdot 10^{-3}$

Table A.5: Viscosity data of mixtures with 88% wax + 10% stearic acid + 2% carbon black at $\dot{\gamma} = 500\ s^{-1}$, between $80°C$ and $190°C$, sampled every $10°C$.

80% Wax + 10% Stearic Acid + 2% Carbon Black					
T $[°C]$	Viscosity $[Pa \cdot s]$ at $\dot{\gamma} = 1000\ s^{-1}$				
	0907	1276	6003	6805	Carlo Erba
80	-	0.7174	$4.721 \cdot 10^{-3}$	$5.770 \cdot 10^{-3}$	$4.439 \cdot 10^{-3}$
90	-	0.5855	$4.246 \cdot 10^{-3}$	$5.090 \cdot 10^{-3}$	$4.021 \cdot 10^{-3}$
100	$1.072 \cdot 10^{-2}$	0.4831	$4.438 \cdot 10^{-3}$	$4.526 \cdot 10^{-3}$	$3.703 \cdot 10^{-3}$
110	$9.503 \cdot 10^{-3}$	0.4024	$4.076 \cdot 10^{-3}$	$4.052 \cdot 10^{-3}$	$3.384 \cdot 10^{-3}$
120	$8.337 \cdot 10^{-3}$	0.3368	$3.594 \cdot 10^{-3}$	$3.707 \cdot 10^{-3}$	$3.225 \cdot 10^{-3}$
130	$7.367 \cdot 10^{-3}$	0.2854	$3.200 \cdot 10^{-3}$	$3.426 \cdot 10^{-3}$	$2.872 \cdot 10^{-3}$
140	$6.572 \cdot 10^{-3}$	0.2441	$2.854 \cdot 10^{-3}$	$3.118 \cdot 10^{-3}$	$2.684 \cdot 10^{-3}$
150	$5.947 \cdot 10^{-3}$	0.2106	$2.576 \cdot 10^{-3}$	$2.868 \cdot 10^{-3}$	$2.510 \cdot 10^{-3}$
160	$5.356 \cdot 10^{-3}$	0.1832	$2.352 \cdot 10^{-3}$	$2.658 \cdot 10^{-3}$	$2.359 \cdot 10^{-3}$
170	$4.906 \cdot 10^{-3}$	0.1572	$2.189 \cdot 10^{-3}$	$2.502 \cdot 10^{-3}$	$2.208 \cdot 10^{-3}$
180	$4.604 \cdot 10^{-3}$	0.1337	$2.082 \cdot 10^{-3}$	$2.369 \cdot 10^{-3}$	$2.046 \cdot 10^{-3}$
190	$4.467 \cdot 10^{-3}$	0.1154	$2.030 \cdot 10^{-3}$	$2.259 \cdot 10^{-3}$	$1.922 \cdot 10^{-3}$

Table A.6: Viscosity data of mixtures with 88% wax + 10% stearic acid + 2% carbon black at $\dot{\gamma} = 1000\ s^{-1}$, between $80°C$ and $190°C$, sampled every $10°C$.

Bibliography

[1] George P. Sutton and Oscar Biblarz. *Rocket Propulsion Elements*. John Wiley & Sons, 2010.

[2] D. Altman. "Highlights in Hybrid Rocket History". In: *10th InternationalWorkshop on Combustion and Propulsion*. 2003.

[3] L. T. De Luca. *Problemi energetici in propulsione aerospaziale*. Politecnico di Milano, 2007.

[4] Space Propulsion Group website. Last visited: 5th December 2013. URL: http://www.spg-corp.com/.

[5] D. Altman. "Hybrid rocket development history". In: *27th AIAA/ASME/SAE/ASEE Joint Propulsion Conference and Exhibit*. 1991.

[6] G. A. Marxman and M. Gilbert. "Turbulent Boundary Layer Combustion in the Hybrid Rocket". In: *9th International Symposium on Combustion*. 1963.

[7] G. A. Marxman, C. E. Wooldridge, and R. J. Muzzy. "Fundamentals of Hybrid Boundary Layer Combustion". In: *Heterogeneous Combustion Conference*. 1963.

[8] L. D. Smoot and C. F. Price. "Regression Rates of Nonmetalized Hybrid Fuels Systems". In: *AIAA Journal* Vol. 3 (1965).

[9] G. Massini. "Time-resolved regression rates of paraffin based fuels for hybrid propulsion". MA thesis. Politecnico di Milano, 2011.

[10] K. K. Kuo et al. *Fundamental Phenomena on Fuel Decomposition and Boundary-Layer Combustion Processes with Applications to Hybrid Rocket Motors, Part I: Experimental Investigation*. Tech. rep. Propulsion Engineering Research Center, 1996.

[11] M. A. Karabeyoglu, B. J. Cantwell, and D. Altman. "Development and Testing of Paraffin-Based Hybrid Rocket Fuels". In: *37st AIAA/ASME/SAE/ASEE Joint Propulsion Conference and Exhibit*. 2001.

[12] F. Maggi et al. "Theoretical Analisys of Hydrides in Solid and Hybrid Rocket Propulsion". In: *International Journal of Hydrogen Energy* 37 (2011), pp. 1760–1769.

[13] M. A. Karabeyoglu, D. Altman, and B. J. Cantwell. "Combustion of Liquefying Hybrid Propellants: Part 1, General Theory". In: *Journal of Propulsion and Power* 18 (2002), pp. 610–620.

[14] M. A. Karabeyoglu and B. J. Cantwell. "Combustion of Liquefying Hybrid Propellants: Part 2, Stability of Liquid Films". In: *Journal of Propulsion and Power* 18 (2002), pp. 621–630.

[15] R. A. Gater and M. R. L. L'Ecuyer. "Entrainment and Deposition Rates in a Dispersed-Film Flow". In: *International Journal of Multiphase Flow* 13 (1970), pp. 1925–1939.

[16] R. Nigmatulin et al. "Entrainment and Deposition Rates in a Dispersed-Film Flow". In: *International Journal of Multiphase Flow* 22 (1996), pp. 19–30.

[17] P. Universit Pavia Mustarelli. Last visited: 26th January 2014. URL: http://chifis.unipv.it/mustarelli/lab_chifis/reologia.pdf.

[18] C. W. Macosko. *Rheology Principles, Measurements, and Applications*. Wiley-VCH, 1994.

[19] Polymer Nanostructures Lab Pennsylvania State University. Last visited: 29th April 2013. URL: http://zeus.plmsc.psu.edu/.

[20] J. J. Marano and G. D. Holder. "General Equation for Correlating the Thermophysical Properties of n-Paraffins, n-Olefins, and Other Homologous Series. 1. Formalism for Developing Asymptotic Behavior Correlations". In: *Industrial Engineering Chemical Research* 36 (1997), pp. 1887–1894.

[21] J. J. Marano and G. D. Holder. "General Equation for Correlating the Thermophysical Properties of n-Paraffins, n-Olefins, and Other Homologous Series. 2. Asymptotic Behavior Correlations for PVT Properties". In: *Industrial Engineering Chemical Research* 36 (1997), pp. 1895–1907.

[22] M. A. Karabeyoglu, B. J. Cantwell, and J. Stevens. "Evaluation of Homologous Series of Normal-Alkanes as Hybrid Rocket Fuels". In: *41st AIAA/ASME/SAE/ASEE Joint Propulsion Conference & Exhibi*. 2005.

[23] J. J. Marano and G. D. Holder. "A General Equation for Correlating the Thermophysical Properties of n-Paraffins, n-Olefins, and Other Homologous Series. 3. Asymptotic Behavior Correlations for Thermal and Transport Properties". In: *Industrial Engineering Chemical Research* 36 (1997), pp. 2399–2408.

[24] J. Bicerano. *Prediction of Polymer Properties*. Marcel Dekker Inc., 1996.

[25] Product information from Carlo Erba Reagenti. Last visited: 3rd October 2013. URL: www.carloerbareagents.com.

[26] Hot melt adhesives brochure from Sasol Wax GmbH. Last visited: 3rd October 2013. URL: www.sasolwax.com.

[27] D. J. Anneken et al. "Ullmann's Encyclopedia of Industrial Chemistry". In: Wiley-VCH, 2006. Chap. Fatty Acids.

[28] C. Paravan. "Ballistics of innovative solid fuel formulations for hybrid rocket engines". PhD thesis. Politecnico di Milano, 2012.

[29] Particle Sizes Explained Nevada Aerospace Science Associates. Last visited: 20th January 2014. URL: www.nassarocketry.com.

[30] J. Carissimi. "Investigation of physical properties of paraffin based hybrid rocket fuels". MA thesis. Politecnico di Milano, 2013.

[31] H. Ciezki. "The M11 Test Complex at DLR in Lampoldshausen". In: *Proceedings of 3rd European Conference for Aerospace Sciences*. 2009.

[32] H. K. Ciezki et al. “Combustion of Solid-Fuel Slabs containing Boron Particles in Step Combustor”. In: *Journal of Propulsion and Power* 19 (2003), pp. 1180–1191.

[33] M. Kobald et al. “Rheological, Optical And Ballistic Investigations Of Paran-Based Fuels For Hybrid Rocket Propulsion Using a 2D Slab-Burner”. In: *5TH European Conference for Aeronautics and Space Sciences (EUCASS)*. 2013.

[34] M. A. Karabeyoglu, B. J. Cantwell, and G. Zilliac. “Development of Scalable SpaceTime Averaged Regression Rate Expressions for Hybrid Rockets”. In: *Journal of Propulsion and Power* 23 (2007).

[35] E. Toson et al. “Rheological and ballistic investigations of paraffin-based fuels for hybrid rocket propulsion using a 2D radial micro-burner”. In: *5TH European Conference for Aeronautics and Space Sciences (EUCASS)*. 2013.

[36] L. Galfetti et al. “Ballistic and rheological characterization of paraffin-based fuels for hybrid rocket propulsion”. In: *47th AIAA/ASME/SAE/ASEE Joint Propulsion Conference & Exhibit*. 2011.

[37] M. A. Karabeyoglu et al. “Scale-Up Tests of High Regression Rate Paraffin-Based Hybrid Rocket Fuels”. In: *Journal of Propulsion and Power* 20 (2004).

[38] I. Nakagawa and S. Hikone. “Study on the Regression Rate of Paraffin-Based Hybrid Rocket Fuels”. In: *Journal of Propulsion and Power* 27 (2011), pp. 1276–1279.